

NASA Technical Paper 1532

LOAN COPY RETURN  
AFVL TECHNICAL LIBR  
KIRTLAND AFB, N. M.



**Turbojet-Exhaust-Nozzle Secondary-  
Airflow Pumping as an Exit Control  
of an Inlet-Stability Bypass System  
for a Mach 2.5 Axisymmetric  
Mixed-Compression Inlet**

Bobby W. Sanders

JANUARY 1980





NASA Technical Paper 1532

**Turbojet-Exhaust-Nozzle Secondary-  
Airflow Pumping as an Exit Control  
of an Inlet-Stability Bypass System  
for a Mach 2.5 Axisymmetric  
Mixed-Compression Inlet**

Bobby W. Sanders  
*Lewis Research Center  
Cleveland, Ohio*

**NASA**

National Aeronautics  
and Space Administration

**Scientific and Technical  
Information Office**

1980



## CONTENTS

	Page
SUMMARY . . . . .	1
INTRODUCTION . . . . .	1
APPARATUS AND PROCEDURE . . . . .	3
General Description . . . . .	3
Inlet Model . . . . .	3
Stability Bypass Entrance and Bleed Region Configuration . . . . .	5
Engine Description . . . . .	5
Upstream Airflow Variation Device . . . . .	6
Instrumentation . . . . .	6
RESULTS AND DISCUSSION . . . . .	7
Basic Inlet Stability Data . . . . .	7
Exhaust Nozzle Pumping . . . . .	9
Steady-State Inlet Stability Performance . . . . .	9
Propulsion System Response to Internal Airflow Disturbances . . . . .	12
Inlet response to engine light . . . . .	12
Engine response to inlet start . . . . .	12
Reductions in overboard bypass airflow . . . . .	13
Reductions in power lever angle . . . . .	14
Reductions in primary-nozzle area . . . . .	14
Propulsion System Response to External Airflow Disturbances . . . . .	15
SUMMARY OF RESULTS . . . . .	17
APPENDIXES	
A - ENGINE AND STABILITY BYPASS AIRFLOWS . . . . .	19
B - SYMBOLS . . . . .	21
REFERENCES . . . . .	24

## SUMMARY

The throat of a Mach 2.5, mixed-compression inlet with 40-percent internal supersonic-area contraction was fitted with a stability bypass system that was designed to provide the inlet with a large stable airflow range. Previous research programs had shown that controlling the stability bypass airflow with pressure-activated poppet valves would provide the inlet with very large stable margins. To further evaluate the concept of stability bypass control for this inlet, we tested an airflow system that used exhaust-nozzle, secondary-airflow pumping as the stability bypass control. A characteristic of the poppet valve that is essential for good stability bypass control - low pressure rise with increasing airflow - also characterizes secondary-airflow pumping. To provide a proper nozzle pumping characteristic, it was necessary to use a complete propulsion system. Therefore, the inlet was attached to a turbojet engine and an ejector nozzle with the stability bypass airflow ducted into the secondary-airflow chamber. Inlet-stability bypass performance was obtained for steady-state conditions and for several transient airflow disturbances, both internal and external. Internal airflow disturbances included pulsed reductions in overboard-bypass-door area, power lever angle, and primary-nozzle area. External airflow disturbances were provided by a flat gust plate upstream of the inlet. Propulsion system response to compressor stall was also obtained.

At the test free-stream Mach number of 2.5 the stability bypass and nozzle pumping control provided greater inlet stability than a conventional bleed system. The addition of the stability bypass system to the inlet did not adversely affect the engine.

## INTRODUCTION

At flight speeds above Mach 2.0 an inlet with a mixture of internal and external compression offers optimum performance by supplying the engine with high-pressure airflow while maintaining minimum drag. In mixed-compression inlets, maintaining the terminal shock at the inlet throat gives the highest pressure recovery and least distortion at the engine entrance. However, mixed-compression inlets have an undesirable airflow characteristic known as "unstart," which may occur when the terminal shock is placed too near the inlet throat. A slight transient reduction in airflow can move the terminal shock forward of the throat, where it is unstable and is abruptly expelled ahead of the inlet cowling. This shock expulsion, or unstart, causes a large, rapid reduction in mass flow and pressure recovery and greatly increases drag. Inlet buzz,

compressor stall, or combustor blowout may also occur. Obviously, an inlet unstart is extremely undesirable because of its adverse effects not only on the propulsion system itself but also on the aircraft's aerodynamic qualities. If an unstart does occur, carefully controlled variations of the inlet geometry are required to reestablish the design operating conditions. An engine relight sequence will also be necessary if blowout occurs.

Both external airflow disturbances (such as atmospheric turbulence) and internal airflow disturbances (such as reduced engine airflow demand) can cause the inlet to unstart. For an internal disturbance the inlet should provide a margin in corrected airflow below the optimum performance level without incurring unstart. This margin is defined as the stable airflow operating range. Conventional mixed-compression inlets can be designed to have a limited stable range: The performance bleed system increases its airflow as the terminal shock moves upstream into the throat bleed region. With fixed bleed exit areas, this limited stable range may not be adequate to absorb many airflow transients encountered by a typical supersonic propulsion system. A larger stable airflow range is currently provided for these inlets by operating them supercritically, with a resultant loss in their performance. Since any loss in inlet performance is reflected directly as a loss in propulsion-system thrust and efficiency, supercritical operation should be avoided.

The necessary system stability can be provided without compromising steady-state performance (i. e. , pressure recovery and distortion) by redesigning the inlet. The throat bleed system can be replaced with large bleed areas that provide a stability bypass system capable of removing large amounts of airflow (ref. 1). (The nomenclature for the throat airflow removal system has been changed since ref. 1 was published from throat-bypass system to inlet-stability bypass system.) This system prevents unstarts by removing airflow from the inlet throat to compensate for reduced diffuser-exit airflow demand. Reference 1 has shown that large increases in stability bypass airflow may be provided without prohibitive amounts of airflow removal during normal inlet operation if the bypass exit area can be controlled to maintain a relatively constant pressure in the bypass plenum. The inlet-stability bypass exit area can be varied by pressure-activated valves (such as the poppet valve in ref. 2) at the bypass exit. The effectiveness of several different stability bleed systems is discussed in references 1 and 3 to 11.

Previous research has shown that a good stability bypass control maintains a nearly constant pressure characteristic as airflow increases. Like the poppet valve, secondary-airflow pumping of the exhaust nozzle of a supersonic propulsion system has this characteristic. Therefore, as an exit control it should provide a sufficient inlet-stability margin. To evaluate this control concept, an inlet incorporating it and attached to a J85-GE-13 turbojet engine was tested in the Lewis 10- by 10- Foot Super-

sonic Wind Tunnel to determine its performance, both steady state and dynamic. The stability bypass airflow was ducted into the secondary-airflow plenum of the exhaust nozzle so that the exhaust nozzle could function as an inlet-stability bypass exit control. The inlet was a Mach 2.5, mixed-compression type with 40 percent of the supersonic-area contraction occurring internally.

Both steady-state and transient data were recorded at the inlet free-stream design Mach number of 2.5. Internal airflow disturbances were obtained by pulsing the overboard-bypass airflow, the power lever angle, or the primary-nozzle area. External airflow disturbances were provided by varying the angle of attack of a large flat plate located upstream of the inlet. A control system was used for fast inlet restart and engine relight when an inlet unstart was obtained.

U. S. customary units were used in designing the test model and recording and computing the experimental data. These units were converted to the International System of Units (SI) for this report.

## APPARATUS AND PROCEDURE

### General Description

An NASA-designed supersonic inlet attached to a General Electric model J85-GE-13 turbojet engine was tested in the Lewis 10- by 10- Foot Supersonic Wind Tunnel at the following nominal free-stream conditions: Mach number, 2.5; total pressure,  $9.4 \text{ N/cm}^2$ ; total temperature, 302 K; Reynolds number,  $4.3 \times 10^6$  (based on the cowl-lip diameter); and specific-heat ratio, 1.4. The engine operated from windmill to 90-percent corrected speed. When data were being taken with the engine running, the tunnel was operating on its propulsion cycle. In this cycle, the airflow downstream of the test section is vented to the atmosphere rather than recirculated as in the aerodynamic cycle. Figure 1 shows the engine and inlet, with nacelle, installed in the wind tunnel.

### Inlet Model

The inlet used in this investigation was a Mach 2.5 axisymmetric, mixed-compression type with 40 percent of the design supersonic-area contraction occurring internally. The inlet was attached to a cylindrical nacelle 0.635 meter in diameter in which a J85-GE-13 engine or a coldpipe, choked-exit plug assembly could be installed. For this study, only the engine was used. At the design Mach number, sizing the inlet to match the J85-GE-13's airflow requirements resulted in a 47.32-centimeter inlet capture diameter. The inlet was started by translating the centerbody. A flight version of this inlet with 40-percent internal contraction would require a collapsing cen-

terbody for starting and off-design operation (ref. 4).

Some basic inlet design details are presented in figure 2. Local theoretical airflow conditions on the cowl and centerbody, inlet contours, and diffuser-area variation are shown for the inlet design Mach number and centerbody position. A computer program (ref. 12) that incorporated the method of characteristics was used to design the supersonic diffuser. Initial supersonic compression was provided by a two-cone surface with half-angles of  $10^\circ$  and  $18.5^\circ$ . The internal oblique shock from the cowl lip was designed to be canceled at its impingement point on the centerbody by turning the surface. The remaining supersonic compression was isentropic for an average theoretical supersonic throat Mach number of 1.30 with an inviscid recovery of 0.9855. At the design centerbody position, the geometric throat was located at an  $x/R_c$  of 3.26. Downstream of the geometric throat, the inlet included a throat region with  $1^\circ$  equivalent conical expansion and a main subsonic diffuser that contained an overboard bypass system. The diffuser-centerbody boundary layer was controlled by vortex generators at an axial distance ratio of 3.965 (fig. 3). Details of the vortex generator design are shown in figure 4. The overall inlet length at design - cone tip to compressor face - was 7.88 cowl-lip radii. Internal surface coordinates of the inlet in terms of the cowl-lip radius are presented in table I. The inlet design characteristics are discussed more completely in reference 13.

Bleed areas were located in the throat region on the inlet cowl and centerbody surfaces. The forward-cowl bleed flow (not used in this test) was dumped directly overboard, as shown in figure 5. Stability bypass flow (to give the inlet a large stable range) was removed through the stability bypass entrance (a large region of normal bleed holes on the cowl side of the throat region). It was then ducted through the cowl-ing to the secondary-airflow chamber of the exhaust nozzle (figs. 3 and 5). Centerbody bleed airflow was ducted through hollow support struts to two centerbody bleed pipe - choked-plug assemblies (fig. 3).

The subsonic portion of the inlet diffuser incorporated two remotely controlled bypass systems: a fast-acting overboard bypass, and a slow-acting ejector bypass for engine and nozzle cooling airflow. For this investigation the ejector bypass was closed. Engine cooling airflow for the forward part of the engine was supplied from an external source. The externally supplied airflow mixed with the inlet-stability bypass airflow in the secondary-airflow chamber (fig. 5(b)). Cascades had been installed in the entrance to the overboard bypass cavity during a previous test program to eliminate resonance (ref. 14).

As shown in the figures, a bulky cowl was used on the test model so that major changes could easily be made to the inlet-stability bleed system and associated ducting during the wind tunnel tests. It was not representative of flight hardware. Figure 6 shows how an inlet-stability bypass system with the stability airflow ducted to the ex-

haust nozzle can be packaged within the low-external-cowl-drag profile essential for supersonic flight.

### Stability Bypass Entrance and Bleed Region Configuration

The stability-bypass configuration used in this test program (fig. 7) was the same as configuration NF of reference 1. As figure 7 shows, all the bleed regions were composed of rows of normal holes arranged in a concentrated, staggered pattern to provide uniform, circumferential bleeding of the boundary layer. The distributed porous hole pattern of 0.3175-centimeter-diameter holes in 15 rows on 0.4763-centimeter centers gave a nominal porosity of 40 percent. Reference 1 indicates that this stability bypass system can provide an inlet-stability margin of 28.4 percent from a high-performance-match operating condition if constant pressure is maintained in the stability bypass plenum to inlet unstart. The available forward and aft cowl bleeds were sealed, and the centerbody bleed gave a performance bleed mass-flow ratio of about 0.025 at the inlet-engine match condition.

### Engine Description

The General Electric J85-GE-13 is an afterburning turbojet with a high thrust-weight ratio. The engine has an eight-stage, axial-flow compressor coupled to a two-stage turbine. It has controlled compressor interstage bleed, variable inlet guide vanes, a throughflow annular combustor, and an afterburner (not used in this test) with a variable-area primary exhaust nozzle. The engine inlet diameter is 40.8 centimeters.

The compressor variable geometry consists of interstage bleed valves on stages 3 to 5 and inlet guide vanes. On a standard engine, the bleed valves and guide vanes are linked together and are controlled by the main fuel control as a function of the engine corrected speed. During this investigation the compressor variable geometry and power lever angle were controlled either by a computer or manually. The primary-nozzle area, which is normally controlled by the afterburner fuel control, was also controlled either by a computer or manually for this test.

The inlet performance for an engine stall condition was assessed by stalling the compressor by slowly closing the primary-nozzle area while maintaining a constant speed. So that the turbine temperature limit would not be exceeded during this procedure, a reduced-area, first-stage turbine stator was installed. Then at any point on the compressor map the turbine was matched to the compressor at a lower turbine-inlet temperature.

## Upstream Airflow Variation Device

A flat gust plate was used to vary the inlet, local, free-stream airflow (figs. 1 and 8). With the inlet and flat gust plate both at  $0^\circ$  angle of attack (fig. 8(a)), the local conditions at the inlet were not changed from the free-stream conditions. Increasing plate angle of attack decreased local Mach number and increased inlet angle of attack (fig. 8(b)).

### Instrumentation

Static-pressure distributions were measured along the top centerlines of the cowl and centerbody at the axial locations given in table II. Subsonic diffuser and bleed pressure instrumentation is shown in figures 9 and 10. Stability-bypass-bleed total pressure was measured by two total-pressure rakes just downstream of the open bleed at an  $x/R_c$  of 4.051. Pressures from these rakes were averaged to determine the stability-bypass-bleed recovery. Secondary total pressure was measured by two probes (fig. 5(b)). Centerbody and overboard-bypass-plenum pressures were measured by single tubes (fig. 10).

Overall inlet total-pressure recovery and distortion were determined from six, 10-tube total-pressure rakes (fig. 9) at the diffuser exit (inlet station 2). Each rake consisted of six equal-area-weighted tubes with additional tubes at the extreme equal-area-weighted tubes in positions corresponding to an 18-tube area-weighted rake. The compressor-face instrumentation and a calibration curve were used to determine engine airflow, as described in appendix A. Two piezoelectric pressure transducers (D8 and D9) were located at the compressor face (fig. 9). Dynamic instrumentation locations are given in table III.

The compressor discharge pressure was measured by 16 steady-state, total-pressure probes mounted in four rakes as shown in figure 11(a). One total-pressure probe (D10) measured both steady-state and transient pressures. A piezoelectric transducer was flush mounted to the inside of the tube 15.2 centimeters downstream of the probe entrance, and the tube was extended to the steady-state recording system so that the tube operated like an infinite line. Turbine discharge total temperature  $T_5$  was measured by eight thermocouples (fig. 11(b)) that were installed by the engine manufacturer and wired in parallel to give an average reading. Primary-nozzle total pressure  $P_8$  was determined by applying a pressure loss factor of 0.0365 ( $P_8 = 0.9635 P_5$ ) to the turbine discharge total pressure measured by the total-pressure instrumentation shown in figure 11(b).

One dynamic total-pressure and eight dynamic static-pressure taps were placed along the inlet duct as shown in figures 9, 10, and 12. Outputs of the strain-gage

absolute-pressure transducers in the cowl-lip static-pressure tap (S1) and the throat total-pressure probe (S2) were used in ratio form (S1/S2) to sense inlet unstart. The S1 and S2 transducers were mounted at the ends of 38.1- and 5.1-centimeter-long lines, respectively. The additional absolute pressure transducer (S3) was used to indicate the terminal shock position for computer control (fig. 12 and ref. 15). The remaining six (piezoelectric) transducers (D1 to D6) were flush mounted on the surface.

Engine speed was measured by a magnetic pickup that sensed the passage of a rotating gear attached to the customer-power takeoff shaft from the engine gearbox. Combustor flame was sensed by a photodiode. The positions of the inlet centerbody, the overboard bypass doors, and the exhaust nozzle were determined from potentiometer measurements.

The analog computer control system used during the tests is diagrammed in figure 13. The computer could be used to control the flat gust plate, the inlet centerbody, the overboard bypass doors, the power lever angle, and the primary-nozzle area.

## RESULTS AND DISCUSSION

### Basic Inlet Stability Data

The development of an effective stability bypass entrance configuration and the required bypass-plenum exit configuration is described in references 1 to 5 and 7. Basic results of these studies are presented in figure 14.

Inlet-stability bypass performance obtained during previous tests is shown in figure 14(a), where the bypass total-pressure recovery is a function of the bypass mass-flow ratio, and in figure 14(b) by a standard inlet-performance plot. The dashed lines represent the performance envelope of the distributed, porous, stability bypass configuration NF of reference 1, which was also used in the investigation reported herein. Data are shown for a fixed bleed exit and for poppet valves. The fixed exit was chosen because it essentially represents the performance of a conventional performance-bleed - small-fixed-exit system sized to provide an acceptable on-design bleed flow rate. This conventional system allows high on-design inlet performance but is not very tolerant of disturbances in diffuser airflow. For example, figure 14(a) shows that the fixed-exit system, which allows an acceptable match bleed of about 0.02 mass-flow ratio increases bleed mass-flow ratio by only about 0.02 when a disturbance moves the terminal shock upstream to the inlet minimum stable condition. This mass-flow change combined with the increase in diffuser-exit recovery provides a tolerance of about 5 percent to corrected airflow changes.

The basic concept of the stability bypass system is to provide the same on-design performance (i. e., recovery and performance-bleed mass-flow rate) but to allow large

increases in bleed rate to aerodynamically compensate for the changes in diffuser-exit airflow demand. Providing this capability requires a stability-bypass-plenum exit area control with a relatively flat pressure-airflow characteristic. The poppet valve shown in figure 14 has this characteristic. It allows the same on-design inlet performance as the small, fixed exit area but provides a very large increase in bleed to the minimum stable condition. This increased bleed also allows the inlet diffuser-exit recovery to increase to 0.947 at the minimum stable condition. From a design recovery of 0.90, the poppet valves gave an inlet-stability margin of 25.6 percent.

Secondary-airflow pumping of an exhaust nozzle also has a relatively flat pressure-airflow characteristic. If connected with an inlet-stability bypass plenum, it should give results like those of the poppet valves. Exhaust-nozzle pumping as a stability bypass exit control is illustrated in figure 15. It is assumed that the nozzle provides the proper design match condition (point A) so that only the required amount of performance bleed is removed. If the nozzle pumping system were carefully matched to the inlet performance bleed, the inlet could be smaller and lighter since it would not have to supply both performance bleed (exhausted overboard) and ejector airflow for engine cooling. The drag caused by the overboard exhaust of the inlet performance bleed would, of course, be eliminated. From the match condition (point A) the stability bypass mass flow could increase substantially to provide the inlet with a large stability margin before the inlet minimum stable condition at point B was reached. Although the slope of the pumping curve (solid line) may vary considerably most of the exhaust nozzles that have recently been considered for supersonic propulsion systems exhibit the desired characteristic of a good stability exit control. The pumping curve in figure 15 represents a single primary area and a single nozzle pressure ratio for match conditions. In an actual application the condition represented by point B might vary along the minimum stable characteristic as a result of changes in these two parameters. These parameters might vary as a result of an airflow transient, or they might cause an airflow transient.

The effect of changes in the ratio of secondary- to primary-nozzle diameter and nozzle pressure ratio on exhaust nozzle pumping is shown in figure 16. Although the pumping curves show the desired trend of a stability bypass exit control, how they are affected by a change from the design nozzle configuration is particularly important. In general, variations in these pumping curves would affect the minimum stable condition (point B in fig. 15). For example, reducing the power lever angle reduces the diffuser-exit airflow demand, thus causing the inlet to proceed toward point B on figure 15. However, reducing power lever angle also reduces nozzle pressure ratio. As shown in figure 16(b), a lower nozzle pressure ratio results in a smaller pressure demand. As the fuel flow is reduced and the terminal shock moves toward unstart at

point B, point B also moves to the right on the minimum stable characteristic and effectively provides an even flatter pressure-airflow control curve.

### Exhaust Nozzle Pumping

Exhaust-nozzle pumping data from the wind tunnel tests are compared with data from a static test (ref. 16) in figure 17. Although the external profiles of the two nozzles were different, the internal dimensions were the same. The data show the same trends and, when extrapolated, they agree with theory (ref. 16) at a corrected secondary airflow of 0.02 but have a slightly higher pressure requirement at a corrected secondary airflow of 0.08. (A higher pressure requirement is normal when data are compared with theoretical predictions.)

Data showing effective stability bypass exit control with exhaust-nozzle pumping are presented in figure 18. The design of the test model resulted in the inlet bleed airflow entering the secondary-airflow plenum downstream instead of in front of the engine as desired (fig. 5(b)). Therefore, externally supplied airflow was used to cool the front of the engine. Instead of exhausting this extra airflow overboard upstream of the nozzle and allowing only the stability bypass airflow to be used as secondary airflow, the two airflows were allowed to mix. This combined airflow into the nozzle effectively moved the airflow characteristic for the inlet bleed to the left, as shown in figure 18. Because the amount of externally supplied cooling airflow was relatively constant, the effective pumping curve (dashed line) more closely simulated a nozzle pumping characteristic that might be obtained in flight. This was desirable since the nozzle pumping curve (solid line) obtained did result in too large an on-design bleed mass-flow ratio because of the relatively low pressure-airflow characteristic. The nozzle pressure ratios that could be provided for this configuration in the wind tunnel were much lower than the nominal flight value of 27 (ref. 18); the externally supplied airflow helps to compensate for some of this mismatch in nozzle pressure ratio. (The effect of pressure ratio on secondary-airflow pumping is shown in fig. 16(b)).

### Steady-State Inlet Stability Performance

Steady-state performance of the inlet with the exhaust nozzle as the inlet-stability bypass exit control is shown in figure 19. Representative cowl surface pressure distributions are given in figures 20 and 21 and the nozzle pumping control is compared with other stability bypass exit controls in figure 22.

The data in figures 19(a) and (b) are like the basic data of figure 14. Figure 19(a) shows that secondary-airflow pumping provides an exit control with characteristics like those shown in figure 15. Closing of the overboard bypass doors (circular symbols in

fig. 19(a)) increased the stability bypass mass-flow ratio by only 0.02. The remaining part of the nominal, bypass mass-flow ratio at match of 0.05 was absorbed by the engine because of an increase in diffuser-exit recovery (fig. 19(b)). Reducing the engine speed from match ( $m_{by}/m_0 = 0.05$ ) to idle (square symbols in fig. 19) increased the stability bypass mass-flow ratio by 0.072 (fig. 19(a)), increased the total-pressure recovery to 0.943 (fig. 19(b)), and reduced the diffuser-exit corrected airflow 11.5 percent (fig. 19(c)).

Changes in bypass area and engine speed are typical causes of airflow variations in a flight propulsion system. The stability bypass exhaust-nozzle pumping system can easily absorb these airflow changes without incurring an inlet unstart, as shown in figure 19(a). Centerbody bleed performance and compressor-face total-pressure distortion are presented in figures 19(d) and (e).

Even when the bypass door area was closed at engine idle speed, the minimum stable condition was not attained (triangular symbols in fig. 19). The difference in mass-flow ratios between the right-most square data point (idle condition) and the triangular data point in figure 19(a) is the bypass variation that would be obtained if the engine speed were reduced to idle and then the bypass area were closed. In this case a difference of about 0.05 in mass-flow ratio was realized. Comparing these two conditions in figure 19(b) (in this figure the left-most symbols for the particular airflow variations) shows that they are at approximately the same recovery. Therefore, as shown figure 19(a), almost all the reduction in overboard bypass airflow was absorbed by a change in bleed airflow.

Inlet minimum stable conditions could only be obtained by almost closing the overboard bypass doors after the engine speed had been reduced to idle and the primary-nozzle area had been reduced. These data are represented by the right triangular symbols in figure 19. The pumping curve that was presented in figures 17 and 18 represents the match condition and pumping that would be obtained by reducing the engine speed to idle, closing the bypass doors at idle, and reducing the primary-nozzle area to inlet unstart. These combined airflow reductions were required to obtain the inlet minimum-stable condition. From an initial engine match operating condition of 90-percent total-pressure recovery (fig. 19(c)), corrected airflow was reduced from 16.58 kg/sec to a minimum stable corrected airflow of 13.36 kg/sec with the exhaust-nozzle-pumping inlet-stability bypass system. Substituting these corrected airflows into the stability index equation,  $SI = 100((16.58-13.36)/16.58)$ , gave a steady-state stability index of 19.4 percent. All these airflow reductions would probably not occur at the same time on an aircraft. Therefore, the exhaust-nozzle-pumping inlet-stability bypass system can absorb all but extreme variations in inlet diffuser-exit airflow.

The left-most data for the critical (or supercritical) conditions did not match the dashed line for supercritical stability bypass performance in figure 19(a) because of

the method used to calculate the bleed airflows. The airflow calculation methods are discussed in appendix A. A subtraction method was used to determine the stability airflow. Since this method used engine airflow, which is very difficult to determine accurately, a small error can be expected. No attempt to shift the curve in figure 19(a) was made. Obviously, the critical conditions should be on the supercritical bleed curve, but a left-positioning of the data that would satisfy the supercritical conditions would further offset the recorded minimum stable condition from the minimum stable characteristic curve.

Cowl surface static distributions for an engine speed variation from match to idle are presented in figure 20. These pressure distributions are for the inlet performance conditions represented by the square symbols in figure 19. The curves in figure 20 show that the terminal shock moved upstream as the engine speed was reduced. At engine idle speed ( $N/N^* \sqrt{\theta}$  of 0.792) the terminal shock had moved upstream over about half of the the stability bypass entrance. This roughly correlates with the data of figure 19(a), which show that at the engine idle condition bleed airflow had increased to about half the total amount at the minimum stable condition.

Cowl surface pressure distributions for the critical and minimum-airflow inlet operating conditions for each method used in decreasing the diffuser-exit airflow are presented in figure 21. All the symbols except the inverted triangle (for critical or match) are consistent with the symbols of figure 19. For example, the right-triangular symbol of figure 21 represents the inlet minimum stable condition of figure 19.

Stability bypass performance with the plenum exit controlled by the exhaust-nozzle secondary-airflow pumping characteristic, the poppet valves, or a fixed exit are compared in figure 22 for the inlet on an operating J85-GE-13 engine. Exhaust-nozzle pumping, like the poppet valves, was superior to the fixed-exit control in greatly increasing bleed as the inlet approached minimum stable conditions. Exhaust nozzle pumping did provide the desired relatively flat pressure-airflow control characteristic, like the poppet-valve characteristic. The first four data points for the stability system with exhaust-nozzle pumping control (key to fig. 22) are for almost the same engine operating conditions (match to idle speed) as the poppet-valve data of reference 7. When the poppet-valve-controlled stability bypass system was tested with a turbojet engine, only the separate changes in each system controlling airflow were investigated. Combinations of changes, as were used during the exhaust-nozzle pumping tests, were not investigated because the coldpipe data had indicated the poppet valve's overall capabilities. The two control curves for the poppet valves differ because a slightly higher valve internal reference pressure was used in the engine tests.

## Propulsion System Response to Internal Airflow Disturbances

The transient airflow disturbance data are presented in two parts: Part (a) of each figure shows the inlet response, which includes inlet throat pressures D1 to D5, diffuser static pressure D6, stability-bypass-plenum pressure D7, overboard bypass area  $A_{by}$ , and inlet centerbody position  $x_{cb}$ . Part (b) of each figure shows the engine response, which includes engine speed  $N$ ; combustor flame sensor; combustor spark source; turbine-exit temperature  $T_5$ ; power lever angle PLA, primary-nozzle area  $A_8$ ; compressor pressures D8, D9, and  $P_3/P_2$ ; and the inlet unstart sensor trace. An increase in any of these parameters is indicated when the trace moves toward the top of the figure.

Inlet response to engine light. - The started inlet responded to an engine light as shown in figure 23. The increase in engine speed and turbine-exit temperature shows that an engine light was obtained at the second spark shown on the trace. As the engine speed increased and consequently the engine required more airflow, the closed-loop overboard bypass control system reduced the bypass area to prevent the inlet terminal shock from moving too far supercritical. The control system was designed to hold a predetermined duct pressure. The nozzle area remained fixed during the engine light. No adverse effects of using the exhaust-nozzle secondary-airflow pumping control were observed. The pressure traces indicate very little pressure variation in the inlet during the engine light.

The unstart inlet responded to an engine light as shown in figure 24. Again the overboard bypass system was in closed-loop control. Results were like those for the started inlet.

Engine response to inlet start. - The engine and inlet responded during an inlet start with the engine running as shown in figure 25. The inlet was started by translating the inlet centerbody upstream. In an actual flight inlet of this configuration, varying the throat area would require a collapsing centerbody (ref. 4). Centerbody translation is shown in figure 25(a): The nozzle area remained fixed during the inlet start and no adverse effects of using the exhaust-nozzle secondary airflow as a bleed control were observed. A sharp change in throat pressure level indicates the point of inlet start. Comparing the throat pressure traces with the centerbody position indicates that the inlet start occurred just before the centerbody reached its most upstream position. The centerbody was adjusted to translate to a location just beyond the restart position and then return to the design position.

In figure 25(b), inlet start is indicated by a sharp increase in the level of the unstart sensor trace. The overboard bypass doors were on closed-loop control during the inlet restart transient. During this investigation the duct pressure schedule for the overboard bypass control was basically a two-pressure-level curve: one level for

started-inlet operation, and a slightly lower level for unstarted-inlet operation. The control command signal to the bypass doors switched to the unstarted pressure level when the inlet unstart sensor exceeded the reference level and commanded the doors to regulate the duct pressure to a predetermined level.

Reductions in overboard bypass airflow. - The inlet and engine responded to a single sine-wave reduction in overboard bypass exit area as shown in figure 26. This response is presented even though it was obvious from the steady-state performance (fig. 19) that reducing bypass area from inlet-match conditions would not cause an inlet unstart. The traces do show, however, the pressure increases for the throat as the terminal shock moved upstream (see trace for transducer D4 at the downstream edge of the open bleed region). Since the stability-bypass-plenum pressure D7 increased very slightly, the stability mass flow must have absorbed the change in diffuser-exit airflow. (The stability bypass design is based on a very small pressure rise in the bleed plenum for a substantial increase in bleed flow.) The data for the poppet-valve-controlled stability bypass configuration of reference 7 were like the data of figure 26 for exhaust-nozzle pumping when the inlet was subjected to similar transients in overboard bypass area.

Inlet unstart from minimum stable conditions (fig. 27) was obtained by a small reduction in overboard bypass area from the minimum stable operating condition (fig. 19). As stated in the discussion of figure 19, exhaust-nozzle pumping provided a very large stability range for the inlet. An inlet unstart could only be obtained by reducing engine speed to idle, reducing nozzle area from match, and almost closing the bypass doors.

Inlet unstart is indicated in figure 27(a) by a sharp drop in the throat pressures from the high, minimum stable pressure level (right-triangular symbol in fig. 21) and by the sudden drop in the unstart sensor trace in figure 27(b). When inlet unstart was indicated by the unstart sensor, the computer control was set to extend the centerbody to restart the inlet, to provide closed-loop overboard bypass control, and to cause the combustor spark source (spark plug at 2 sparks/sec) to relight the engine if the unstart had caused a blowout. The inlet restarted in about 0.2 second (limited by the centerbody translation rate) as indicated by the inlet unstart sensor.

Figure 27 shows some of the very undesirable characteristics that are associated with an inlet unstart. Combustor blowout occurred, as indicated by the steady-state character of the flame sensor trace just after unstart. The compressor probably did not stall as a hammershock pressure spike (which normally occurs in the inlet as a result of stall) was not evident. The compressor-face total pressure D9 shows an extremely large drop in recovery immediately after unstart. This drop in pressure ( $\Delta P/P_0 = 0.78$  (4 lines) and 0.195 per line) represents a change in compressor-face recovery from 0.94 at the minimum stable condition to 0.16 just after unstart. The combustor was

relighted about 0.50 second after inlet unstart, as indicated by comparing the spark source trace with the flame sensor and engine speed traces.

Reductions in power lever angle. - Inlet and engine responses to a reduction in power lever angle are presented in figure 28. Reducing the power lever angle decreased fuel flow, which in turn decreased engine speed, as indicated in figure 28(b). Reducing engine speed required a reduced diffuser-exit airflow demand since the overboard bypass control was not activated. The pressure signal from transducer D4 indicated that the terminal shock moved upstream to compensate for the reduced airflow demand but that the inlet did not unstart. Figure 19 has shown that the inlet could not be unstarted by varying the power lever angle from a match engine speed of about 0.873. The exhaust-nozzle-pumping stability bypass system provided such a large stability range that the inlet did not unstart even when the engine speed was reduced to idle.

Reductions in primary-nozzle area. - The propulsion system responded to a reduction in the primary-nozzle area and consequently to a reduction in diffuser airflow demand as shown in figure 29. The results are like those for reductions in overboard bypass airflow and power lever angle. Reducing primary-nozzle area reduced engine speed. The lower engine speed moved the terminal shock upstream since less diffuser-exit airflow was required because the bypass door control was not activated. The pressure rise for transducer D4 indicates the shock movement. A slight rise in the stability-bypass-plenum pressure D7 would indicate that the transient change in airflow was absorbed by the stability system and that inlet unstart did not occur. The trace for transducer D5 indicates that the shock moved downstream over this transducer just after the transient but then returned to its original position.

The propulsion system responded to a compressor stall as shown in figure 30. For this transient, the compressor was stalled by a slow manual closing of the primary nozzle to backpressure the engine while manually advancing the power lever angle to maintain a constant corrected engine speed of 90.1 percent. Compressor performance is presented in figure 31. In figure 30(b) the primary-nozzle area before compressor stall appears to be constant because of the very slow manual closing of the primary nozzle. Stall hammershock shows up as the large initial pressure spike on all the pressure transducers in figure 30(a). Figure 30(b) indicates that combustor blowout occurred at the same time that the compressor pressure ratio indicated stall. The inlet unstart sensor indicated inlet unstart about 0.01 second later. The inlet unstarted because the stability bypass system did not have the capability to absorb the airflow reduction associated with an engine stall. At inlet unstart the overboard bypass system was switched to closed-loop control. After stall, the command (scram) to completely open the nozzle and chop the fuel flow was given by the control system. Engine relight was not attempted.

## Propulsion System Response to External Airflow Disturbances

The propulsion system responded to variations in external airflow as shown in figures 32 to 37. External airflow disturbances that reduce inlet free-stream Mach number or increase angle of attack can induce inlet unstart. For some supersonic inlets, unstart results from a local overcompression of the airflow near the throat region to a subsonic condition. When the inlet is operated at an angle of attack, this overcompression occurs on the leeward side of the inlet. Reference 1 indicates that local overcompression can be delayed to larger angles of attack by locating bleed forward in the supersonic diffuser in the overcompression region and by removing bleed airflow from a large axial region on the cowl surface with additional bleed airflow removal. Reference 19 indicates that for a reduction in inlet free-stream Mach number the local overcompression again appears forward of the throat but circumferentially encompasses the entire inlet flow field.

The external airflow was varied by pulsing (single sine wave) or by a slow manual change of the flat-plate angle of attack (fig. 11) upstream of the inlet. Increasing the plate angle of attack from  $0^\circ$  lowered the local Mach number and increased the local angle of attack - for a combination of changes in the external airflow.

For this test the inlet diffuser dynamic pressure instrumentation was on the side ( $\varphi = 90^\circ$ ) of the inlet. Therefore, increasing the plate angle, which caused a local downflow into the inlet, resulted in the dynamic-pressure instrumentation being between the windward ( $\varphi = 0^\circ$ ) and the leeward ( $\varphi = 180^\circ$ ) sides of the inlet. The inlet throat transducers do show a local pressure increase because the disturbance was largely due to Mach number reduction. But they do not show the maximum pressure rise in the inlet throat since the combination of Mach number and angle of attack would produce the maximum change on the leeward (bottom centerline) side.

The system responded to pulses in the flat-gust-plate angle of attack as shown in figures 32 and 33. Changing the gust-plate angle from  $0^\circ$  to  $1^\circ$  (fig. 32) increased pressure in the inlet throat and in the stability bypass plenum. The inlet did not unstart, and no noticeable change in the engine parameters was observed.

Changing the gust-plate angle from  $0^\circ$  to  $1.2^\circ$  (fig. 33) resulted in an inlet unstart. A rather large increase in surface pressure on the forward cowl (transducer D1) occurred just before unstart; and, as indicated earlier, the pressure rise on the leeward side should have been even larger (i. e., increased to sonic conditions, which would result in an inlet unstart). The inlet unstart did not cause combustor blowout or compressor stall because the unstart pressure transients were not severe. Therefore, only an inlet restart was required to reestablish the initial operating conditions. The inlet restarted in about 0.2 second, with an additional 0.3 second to reset the centerbody to the design position. The overboard bypass trace shows that the bypass doors

went into a computer-controlled, closed-loop operation upon inlet unstart. Normally, for a conventional inlet, the bypass doors must be controlled upon inlet unstart to prevent buzz. For this inlet configuration, however, overboard bypass control is probably not required because the stability bleed should perform the function of the overboard bypass upon unstart. If upon unstart the bypass door area allows the stability system to function within the unstarted-buzz-limit bleed characteristic curves, the stability system will prevent inlet buzz. The stability bypass system as an inlet buzz control during unstart is discussed in reference 7. Reference 7 also states that, when a conventional inlet system with small bleed plenum and small fixed exit was unstarted by an external disturbance similar to that of figure 33, combustor blowout and stall always occurred. Again figure 33 shows the superiority of the exhaust-nozzle-pumping stability bypass system since neither blowout nor stall occurred.

An inlet unstart created by a slow, manual variation of the gust-plate angle of attack is presented in figure 34. The nearly constant level of the gust-plate angle before inlet unstart was the result of the slow manual variation of the plate angle. At inlet unstart the computer commanded the plate to return to  $0^\circ$ . Basically, the results of the unstart shown in figure 34 were the same as for that shown in figure 33. Neither combustor blowout nor compressor stall occurred. However, unlike the test conditions of figure 33, the overboard bypass doors were not set to go into the computer-controlled mode upon unstart for the test conditions of figure 34. Inlet buzz did not occur. These data show that the stability bypass system can function during an unstarted-inlet condition to help prevent buzz.

When the conditions of figure 34 were repeated about 45 seconds later, another inlet unstart occurred (fig. 35). Compressor stall and combustor blowout occurred just after inlet unstart. The inlet was restarted by extending the centerbody, but the engine was not relighted because the combustor spark source was not activated for relight. However, without combustor relight the decrease in engine speed and consequently in diffuser-exit airflow demand caused an upstream movement of the terminal shock, as indicated by the inlet throat transducers, and resulted in another inlet unstart. The stability-bypass-plenum transducer D7 indicated an increase in pressure before the second inlet unstart.

From figure 19(a) a reasonable increase in plenum pressure would indicate that a large amount of airflow was removed as the terminal shock moved upstream. However, this system did not have the capacity to absorb the reduction in airflow from match to the almost windmill conditions (indicated by the nearly constant level at the end of the engine speed trace in fig. 35(b)) that occurred before the second inlet unstart. With the engine at windmill, the overboard bypass doors at the initial match condition, and the inlet unstarted, the stability bypass system could not prevent inlet buzz after the second inlet unstart. Thus, even though the stability bypass system can greatly reduce the re-

quirements of the propulsion control system during inlet unstart, a simple overboard bypass system is still required for such extreme conditions as shown in figure 35.

Manual scram of the system was begun about 0.1 second after the second unstart. During the test program, there were 16 inlet unstarts from external airflow disturbances. Only three of these unstarts caused the compressor to stall. Two of these stalls occurred when an inlet unstart condition was duplicated less than a minute after the first unstart condition. Figures 34 and 35 show these duplicate test conditions.

During inlet unstart-restart and engine relight, with (fig. 36) or without (fig. 37) overboard bypass control after unstart, inlet buzz did not occur. Neither combustor blowout nor compressor stall occurred. These data are for conditions like those of the previous figures except that the primary-nozzle area was slightly larger.

## SUMMARY OF RESULTS

The throat of a Mach 2.5, mixed-compression inlet with 40-percent internal supersonic-area contraction was fitted with an inlet-stability bypass system designed to provide the inlet with a large, stable airflow range. This system allows the inlet to be operated at nearly the optimum performance condition without being susceptible to an inlet unstart as a result of small variations in inlet airflow. Previous research programs have shown that pressure-activated poppet-valve control of the stability bypass airflow results in very large, stable airflow margins for the inlet. For further evaluation of the inlet-stability bypass system, the inlet was tested on a turbojet engine. The stability bypass airflow was ducted into the secondary-airflow plenum of the turbojet ejector nozzle. This arrangement allows the secondary-airflow pumping characteristic of the exhaust nozzle to function as an inlet-stability bypass exit control. The relatively flat pressure-airflow characteristic of the nozzle pumping should provide results like those for the poppet valves. Inlet and engine response were obtained for several transient airflow disturbances, both external and internal. The test was conducted in the Lewis 10- by 10-Foot Supersonic Wind Tunnel at a Mach number of 2.5, with the following results:

1. The supersonic-exhaust-nozzle-controlled inlet-stability bypass system had no adverse effects on the performance of the inlet or engine.
2. With the inlet operating at a high performance condition, a large, stable airflow range can be provided by using exhaust-nozzle secondary-airflow pumping as an exit control for an inlet stability-bypass system. From an initial inlet operating condition of 90-percent total pressure recovery, it provided a steady-state stability index of 19.4 percent.
3. The inlet-stability bypass with the exhaust-nozzle pumping as an exit control prevented the inlet from unstating for all but extreme downstream disturbances. For

example, inlet unstart could only be obtained by stalling the engine or by a combined reduction in subsonic diffuser airflow that was obtained by reducing the engine speed from match to idle, reducing the turbojet primary-nozzle area, and closing the overboard bypass doors.

4. No difficulty was experienced in lighting the engine (with the inlet started or unstarted) or in starting the inlet with the engine running.

5. When the engine was relighted during an inlet unstart with or without overboard bypass control, inlet buzz did not occur. Inlet buzz did occur after one inlet unstart without overboard bypass control in which the engine was not relighted but was allowed to coast down to windmill conditions.

6. Combustor blowout occurred during only 3 of the 16 inlet unstarts that were caused by external airflow disturbances.

7. Combustor blowout occurred for both inlet unstarts that were caused by internal airflow disturbances. For one unstart, the inlet restarted in about 0.2 second (limited by the centerbody translation rate) and the combustor relighted about 0.2 second later. Relight was not attempted when the inlet was unstarted by stalling the engine.

8. The nozzle pumping characteristics obtained in the wind tunnel tests agreed with those obtained in a static test facility.

Lewis Research Center,

National Aeronautics and Space Administration,

Cleveland, Ohio, July 24, 1978,

505-04.

## APPENDIX A

### ENGINE AND STABILITY BYPASS AIRFLOWS

Engine corrected airflow and stability bypass mass flow were determined by the following procedure.

#### Engine Airflow

It is very difficult to measure engine airflow either in a wind tunnel or in flight. Therefore, the engine is usually extensively calibrated in a static test facility before, and perhaps after, the propulsion test program. A different approach to obtaining the engine airflow was used in this investigation.

During the coldpipe investigation of this inlet (ref. 1) the airflow calculated from compressor-face instrumentation was compared with the airflow measured by the choked-exit mass-flow plug system. From this calibration the compressor-face calculated airflow can be corrected during an engine test to accurately represent engine airflow. The compressor-face calculated airflow  $W_{\text{corr, cf}}$  and choked-exit-plug-measured airflow  $W_{\text{corr, cep}}$  are compared in figure 38.

Compressor-face airflow was calculated by the following equation:

$$W_{\text{corr, cf}} = \frac{16.102 \left( \frac{m_{\text{cf}}}{m_0} \right) (A_i) \left( \frac{A^*}{A} \right)_0}{\left( \frac{P_{\text{cf}}}{P_0} \right)}$$

where  $A_i$  is the inlet capture area of  $0.1757 \text{ m}^2$ ;  $P_{\text{cf}}/P_0$  is the compressor-face, total-pressure recovery (also  $P_2/P_0$ ),  $(A^*/A)_0$  is the area ratio for the free-stream Mach number, and  $m_{\text{cf}}/m_0$  was determined from

$$\frac{m_{\text{cf}}}{m_0} = \frac{P_{\text{cf}} A_{\text{cf}} \left( \frac{A^*}{A} \right)_{\text{cf}}}{P_0 A_i \left( \frac{A^*}{A} \right)_0}$$

where  $A_{\text{cf}}$  is the  $0.1177\text{-m}^2$  annulus flow area at the compressor-face rake station and where

$$\left( \frac{A^*}{A} \right)_{\text{cf}} = f(M_{\text{cf}})$$

(The compressor-face Mach number  $M_{cf}$  was determined from the average static and total pressures at the rake station.)

As shown in figure 38, the calculated, compressor-face corrected airflow was larger than the actual corrected airflow as determined by the choked plug. Therefore, during the engine test program, the engine corrected airflow ( $W_{corr,2}$  or  $W_{corr,cep}$ ) was obtained by applying the calibration curve in figure 38 to measured compressor-face airflows  $W_{corr,cf}$ . If engine mass-flow  $m_2/m_0$  is required, the corrected airflow equation and the value for  $W_{corr,2}$  are used to obtain the correct value.

#### Stability Bypass Airflow

The stability bypass mass-flow ratio was determined by subtraction, as follows

$$\frac{m_{sb}}{m_0} = \frac{m_i}{m_0} - \frac{m_2}{m_0} - \frac{m_{by}}{m_0} - \frac{m_{cb}}{m_0}$$

where  $m_i/m_0$  is the capture mass-flow ratio (1.0 for the inlet cruise Mach number),  $m_2/m_0$  was determined from the calibration curves for the engine-face rake station, and  $m_{by}/m_0$  and  $m_{cb}/m_0$  are measured values of overboard bypass and centerbody mass flows.

## APPENDIX B

### SYMBOLS

A	flow area, $m^2$
$A_c$	cowl-lip capture area, $0.1757 m^2$
$A_8$	primary-nozzle area, $m^2$
CO	converging-vortex generator pair
CPR	compressor pressure ratio, $P_3/P_2$
D	inlet compressor-face distortion, $D_2 = [(P_{\max} - P_{\min})/P_{av}]_2$
DI	diverging-vortex generator pair
d	diameter, cm
f	pulse frequency, $1/\tau$ , $sec^{-1}$
H	annulus or rake height at local diffuser station, cm
h	distance from inlet surface, cm
M	Mach number
m	mass flow, kg/sec
$m_0$	free-stream mass flow based on $A_c$ , kg/sec
$m/m_0$	mass-flow ratio
N	engine speed, rpm
$N^*$	rated engine speed, 16 500 rpm
$N/N^*\sqrt{\theta}$	corrected engine speed
P	total pressure, $N/m^2$
$\Delta P$	fluctuating component of local pressure
PLA	power lever angle (throttle), deg
p	static pressure, $N/m^2$
$R_c$	inlet cowl-lip radius, 23.66 cm
r	radius, cm
SI	stability index, $SI = 100 \left( 1 - \frac{W_{\text{corr, min s, 2}}}{W_{\text{corr, op, 2}}} \right)$ , percent
T	total temperature, K

W	weight flow rate, kg/sec
$W_{\text{corr}}$	corrected airflow, $W \sqrt{\theta/\delta}$ , kg/sec
x	axial station, cm
$x_{\text{cb}}$	centerbody position measured from $M_0 = 2.5$ design cone tip position, cm
$x/R_c$	axial distance ratio, inlet radii
$\alpha$	angle of attack, deg
$\delta$	$P/(10.13 \times 10^4 \text{ N/m}^2)$
$\theta$	$T/288.2 \text{ K}$
$\dot{\theta}_l$	cowl-lip position parameter, $\tan^{-1} \left( \frac{1}{\frac{x}{R_c}} \right)$
$\tau$	transient pulse width, sec
$\varphi$	circumferential position, deg

Subscripts:

av	average
b	bleed
bp	bleed plenum
by	overboard bypass
cb	inlet centerbody
cep	choked exit plug
cf	compressor face
de	subsonic diffuser exit (engine plus overboard bypass)
e	exhaust
ea	external cooling airflow
fp	flat plate
i	inlet capture
l	local
max	maximum
min	minimum
min s	minimum stable inlet operating point

op	inlet operating point
p	primary
ref	reference
s	nozzle secondary
sb	stability bypass
t	transient
uns	unstart
0	free stream
2	compressor-face station
3	compressor discharge station
5	turbine-exit station
8	exhaust station (primary nozzle)

## REFERENCES

1. Sanders, Bobby W. ; and Mitchell, Glenn A. : Throat-Bypass Bleed Systems for Increasing the Stable Airflow Range of a Mach 2.50 Axisymmetric Inlet with 40-Percent Internal Contraction. NASA TM X-2779, 1973.
2. Mitchell, Glenn A. ; and Sanders, Bobby W. : Airflow Control System for Supersonic Inlets. U. S. Patent 3,799,475, Mar. 1974.
3. Sanders, Bobby W. ; and Mitchell, Glenn A. : Increasing the Stable Operating Range of a Mach 2.5 Inlet. AIAA Paper 70-686, June 1970.
4. Bowditch, David N. ; et al. : Supersonic Cruise Inlets. Aircraft Propulsion. NASA SP-259, 1971, pp. 283-312.
5. Mitchell, Glenn A. ; and Sanders, Bobby W. : Pressure-Activated Stability-Bypass-Control Valves to Increase the Stable Airflow Range of a Mach 2.5 Inlet with 40-Percent Internal Contraction. NASA TM X-2972, 1974.
6. Mitchell, Glenn A. ; and Sanders, Bobby W. : Poppet Valve Control of a Throat Stability Bypass to Increase the Stable Airflow Range of a Mach 2.5 Inlet with 60-Percent Internal Contraction. NASA TM X-3297, 1975.
7. Sanders, Bobby W. : Dynamic Response of a Mach 2.5 Axisymmetric Inlet and Turbojet Engine with a Poppet-Valve-Controlled Inlet-Stability Bypass System When Subjected to Internal and External Airflow Transients. NASA TP-1531, 1979.
8. Shaw, Robert J. ; Mitchell, Glenn A. ; and Sanders, Bobby W. : Forward Slanted Slot Throat Stability Bypass to Increase the Stable Airflow Range of a Mach 2.5 Inlet with 60-Percent Internal Contraction. NASA TM X-2973, 1974.
9. Shaw, Robert J. ; Mitchell, Glenn A. ; and Sanders, Bobby W. : Distributed Porous Throat Stability Bypass to Increase the Stable Airflow Range of a Mach 2.5 Inlet with 60-Percent Internal Contraction. NASA TM X-2974, 1974.
10. Shaw, Robert J. ; Mitchell, Glenn A. ; and Sanders, Bobby W. : Distributed Educated Throat Stability Bypass to Increase the Stable Airflow Range of a Mach 2.5 Inlet with 60-Percent Internal Contraction. NASA TM X-2975, 1974.
11. Mitchell, Glenn A. ; Sanders, Bobby W. ; and Shaw, Robert J. : Throat Stability-Bypass Systems to Increase the Stable Airflow Range of a Mach 2.5 Inlet with 60-Percent Internal Contraction. NASA TM X-2976, 1974.
12. Anderson, Bernhard H. : Design of Supersonic Inlets by a Computer Program Incorporating the Method of Characteristics. NASA TN D-4960, 1969.

13. Wasserbauer, Joseph F.; and Choby, David A.: Performance of a Bicone Inlet Designed for Mach 2.5 with Internal Distributed Compression and 40-Percent Internal Contraction. NASA TM X-2416, 1972.
14. Coltrin, Robert E.; and Calogeras, James E.: Supersonic Wind Tunnel Investigation of Inlet-Engine Compatibility. AIAA Paper 69-487, June 1969.
15. Cole, Gary L.; Neiner, George H.; and Crosby, Michael J.: An Automatic Restart Control System for an Axisymmetric Mixed-Compression Inlet. NASA TN D-5590, 1969.
16. Samanich, Nick E.; and Huntley, Sidney C.: Thrust and Pumping Characteristics of Cylindrical Ejectors Using Afterburning Turbojet Gas Generator. NASA TM X-52565, 1969.
17. Kochendorfer, Fred D.; and Rousso, Morris D.: Performance Characteristics of Aircraft Cooling Ejectors Having Short Cylindrical Shrouds. NACA RM E51E01, 1951.
18. Bresnahan, Donald L.: Performance of an Aerodynamically Positioned Auxiliary Inlet Ejector Nozzle at Mach Numbers from 0 to 2.0. NASA TM X-2023, 1970.
19. Choby, David A.: Tolerance of Mach 2.50 Axisymmetric Mixed-Compression Inlets to Upstream Flow Variations. NASA TM X-2433, 1972.

TABLE I. - INLET COORDINATES

(a) Centerbody				(b) Cowl			
Axial distance from center-body tip, $x/R_c$	Inlet cowl-lip radius ratio, $r/R_c$	Axial distance from center-body tip, $x/R_c$	Inlet cowl-lip radius ratio, $r/R_c$	Axial distance from center-body tip, $x/R_c$	Inlet cowl-lip radius ratio, $r/R_c$	Axial distance from center-body tip, $x/R_c$	Inlet-cowl lip radius ratio, $r/R_c$
0	0	4.750	0.5825	2.117	1.0000	4.600	0.9374
10° Conical section		4.800	.5700	2.150	1.0028	4.650	.9324
1.0323	0.1820	4.850	.5573	2.200	1.0070	4.700	.9276
18.5° Conical section		4.900	.5448	2.250	1.0111	4.750	.9232
		4.950	.5320	2.300	1.0154	4.800	.9191
2.7620	0.7608	5.000	.5195	2.350	1.0193	4.850	.9153
2.800	.7696	5.050	.5075	2.400	1.0228	4.900	.9120
2.850	.7794	5.100	.4983	2.450	1.0261	4.950	.9087
2.900	.7874	5.150	.4895	2.500	1.0290	5.000	.9050
2.950	.7937	5.200	.4805	2.550	1.0317	5.050	.9044
3.000	.7986	5.250	.4715	2.600	1.0340	5.100	.9049
3.050	.8025	5.300	.4622	2.650	1.0360	5.150	.9058
3.100	.8045	5.350	.4534	2.700	1.0373	5.200	.9071
3.150	.8043	5.400	.4444	2.750	1.0382	5.250	.9086
3.200	.8030	5.450	.4352	2.800	1.0386	5.300	.9102
3.250	.8015	5.500	.4264	2.850	1.0386	5.350	.9118
3.300	.8000	5.550	.4175	2.900	1.0381	5.400	.9132
3.350	.7982	5.600	.4085	2.950	1.0370	5.450	.9145
3.400	.7964	5.650	.3995	3.000	1.0356	5.500	.9157
3.450	.7944	5.700	.3900	3.050	1.0337	5.550	.9166
3.500	.7925	5.750	.3815	3.100	1.0320	5.600	.9173
3.550	.7906	5.800	.3732	3.150	1.0304	5.650	.9177
3.600	.7886	5.850	.3650	3.200	1.0290	5.700	.9179
3.650	.7862	5.900	.3566	3.250	1.0275	Cylinder	
3.700	.7834	5.950	.3488	3.300	1.0262		
3.750	.7798	6.000	.3412	3.350	1.0251	6.1747	0.9179
3.800	.7757	6.050	.3339	3.400	1.0239	Bypass gap	
3.850	.7711	6.100	.3266	3.450	1.0227		
3.900	.7655	6.150	.3196	3.500	1.0215	6.7847	0.8868
3.950	.7590	6.200	.3130	3.550	1.0204	6.800	.8865
4.000	.7513	6.250	.3068	3.600	1.0192	6.850	.8855
4.050	.7426	6.300	.2985	3.650	1.0176	6.900	.8846
4.100	.7330	6.350	.2910	3.700	1.0160	6.950	.8837
4.150	.7230	6.400	.2845	3.750	1.0144	7.000	.8823
4.200	.7133	6.450	.2780	3.800	1.0124	7.050	.8805
4.250	.7036	6.500	.2716	3.850	1.0100	7.100	.8785
4.300	.6924	6.550	.2655	3.900	1.0071	7.150	.8760
4.350	.6810	6.600	.2597	3.950	1.0037	7.200	.8734
4.400	.6692	6.650	.2545	4.000	1.0000	7.250	.8707
4.450	.6577	6.700	.2501	4.050	.9955	7.300	.8677
4.500	.6455	6.750	.2464	4.100	.9908	7.350	.8654
4.550	.6330	6.800	.2430	4.150	.9858	7.400	.8639
4.600	.6205	6.850	.2410	4.200	.9808	7.450	.8631
4.650	.6085	6.900	.2400	4.250	.9756	7.500	.8627
4.700	.5960	6.950	.2396	4.300	.9702	7.550	.8623
		7.000	.2394	4.350	.9659	7.600	.8621
		Cylinder		4.400	.9595	Cylinder	
		7.8858	0.2394	4.450	.9538		
				4.500	.9481	7.8858	0.8621
				4.550	.9426		

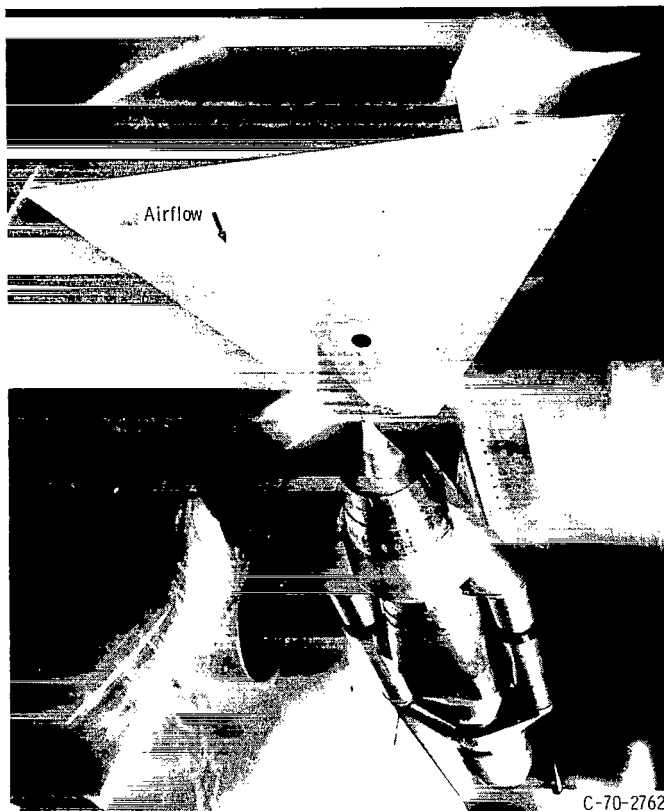
TABLE II. - COWL AND CENTERBODY STATIC-  
PRESSURE TAP LOCATIONS

[Top centerline.]

(a) Cowl		(b) Centerbody	
Axial distance from center- body tip, $x/R_c$			
2.684	3.380	2.308	3.389
2.807	3.434	2.670	3.441
2.859	3.489	2.751	3.489
2.894	3.564	2.802	3.543
2.930	3.639	2.834	3.586
2.964	3.714	2.858	3.629
2.999	3.950	2.893	3.671
3.038	4.192	2.963	3.714
3.066	4.519	3.030	3.795
3.101	4.847	3.102	3.875
3.136	5.202	3.140	3.951
3.170	5.529	3.173	4.192
3.205	6.119	3.210	4.519
3.240	6.742	3.247	4.847
3.275	7.311	3.285	5.202
3.310			7.311
3.345		3.317	
		3.353	

TABLE III. - DYNAMIC INSTRUMENTATION LOCATIONS

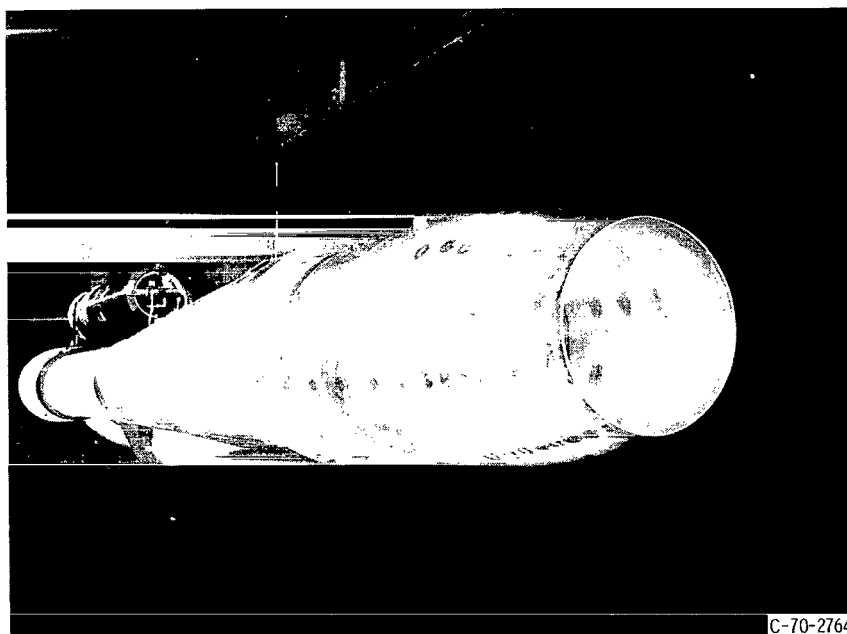
Probe no.	Description	Reference figure	Comments
D1	Cowl static pressure	12	Inlet dynamics
D2	↓	↓	↓
D3			
D4			
D5			
D6	↓	10	
D7	Stability-bypass-plenum total pressure	12	
D8	Compressor-face static pressure	9	
D9	Compressor-face total pressure	9	
D10	Compressor-exit total pressure	11	Used to obtain compressor pressure ratio
S1	Cowl static pressure	12	(Inlet unstart sensor pickups)
S2	Inlet throat total pressure	12	
S3	Terminal shock position sensor	12	Analog computer



(a) Bottom view from an upstream location.

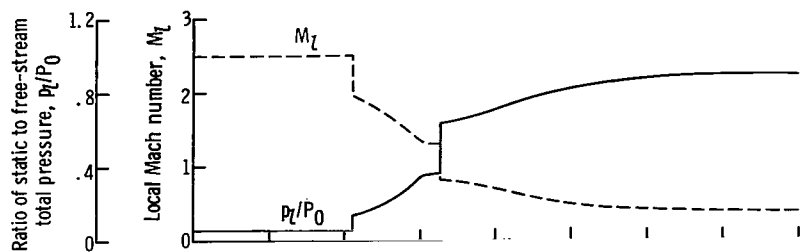


(b) Bottom view from a downstream location.

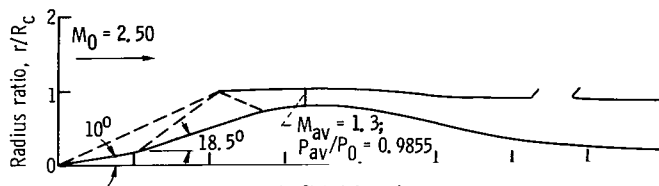


(c) Rear view.

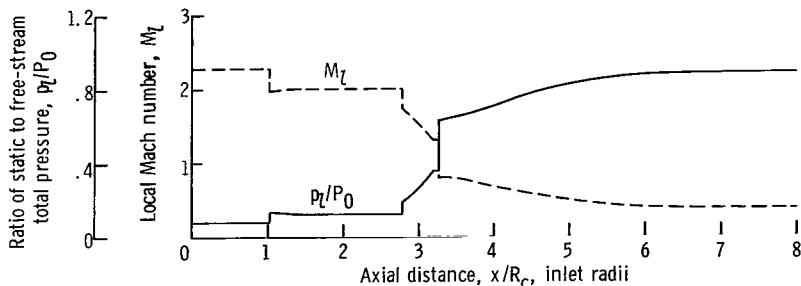
Figure 1. - Model installed in Lewis 10- by 10-Foot Supersonic Wind Tunnel.



(a-1) Cowl surface conditions.

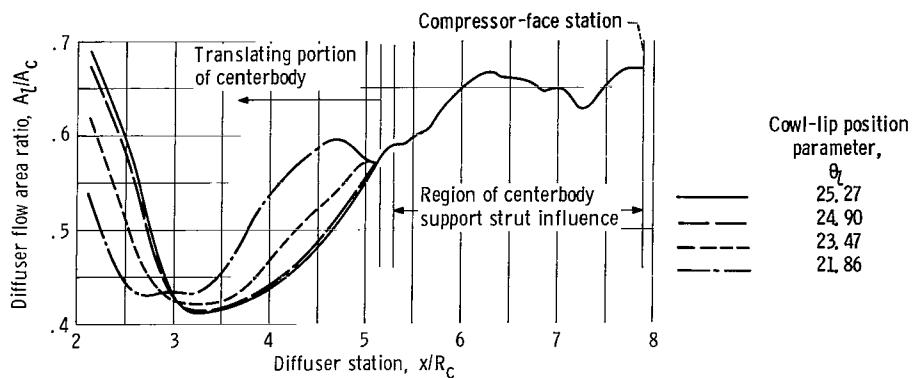


(a-2) Inlet contours.



(a-3) Centerbody surface conditions.

(a) Inlet dimensions and airflow conditions. Free-stream Mach number,  $M_0 = 2.5$ .



(b) Diffuser area variation.

Figure 2. - Aerodynamic details. Cowl-lip position parameter,  $\theta_L = 25.27^\circ$ .

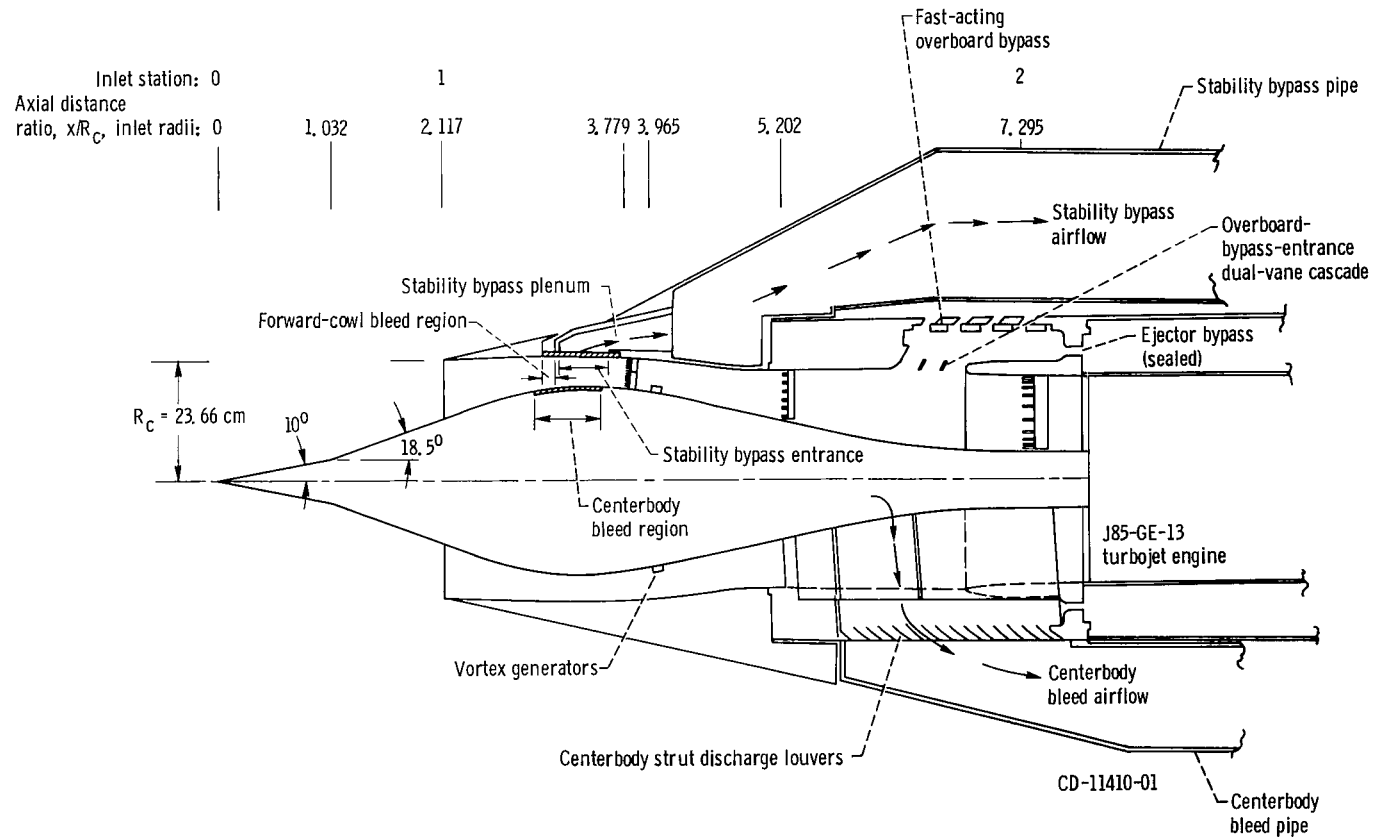


Figure 3. - Inlet details. (Pipes for ducting bleed airflow are not shown in true circumferential positions.)

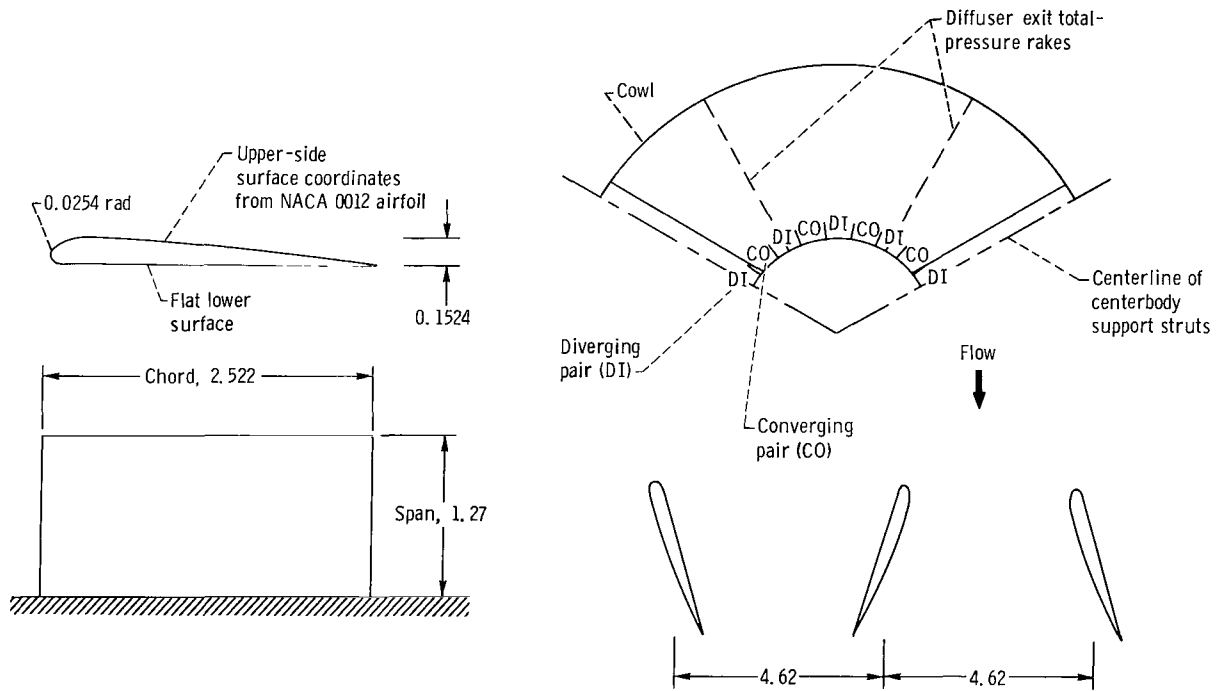
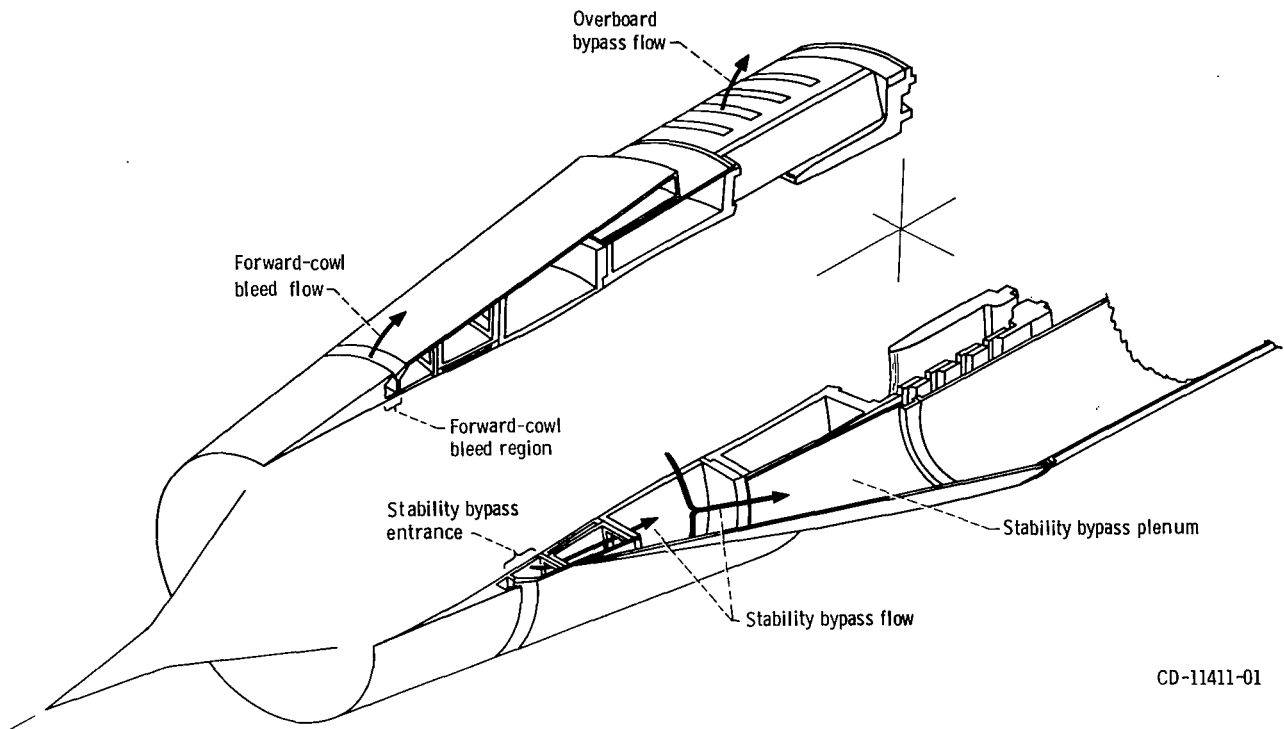
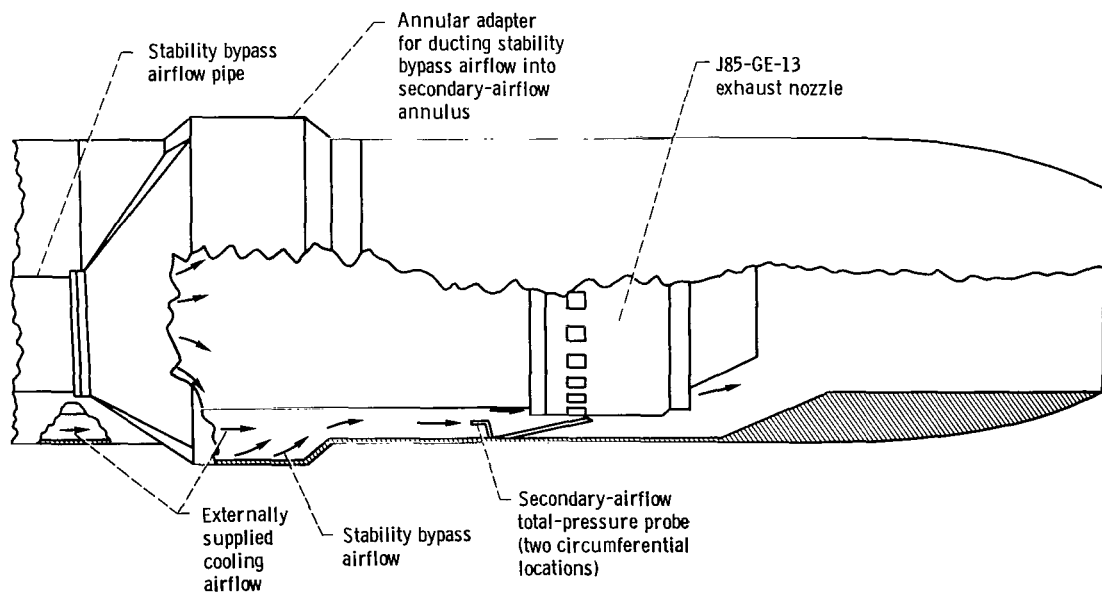


Figure 4 - Vortex generator design. (Dimensions are in cm.)



CD-11411-01

(a) Sketch of inlet cowl showing cowl bleed and bypass ducting.



(b) Sketch of exhaust nozzle showing ducting of airflow.

Figure 5. - Inlet and nozzle airflow ducting.

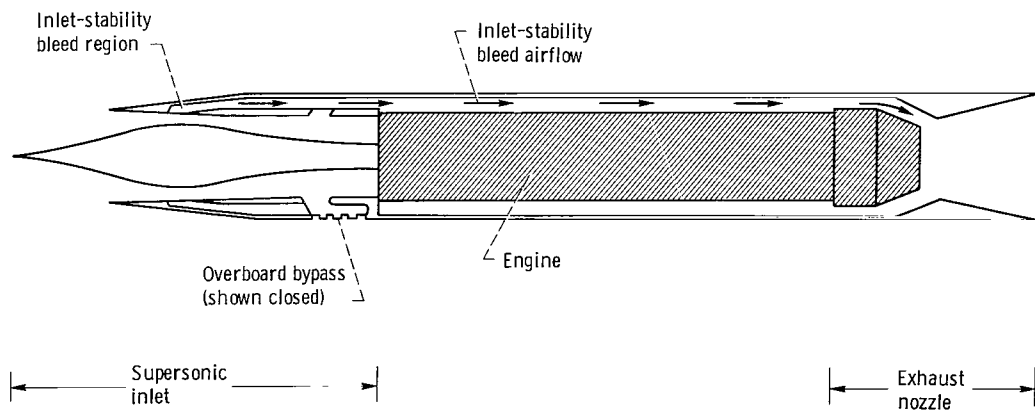
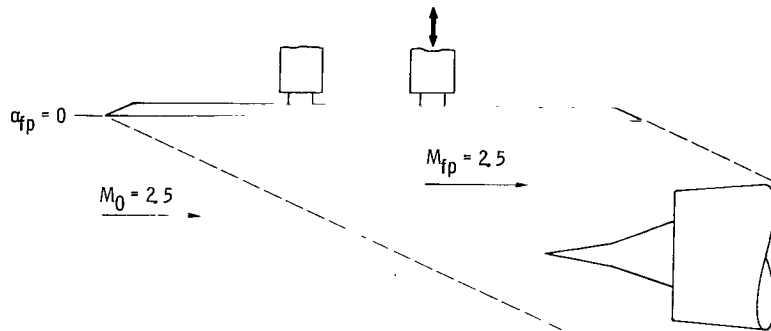
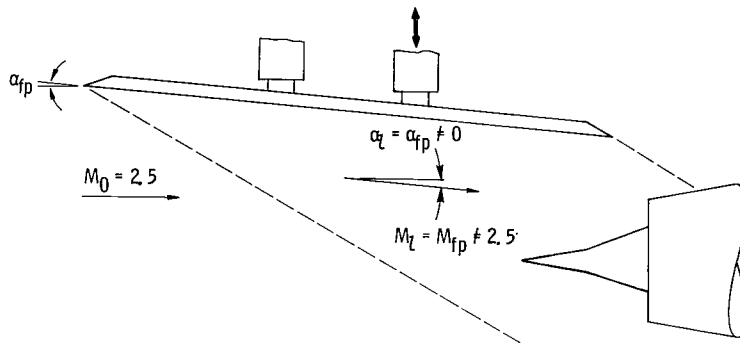


Figure 6. - Possible arrangement of flight inlet incorporating a supersonic-exhaust-nozzle-controlled inlet-stability bypass system.





(a) Inlet operating at uniform design conditions: Free-stream Mach number,  $M_0$ , 2.5; angle of attack,  $\alpha$ ,  $0^\circ$ .



(b) Inlet operating at off-design conditions: Local Mach number,  $M_l \neq 2.5$ ; local angle of attack,  $\alpha_l \neq 0$ .

Figure 8. - Typical installation of Mach 2.5 inlet with flat plate, where local inlet Mach number is function of flat-plate angle.

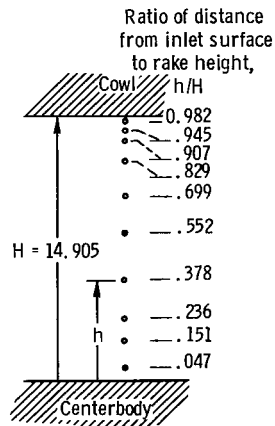
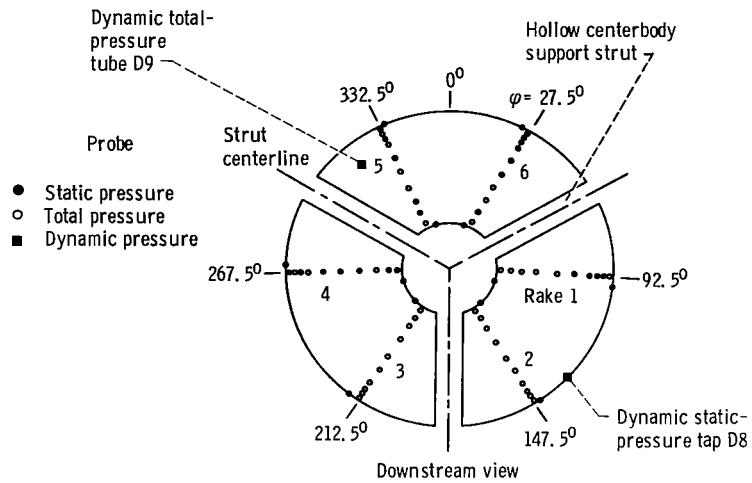


Figure 9. - Subsonic diffuser pressure instrumentation, showing typical exit rake and rake position at inlet station 2.

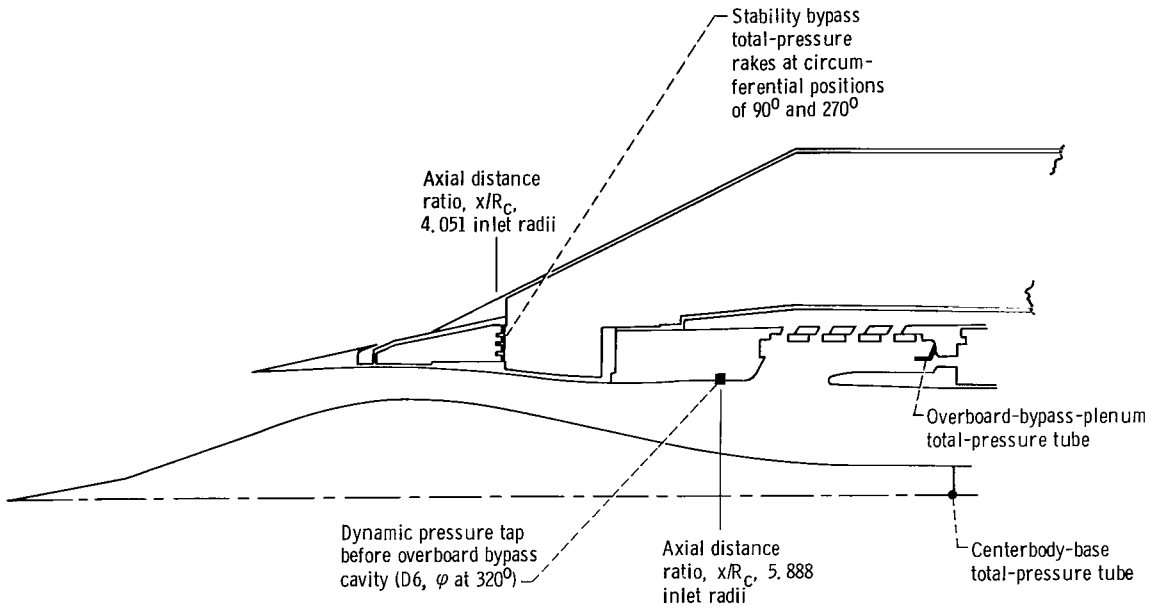


Figure 10. - Bleed and bypass pressure instrumentation.

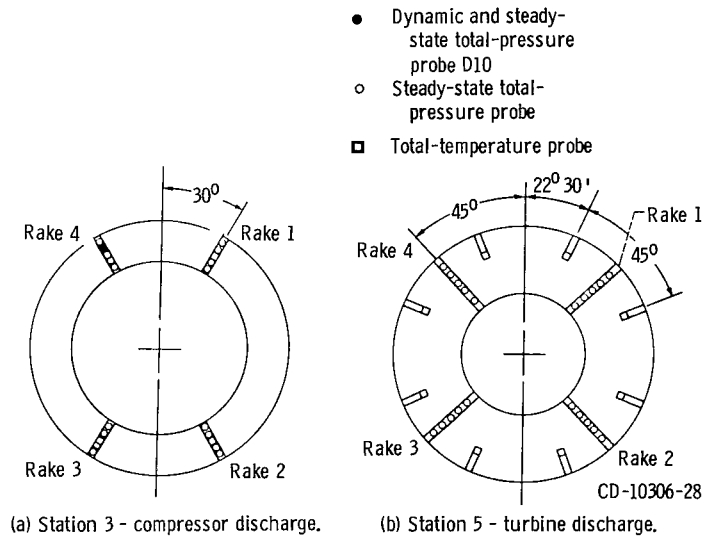


Figure 11. - J85-GE-13 engine instrumentation (downstream view).

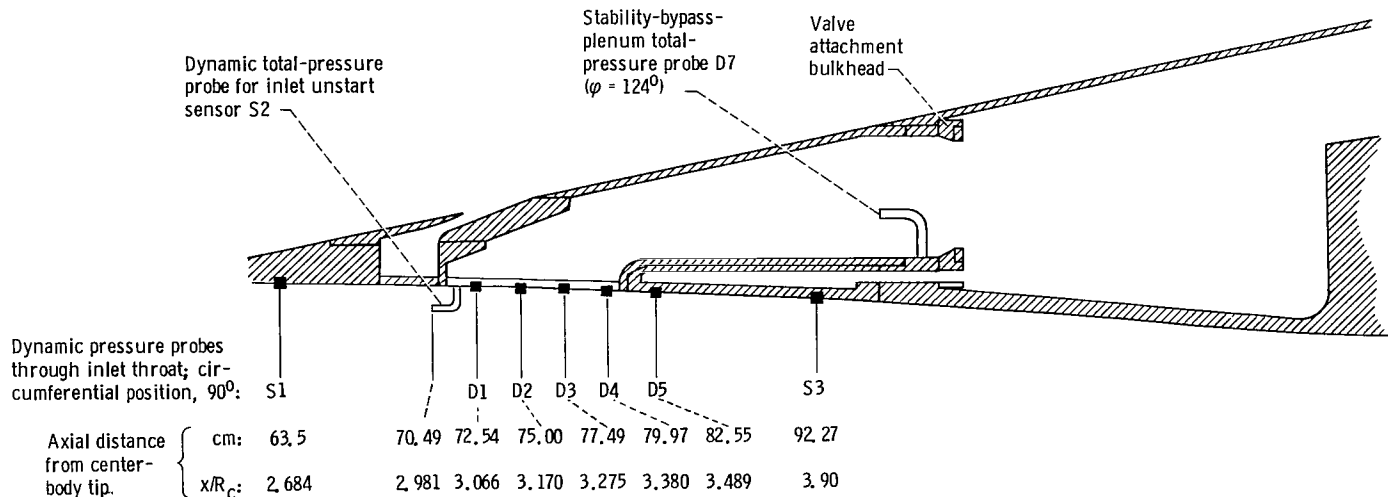


Figure 12. - Inlet-throat-region dynamic pressure instrumentation.

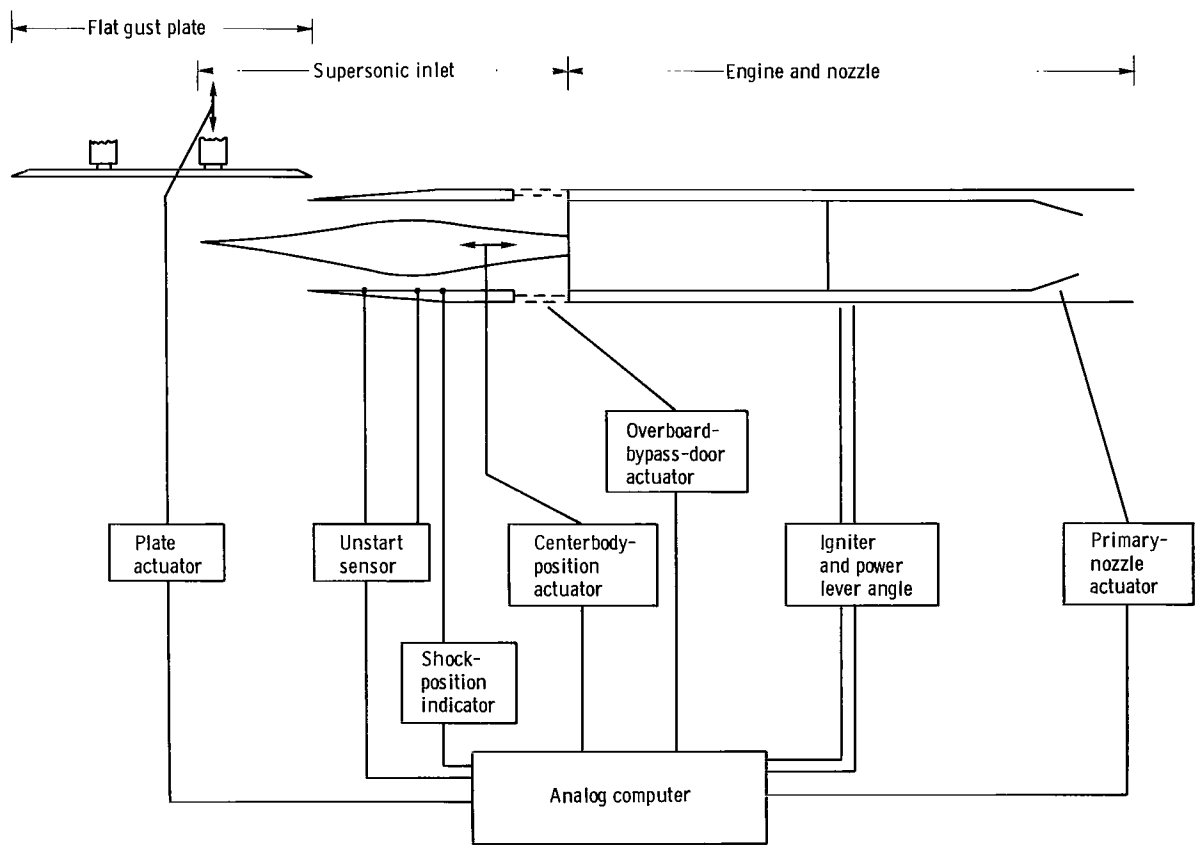


Figure 13. - Block diagram of propulsion system control.

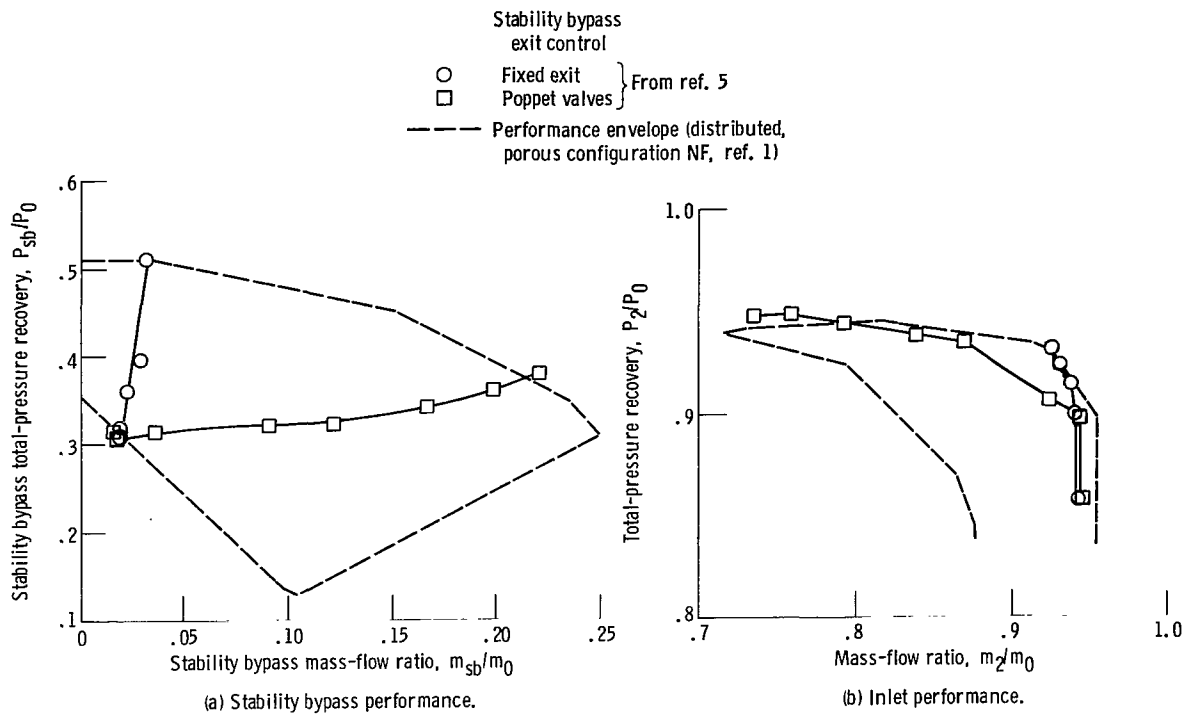


Figure 14. - Steady-state performance of inlet configuration as determined from previous coldpipe studies with fixed and poppet-valve stability bypass exit controls. Free-stream Mach number,  $M_0$  2.5.

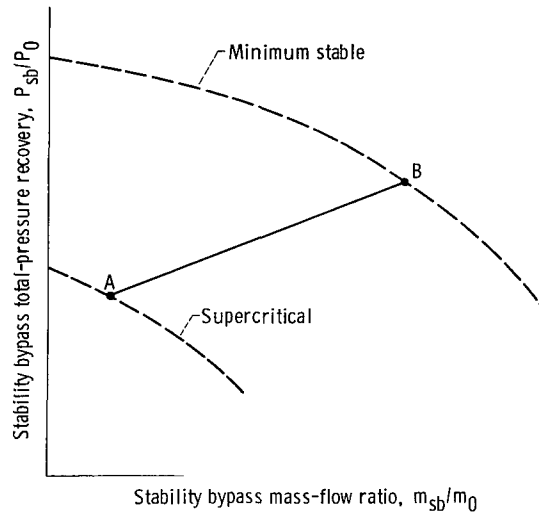
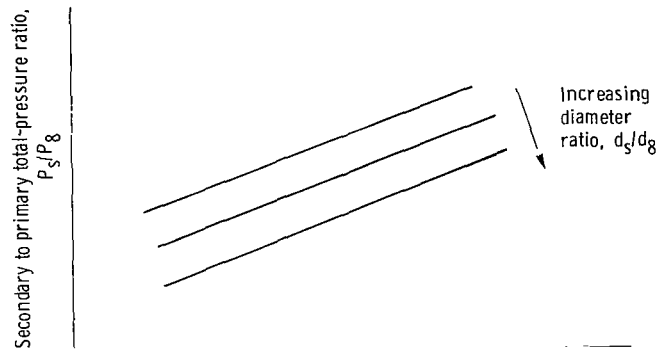
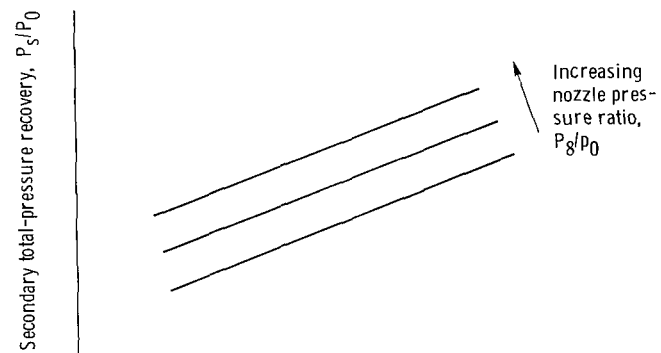


Figure 15. - Exhaust-nozzle secondary-airflow pumping as exit control for stability bypass airflow of supersonic inlet.



(a) Effect of change in ratio of nozzle secondary to primary diameters.



Corrected secondary weight flow ratio,  $W_s\sqrt{T_s}/W_8\sqrt{T_8}$

(b) Effect of change in nozzle pressure ratio for constant primary-nozzle area.

Figure 16. - Exhaust nozzle pumping.

	Corrected engine speed, $N/N^* \sqrt{\theta}$	Ratio of secondary to primary nozzle diameter, $d_s/d_g$	Nozzle pressure ratio, $P_g/P_0$	Ratio of overboard bypass area to inlet area, $A_{by}/A_i$
○	0.873	1.487	19.24	0.0274
□	.854	1.484	18.01	.0309
◇	.827	1.483	16.31	.0309
△	.792	1.483	14.26	.0309
▵	.789	1.483	14.25	0
▹	.762	1.535	13.27	.0179

Data from ref. 16, ejector 1, at diameter ratio  $d_s/d_g$  of -

- 1.17
- - - 1.22
- 1.42

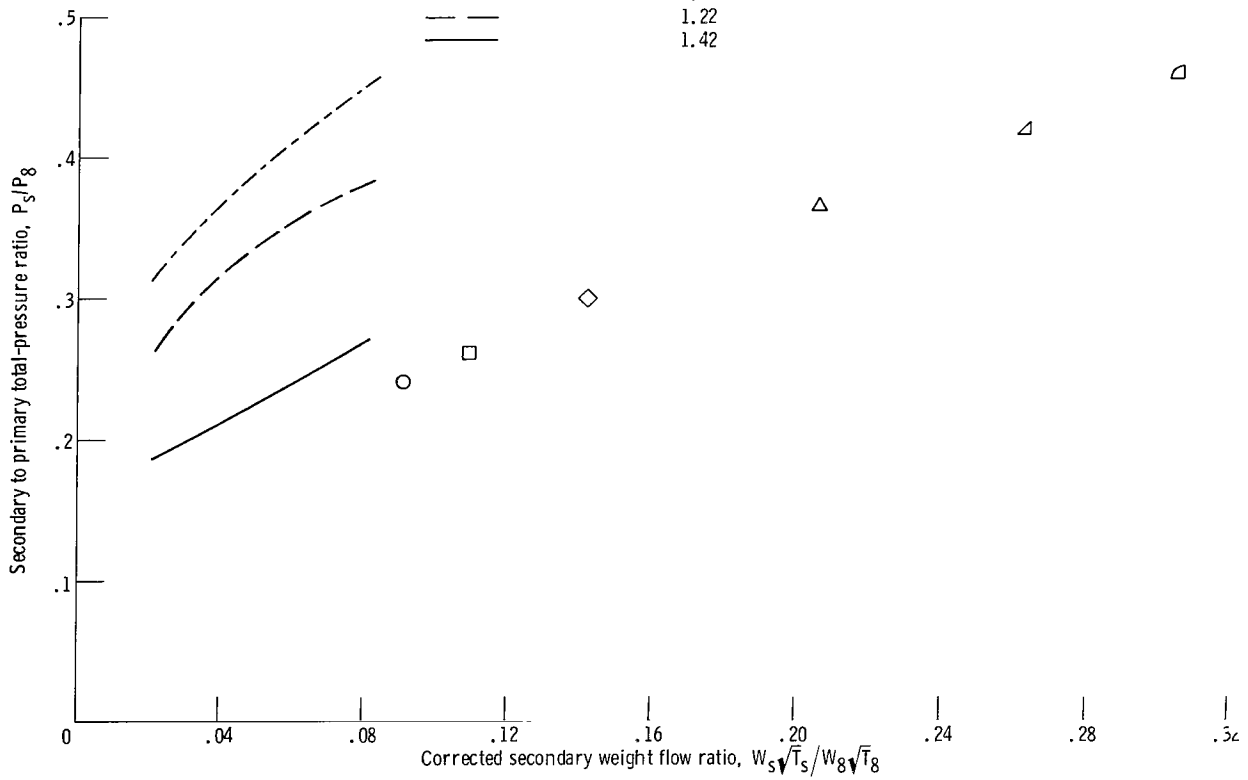


Figure 17. - Comparison of exhaust-nozzle pumping characteristics from wind tunnel and static tests. Free-stream Mach number,  $M_0 = 2.5$ .

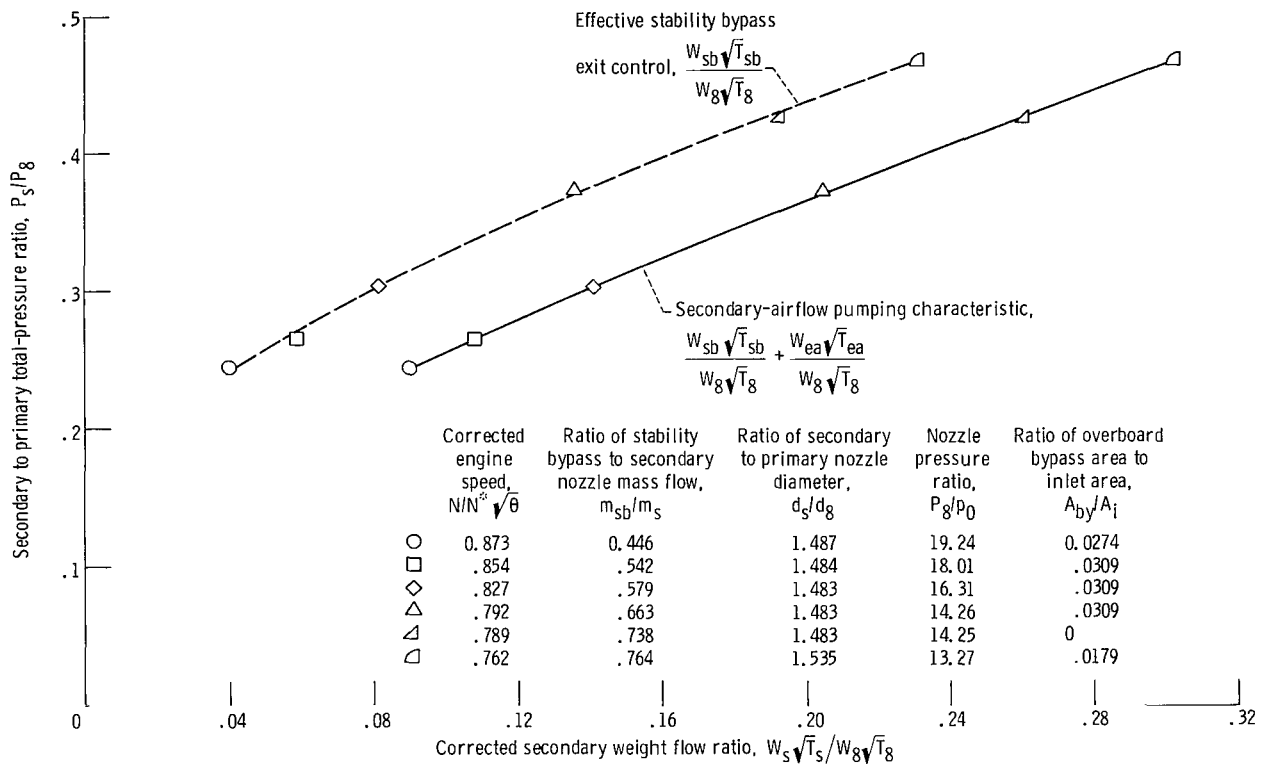


Figure 18. - Exhaust-nozzle pumping characteristics and effective exhaust-nozzle pumping control of inlet-stability bypass airflow. Free-stream Mach number,  $M_0$ , 2.5.

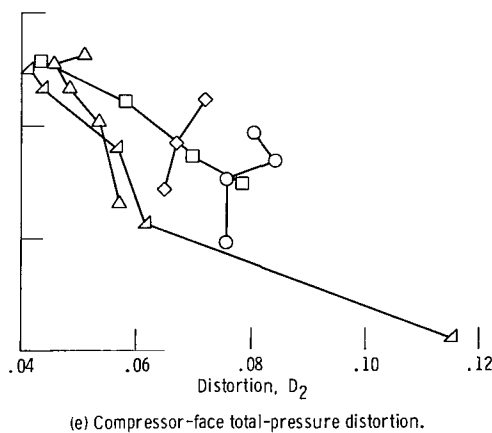
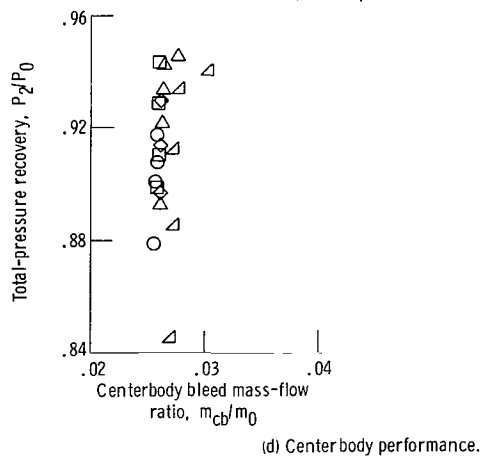
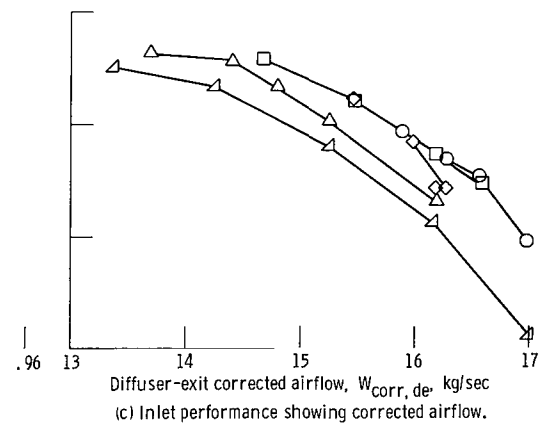
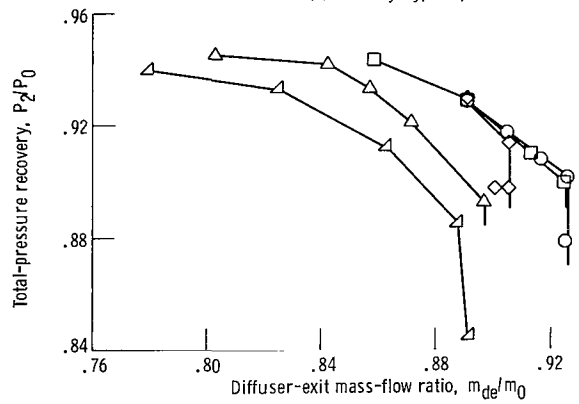
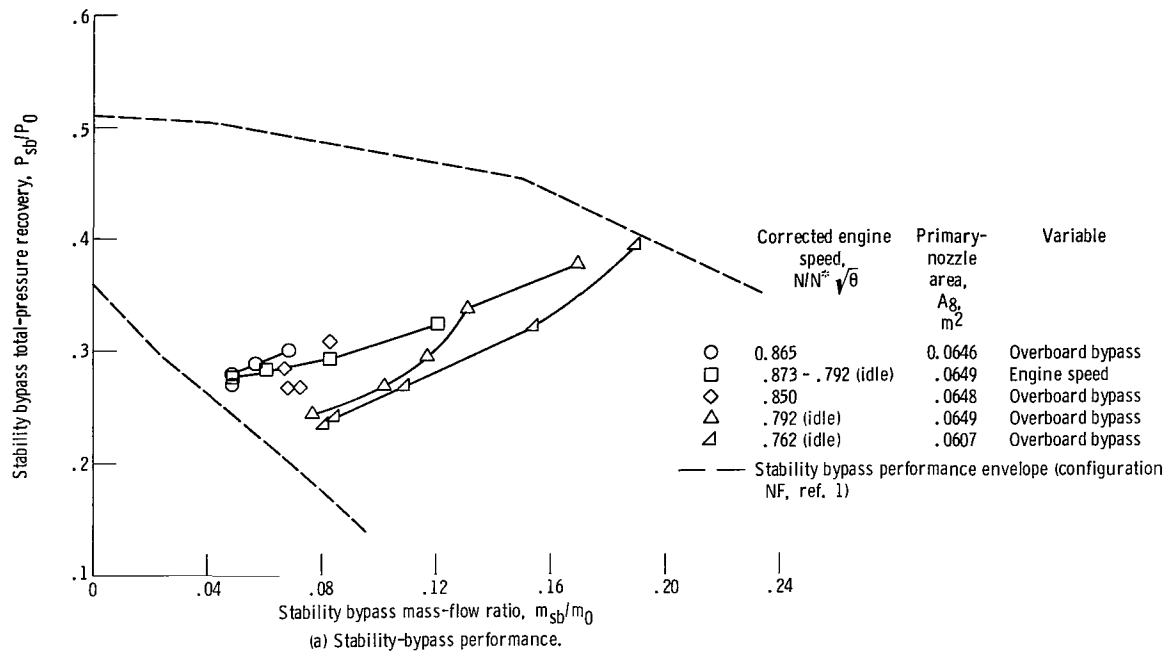


Figure 19. - Steady-state performance of inlet configuration when using exhaust-nozzle pumping as inlet-stability bypass exit control. Free-stream Mach number,  $M_0$ , 2.5.

	Corrected engine speed, $N/N^* \sqrt{\theta}$	Total-pressure recovery, $P_2/P_0$	Stability-bypass total-pressure recovery, $P_{sb}/P_0$	Stability bypass mass-flow ratio, $m_{sb}/m_0$
—□—	0.873	0.899	0.278	0.048
- - □ - -	.854	.909	.283	.061
- · □ - ·	.827	.928	.292	.083
- · · □ - · ·	.792	.943	.323	.121

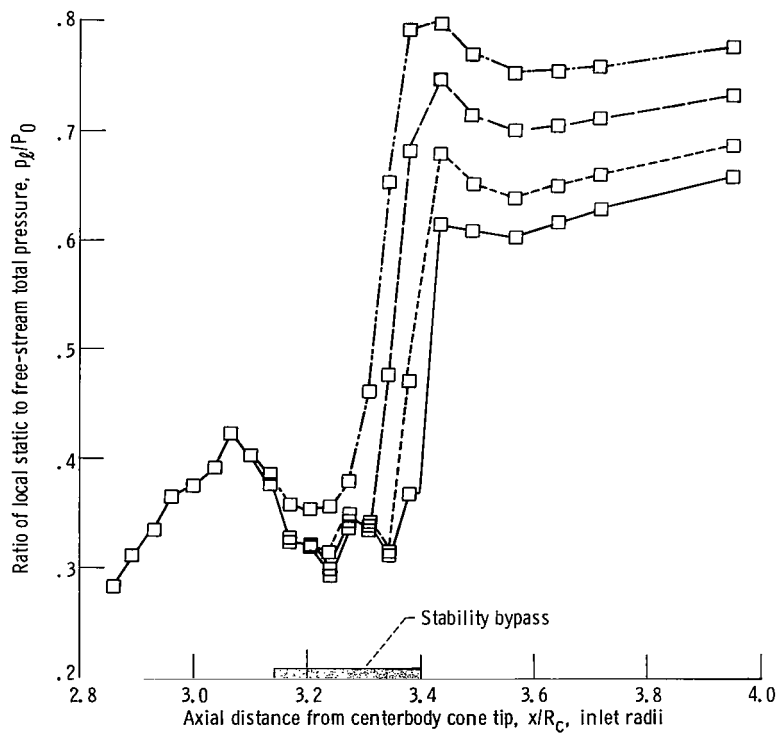


Figure 20. - Cowl surface static-pressure distributions with inlet started for variation in engine speed from match to idle. Free-stream Mach number,  $M_0$ , 2.5.

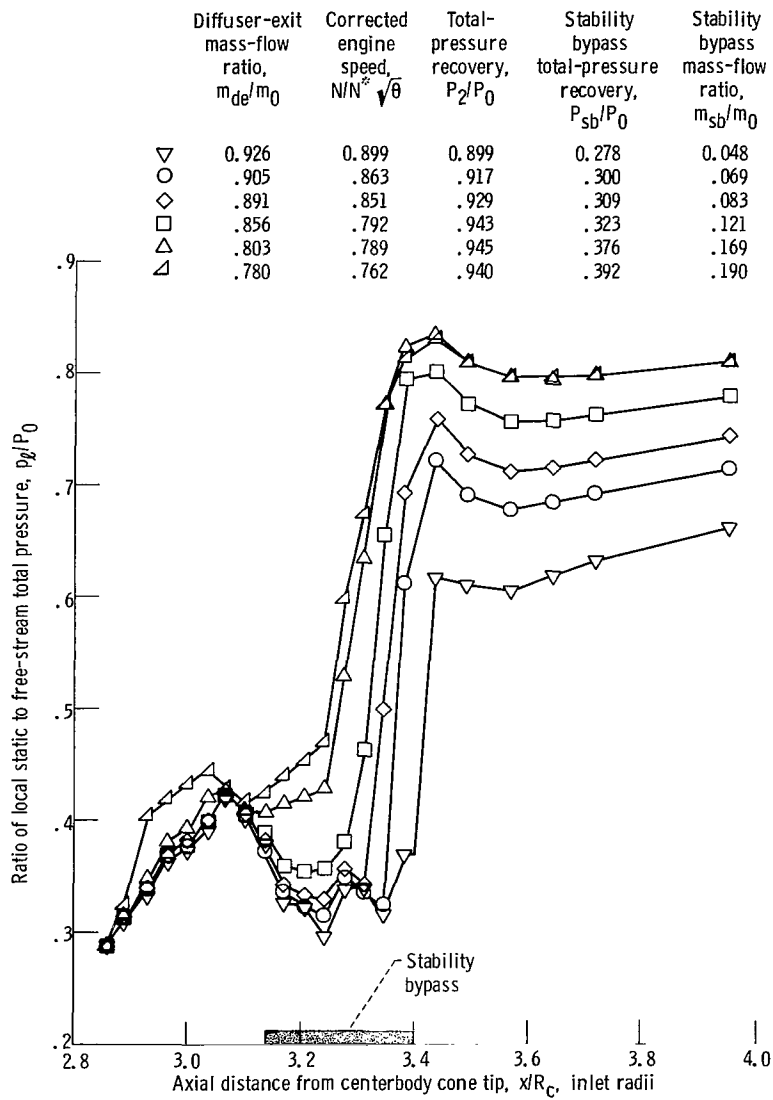


Figure 21. - Cowl surface static-pressure distributions with inlet started for variation in diffuser airflow from critical to minimum stable conditions. Free-stream Mach number,  $M_0$ , 2.5.

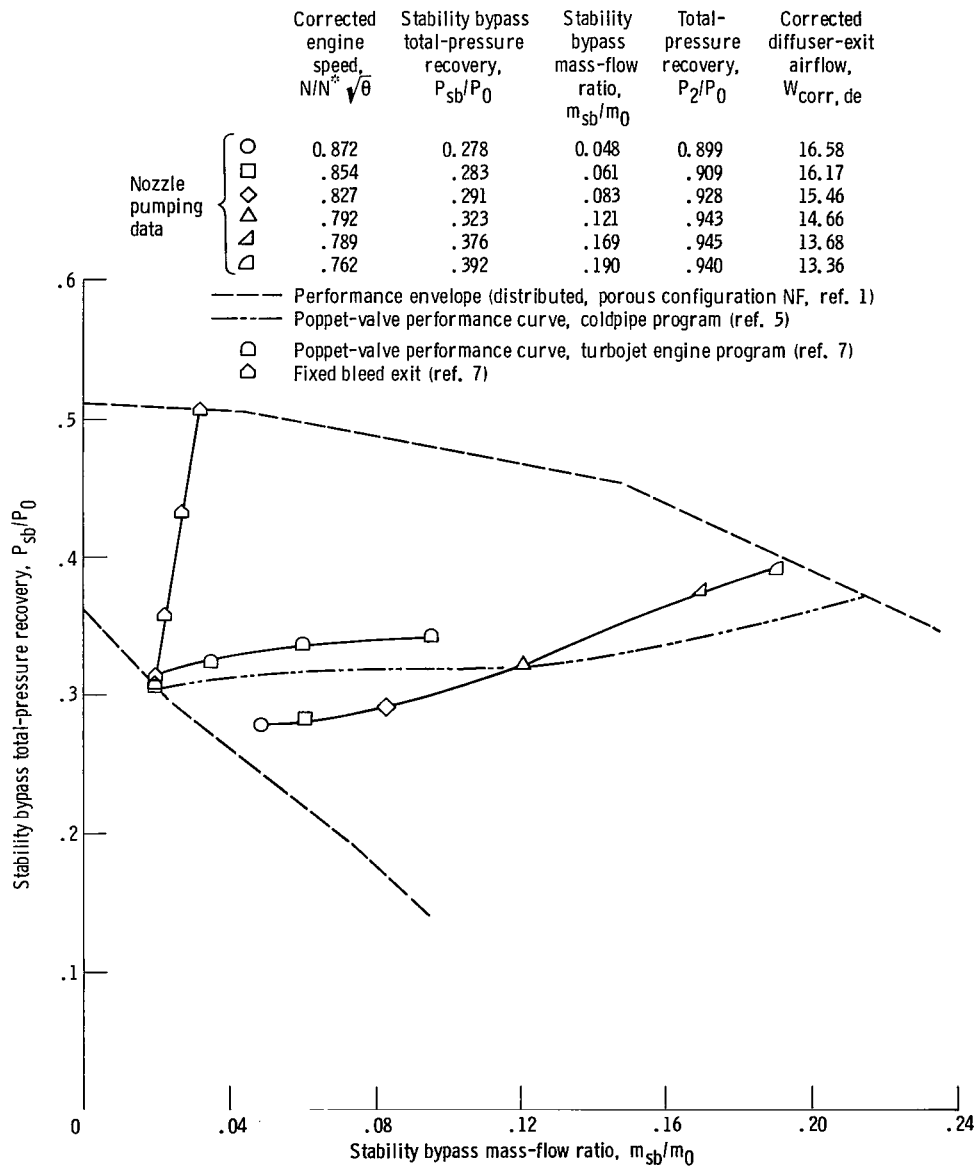
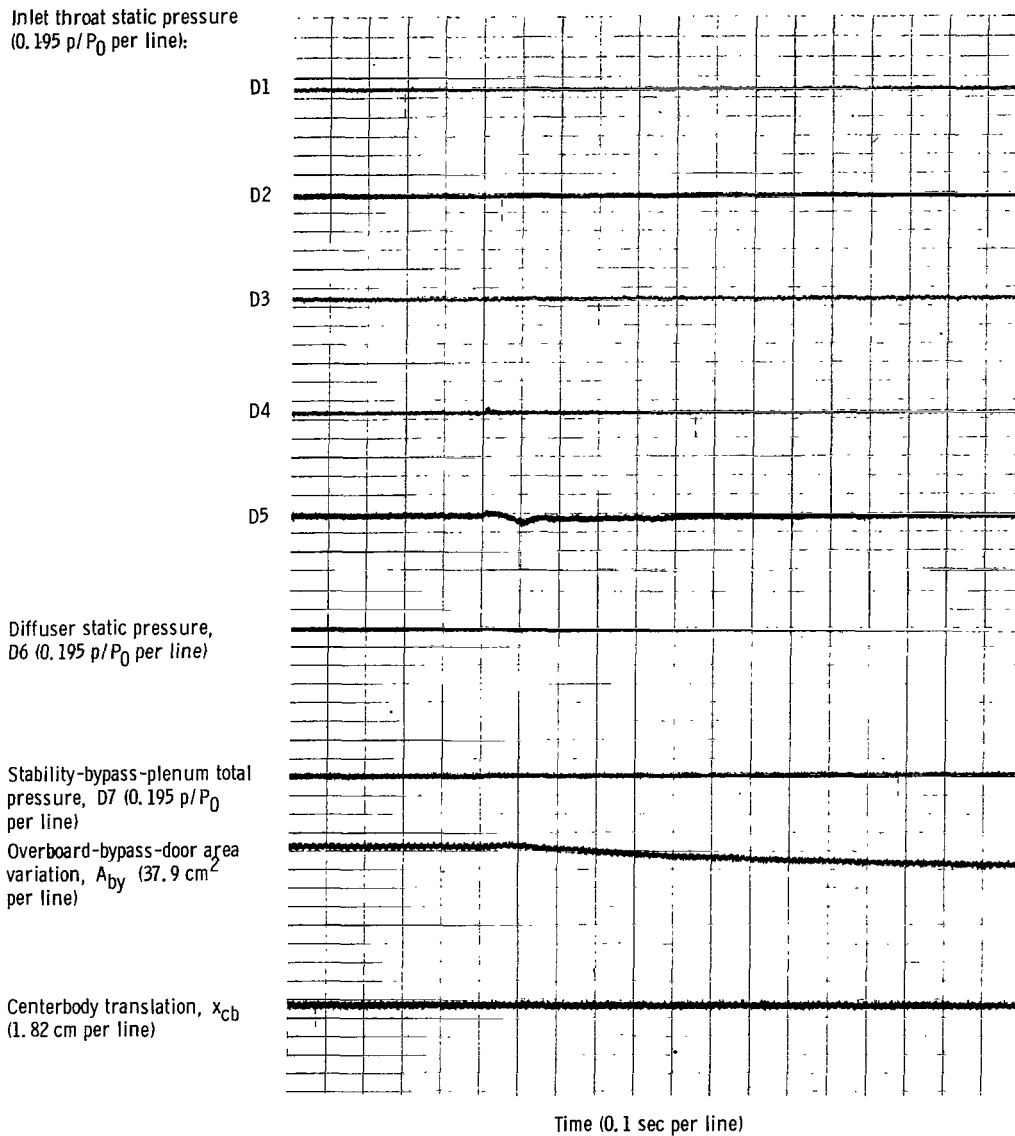
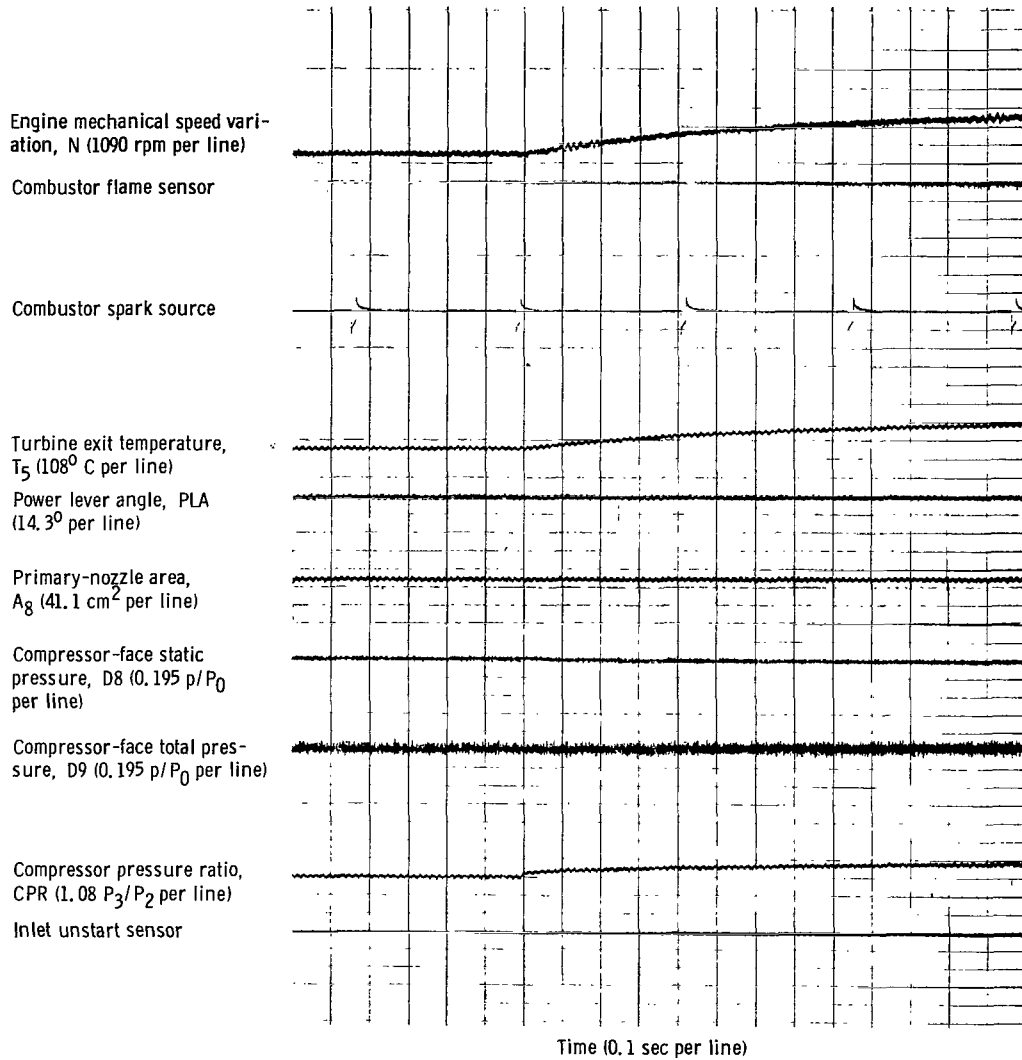


Figure 22. - Comparison of exhaust-nozzle secondary-airflow pumping, poppet-valve, and fixed-exit stability bypass exit controls. Free-stream Mach number,  $M_0$ , 2.5.



(a) Inlet response.

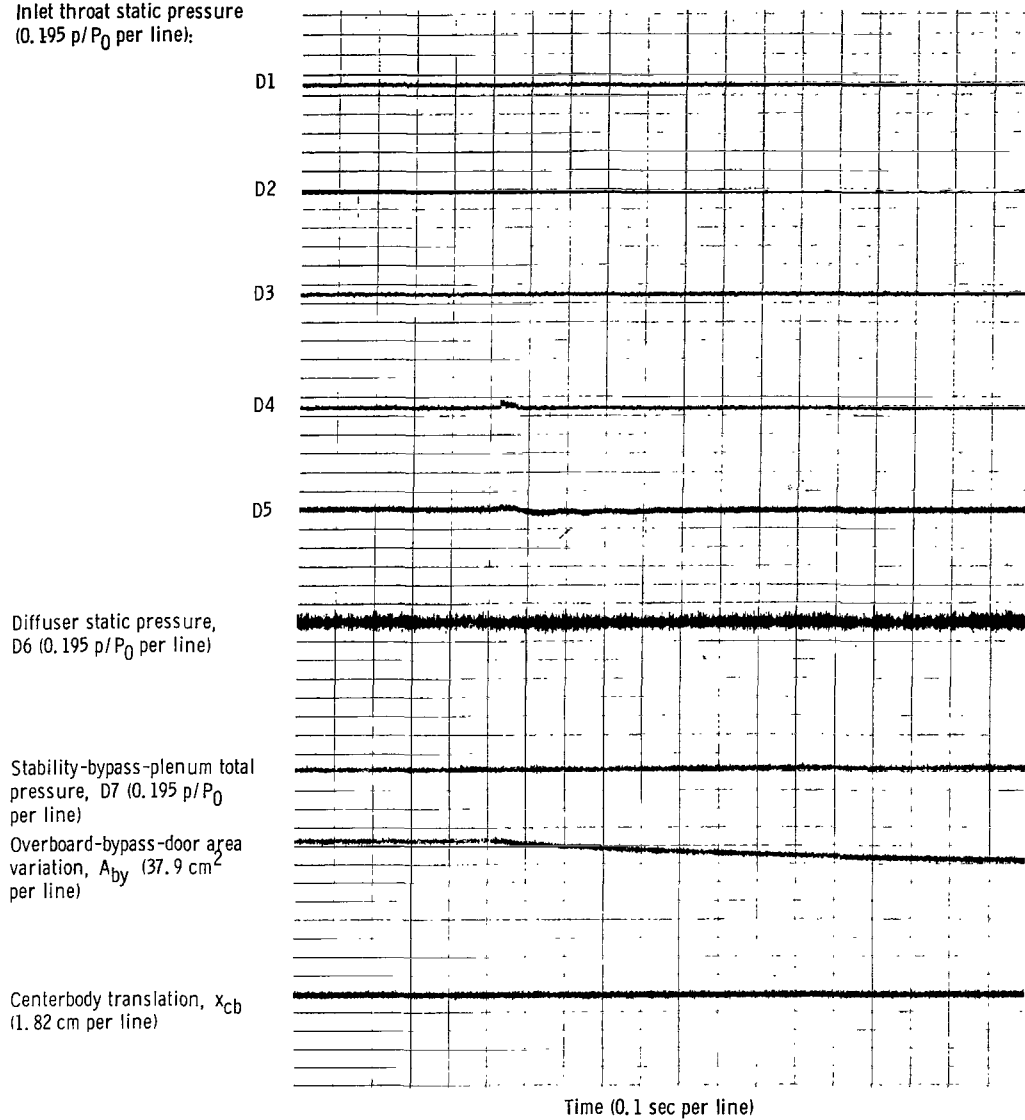
Figure 23. - Started-inlet response to engine light. Free-stream Mach number,  $M_0$ , 2.5; corrected engine speed,  $N/N^* \sqrt{\theta}$ , 0.628; total-pressure recovery,  $P_2/P_0$ , 0.877; stability bypass total-pressure recovery,  $P_{sb}/P_0$ , 0.207; primary nozzle area,  $A_8$ , 0.064 square meter.



(b) Engine response.

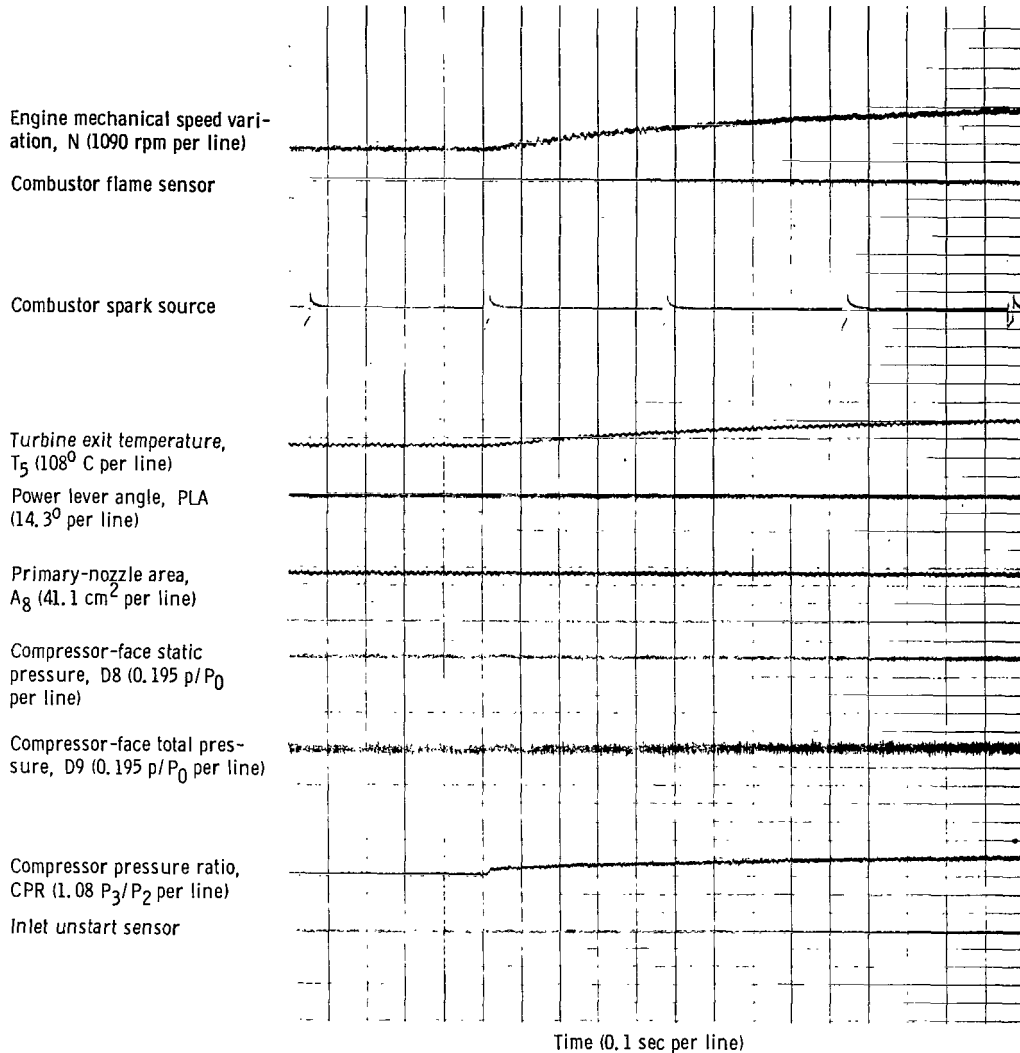
Figure 23. - Concluded.

Inlet throat static pressure  
(0.195 p/P<sub>0</sub> per line):



(a) Inlet response.

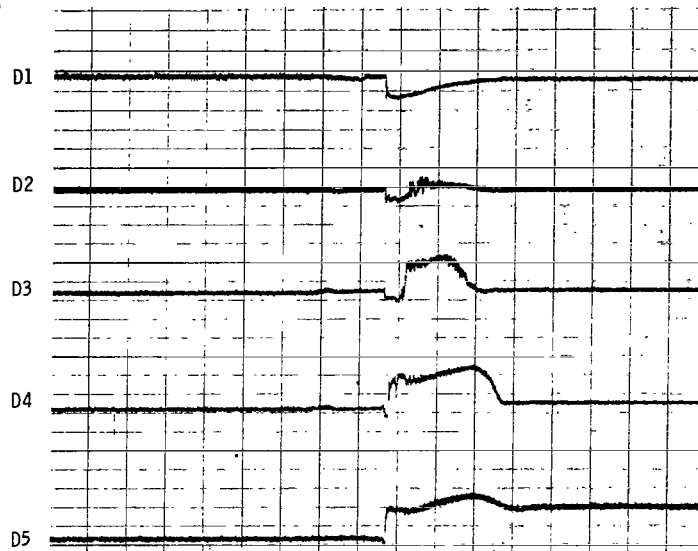
Figure 24. - Unstarted-inlet response to engine light. Free-stream Mach number,  $M_0$ , 2.5; corrected engine speed,  $N/N^* \sqrt{\theta}$ , 0.627; total-pressure recovery,  $P_2/P_0$ , 0.761; stability bypass total-pressure recovery,  $P_{sb}/P_0$ , 0.186; primary-nozzle area,  $A_8$ , 0.0648 square meter.



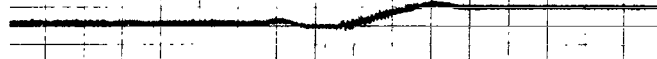
(b) Engine response.

Figure 24. - Concluded.

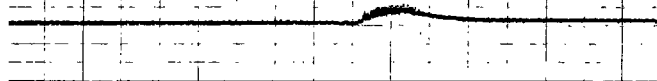
Inlet throat static pressure  
(0.195 p/P<sub>0</sub> per line):



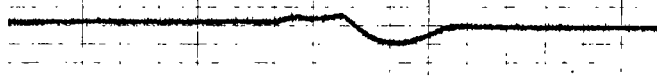
Diffuser static pressure,  
D6 (0.195 p/P<sub>0</sub> per line)



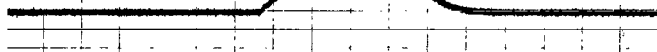
Stability-bypass-plenum total  
pressure, D7 (0.195 p/P<sub>0</sub>  
per line)



Overboard-bypass-door area  
variation, A<sub>by</sub> (37.9 cm<sup>2</sup>  
per line)



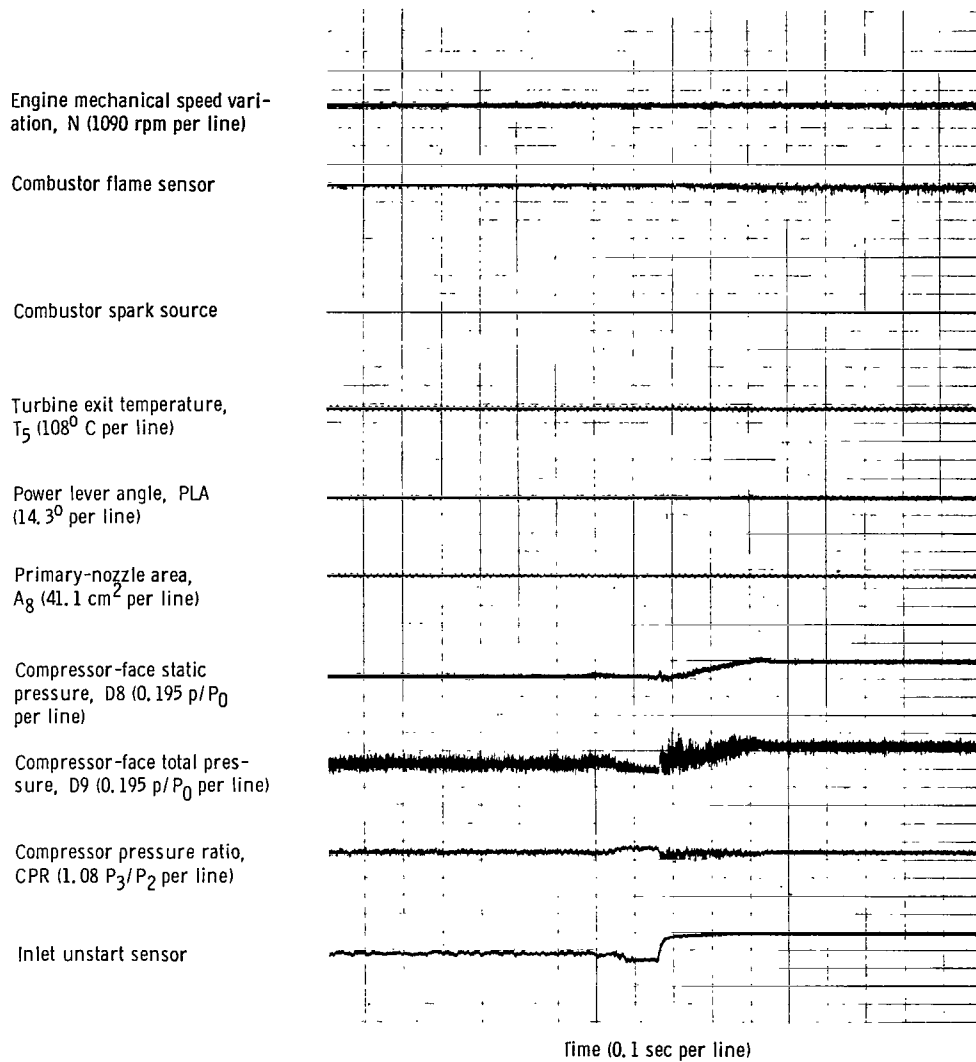
Centerbody translation, x<sub>cb</sub>  
(1.82 cm per line)



Time (0.1 sec per line)

(a) Inlet response.

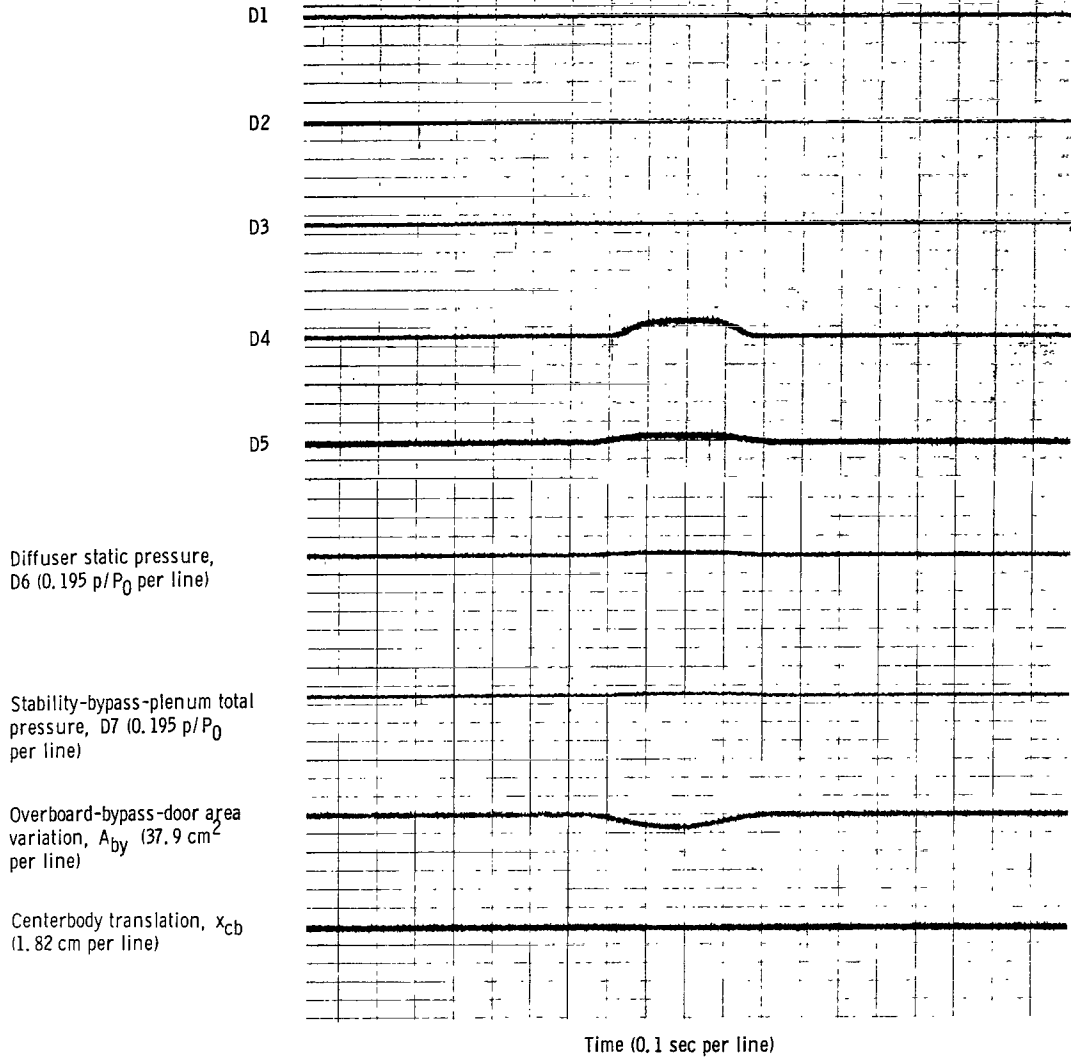
Figure 25. - Inlet restart with engine running. Free-stream Mach number, M<sub>0</sub> 2.5.



(b) Engine response.

Figure 25. - Concluded.

Inlet throat static pressure  
(0.195 p/P<sub>0</sub> per line):



(a) Inlet response.

Figure 26. - Transient reduction in overboard bypass area. Free-stream Mach number,  $M_0$ , 2.5; transient overboard bypass area,  $A_{by}$ , 30.3 square centimeters; transient pulse frequency,  $1/\tau$ , 2 seconds<sup>-1</sup>; corrected engine speed,  $N/N^*$ , 1.0; total-pressure recovery,  $P_2/P_0$ , 0.899; mass-flow ratio,  $m_2/m_0$ , 0.877; stability bypass total-pressure recovery,  $P_{sb}/P_0$ , 0.278; primary-nozzle area,  $A_8$ , 0.0647 square meter.

Engine mechanical speed variation,  $N$  (1090 rpm per line)

Combustor flame sensor

Combustor spark source

Turbine exit temperature,  $T_5$  ( $108^\circ$  C per line)

Power lever angle, PLA ( $14.3^\circ$  per line)

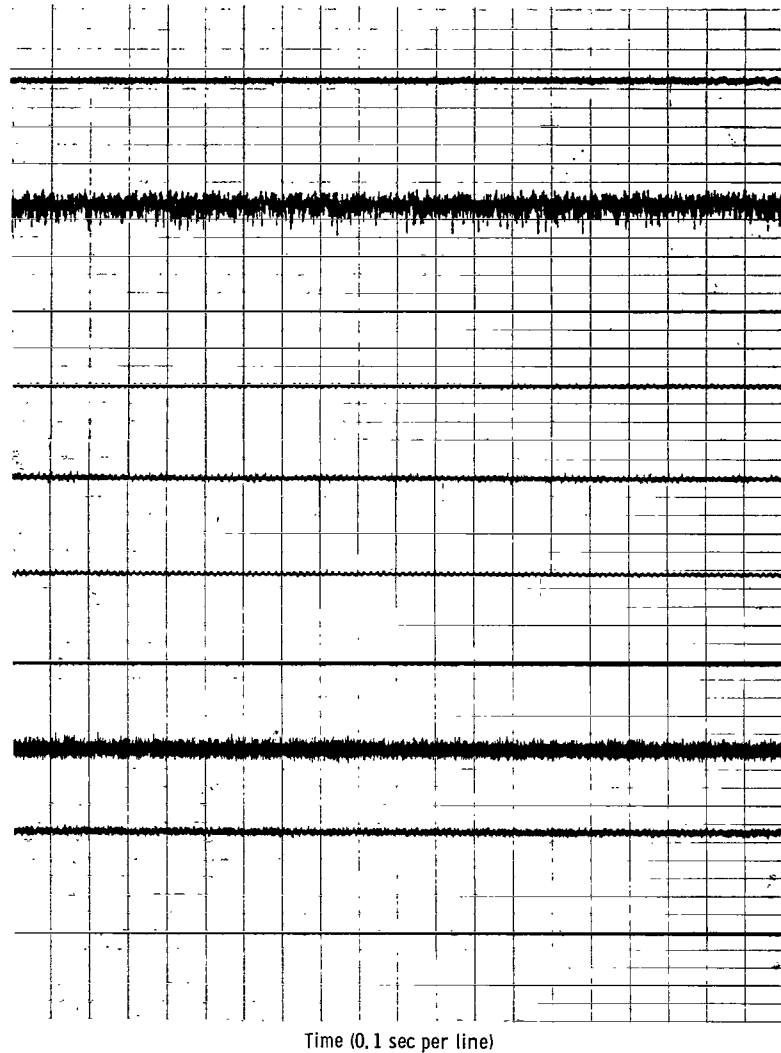
Primary-nozzle area,  $A_8$  ( $41.1 \text{ cm}^2$  per line)

Compressor-face static pressure,  $D_8$  ( $0.195 p/P_0$  per line)

Compressor-face total pressure,  $D_9$  ( $0.195 p/P_0$  per line)

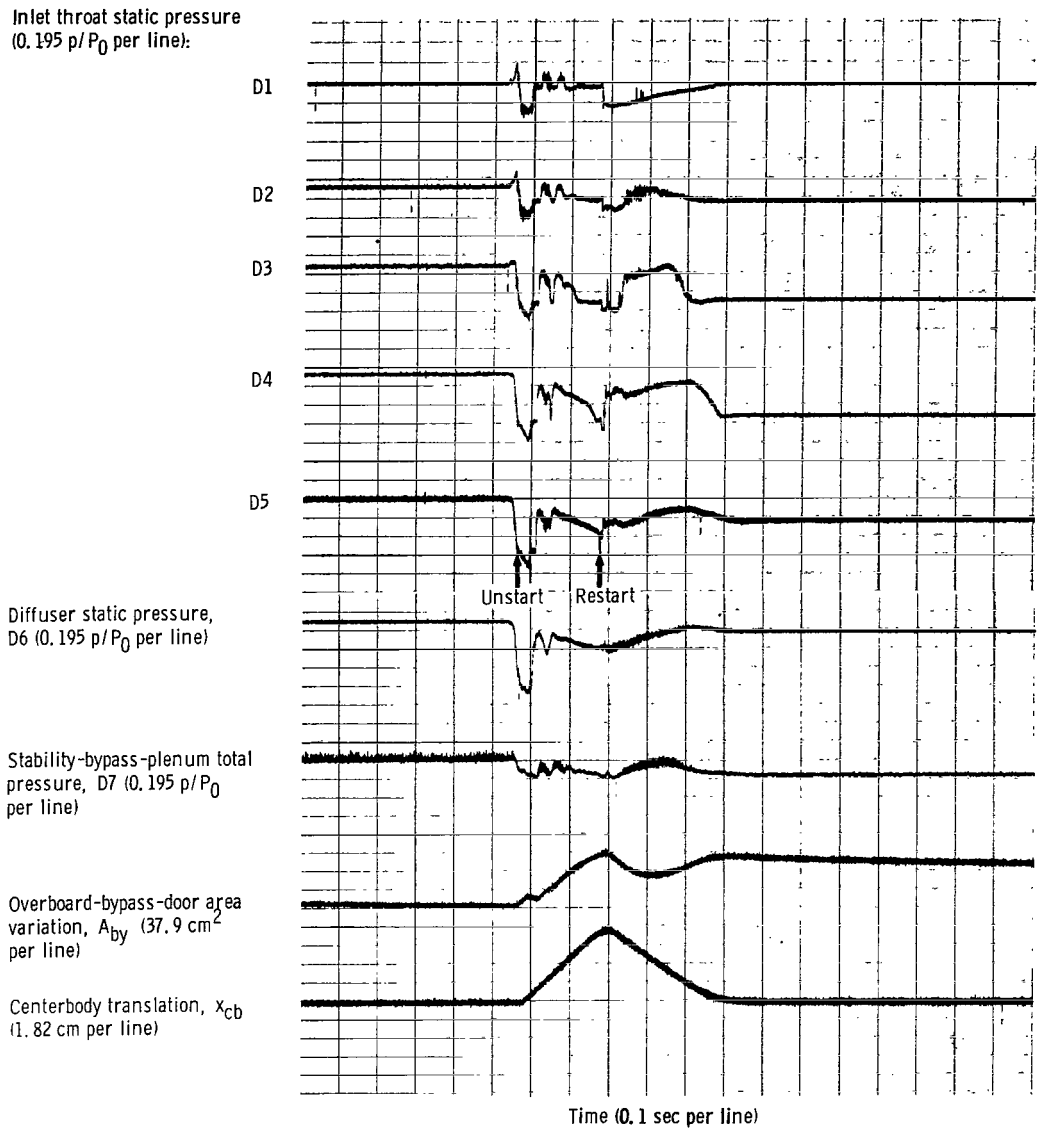
Compressor pressure ratio, CPR ( $1.08 P_3/P_2$  per line)

Inlet unstart sensor



(b) Engine response.

Figure 26. - Concluded.



(a) Inlet response.

Figure 27. - Slow, manual reduction in overboard bypass area from inlet minimum stable condition to inlet unstart. Free-stream Mach number,  $M_0$ , 2.5; corrected engine speed,  $N/N^* \sqrt{\theta}$ , 0.762 (idle); overboard bypass mass-flow ratio,  $m_{by}/m_0$ , 0.037; total-pressure recovery,  $P_2/P_0$ , 0.9399; mass-flow ratio,  $m_p/m_0$ , 0.743; diffuser-exit mass flow ratio,  $m_{de}/m_0$ , 0.780; nozzle pressure ratio,  $P_8/P_0$ , 13.273; stability bypass total-pressure recovery,  $P_{sb}/P_0$ , 0.392; primary-nozzle area,  $A_8$ , 0.0607 square meter.

Engine mechanical speed variation, N (1090 rpm per line)

Combustor flame sensor

Combustor spark source

Turbine exit temperature,  $T_5$  ( $108^\circ\text{C}$  per line)

Power lever angle, PLA ( $14.3^\circ$  per line)

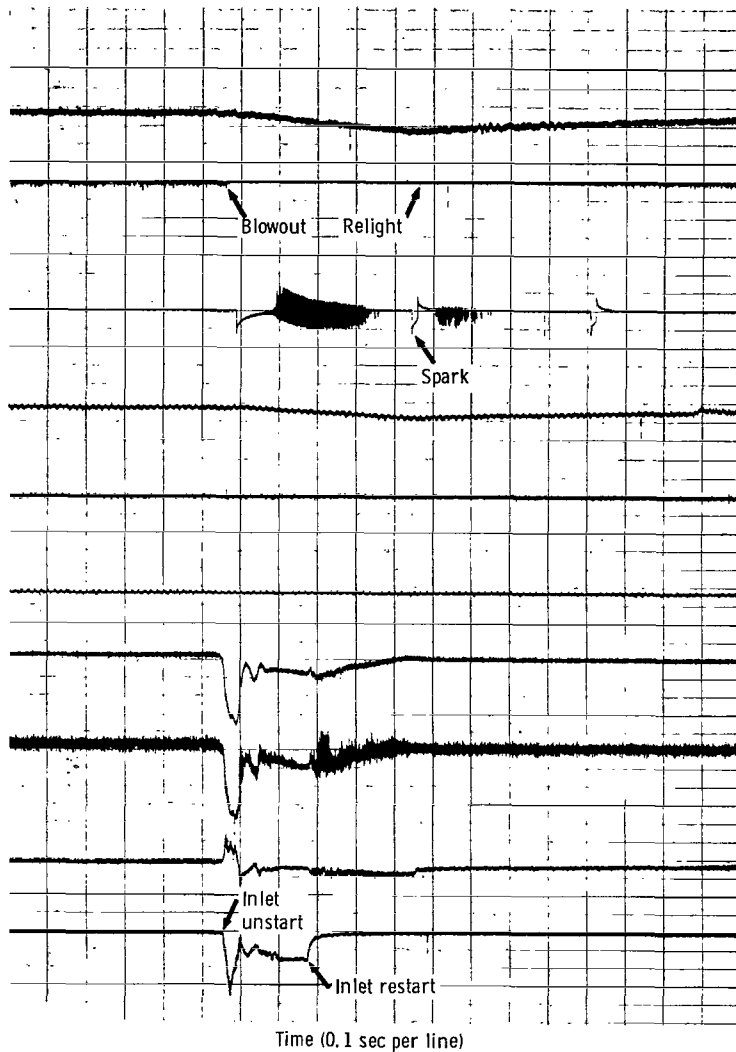
Primary-nozzle area,  $A_8$  ( $41.1\text{ cm}^2$  per line)

Compressor-face static pressure, D8 ( $0.195 p/P_0$  per line)

Compressor-face total pressure, D9 ( $0.195 p/P_0$  per line)

Compressor pressure ratio, CPR ( $1.08 P_3/P_2$  per line)

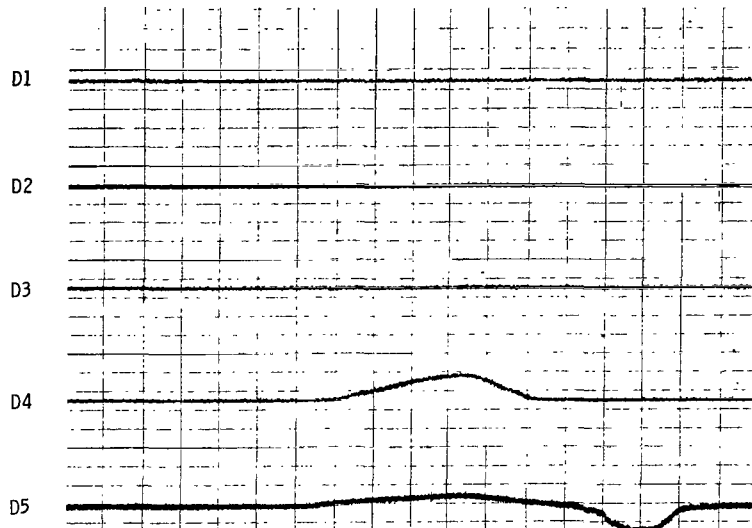
Inlet unstart sensor



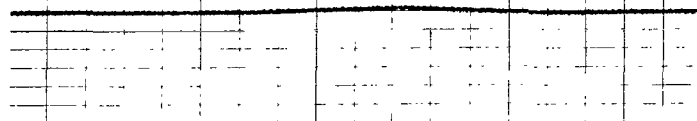
(b) Engine response.

Figure 27. - Concluded.

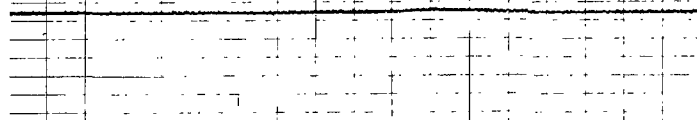
Inlet throat static pressure  
(0.195 p/P<sub>0</sub> per line):



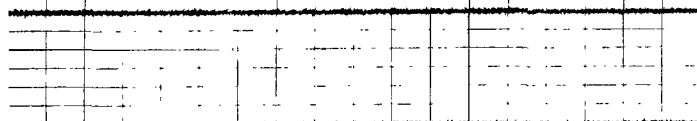
Diffuser static pressure, D6 (0.195 p/P<sub>0</sub> per line)



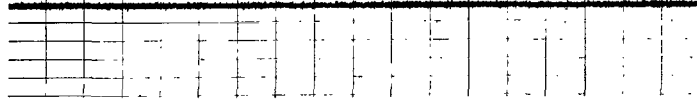
Stability-bypass-plenum total pressure, D7 (0.195 p/P<sub>0</sub> per line)



Overboard-bypass-door area variation, A<sub>by</sub> (37.9 cm<sup>2</sup> per line)



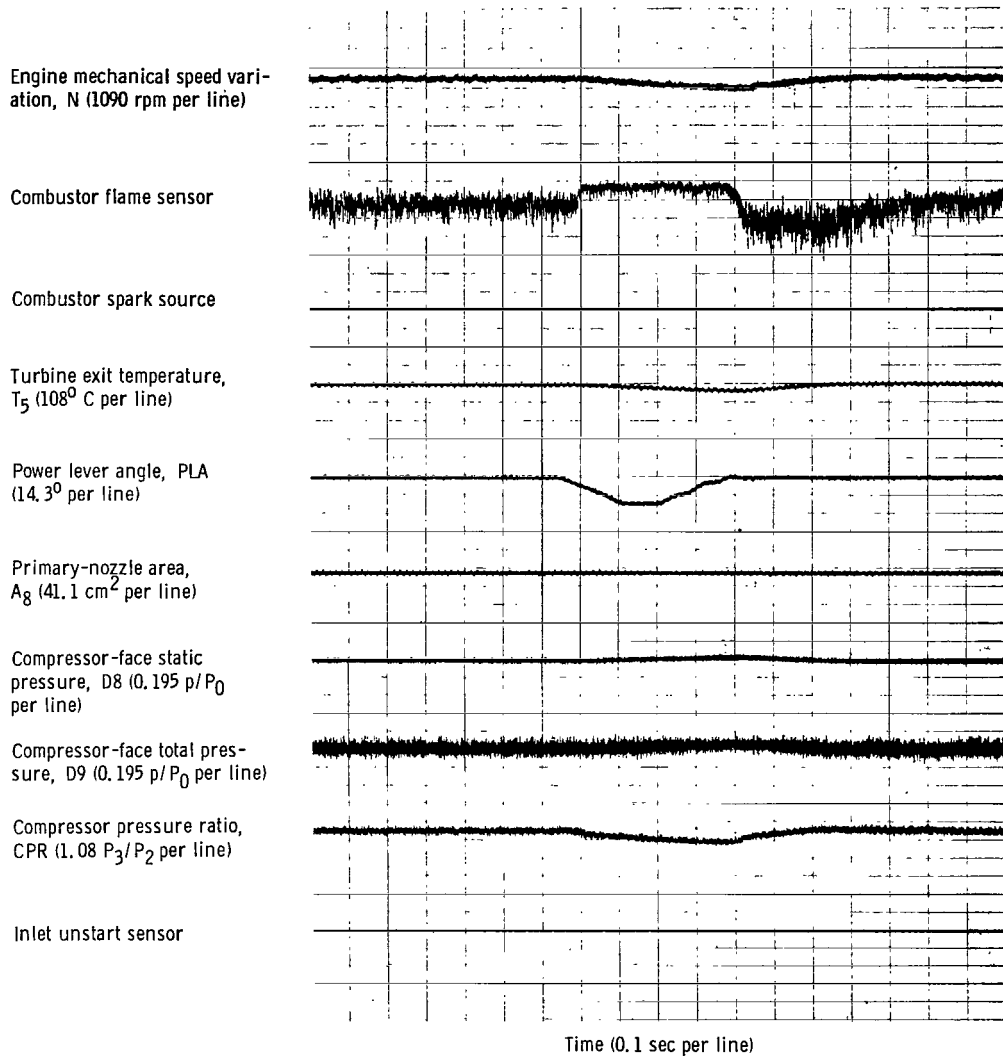
Centerbody translation, x<sub>cb</sub> (1.82 cm per line)



Time (0.1 sec per line)

(a) Inlet response.

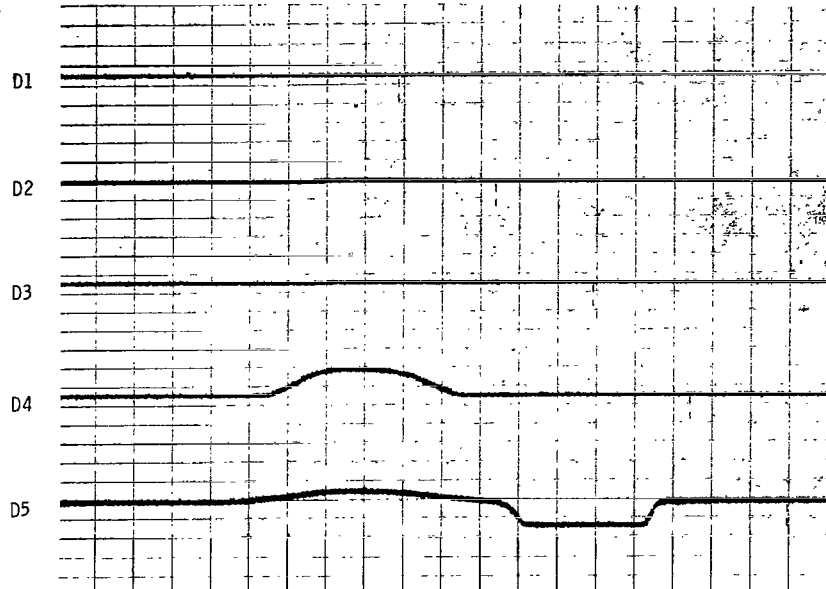
Figure 28. - Transient reduction in power lever angle. Free-stream Mach number, M<sub>0</sub>, 2.5; transient power lever angle, PLA<sub>t</sub>, 30°; transient pulse frequency, 1/τ, 2 seconds<sup>-1</sup>; corrected engine speed, N/N\*√6, 0.873; total-pressure recovery, P<sub>2</sub>/P<sub>0</sub>, 0.899; mass-flow ratio, m<sub>2</sub>/m<sub>0</sub>, 0.877; stability bypass total-pressure recovery, P<sub>sb</sub>/P<sub>0</sub>, 0.278; primary-nozzle area, A<sub>g</sub>, 0.0647 square meter.



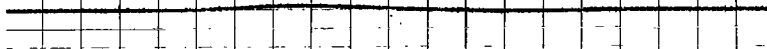
(b) Engine response.

Figure 28. - Concluded.

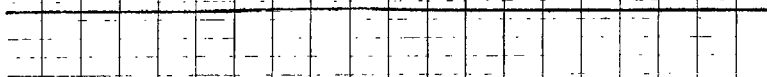
Inlet throat static pressure  
(0.195 p/P<sub>0</sub> per line):



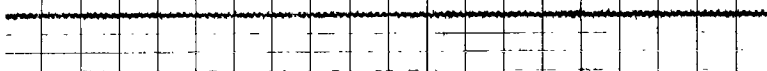
Diffuser static pressure, D6  
(0.195 p/P<sub>0</sub> per line)



Stability-bypass-plenum total  
pressure, D7 (0.195 p/P<sub>0</sub>  
per line)



Overboard-bypass-door area  
variation, A<sub>by</sub> (37.9 cm<sup>2</sup>  
per line)



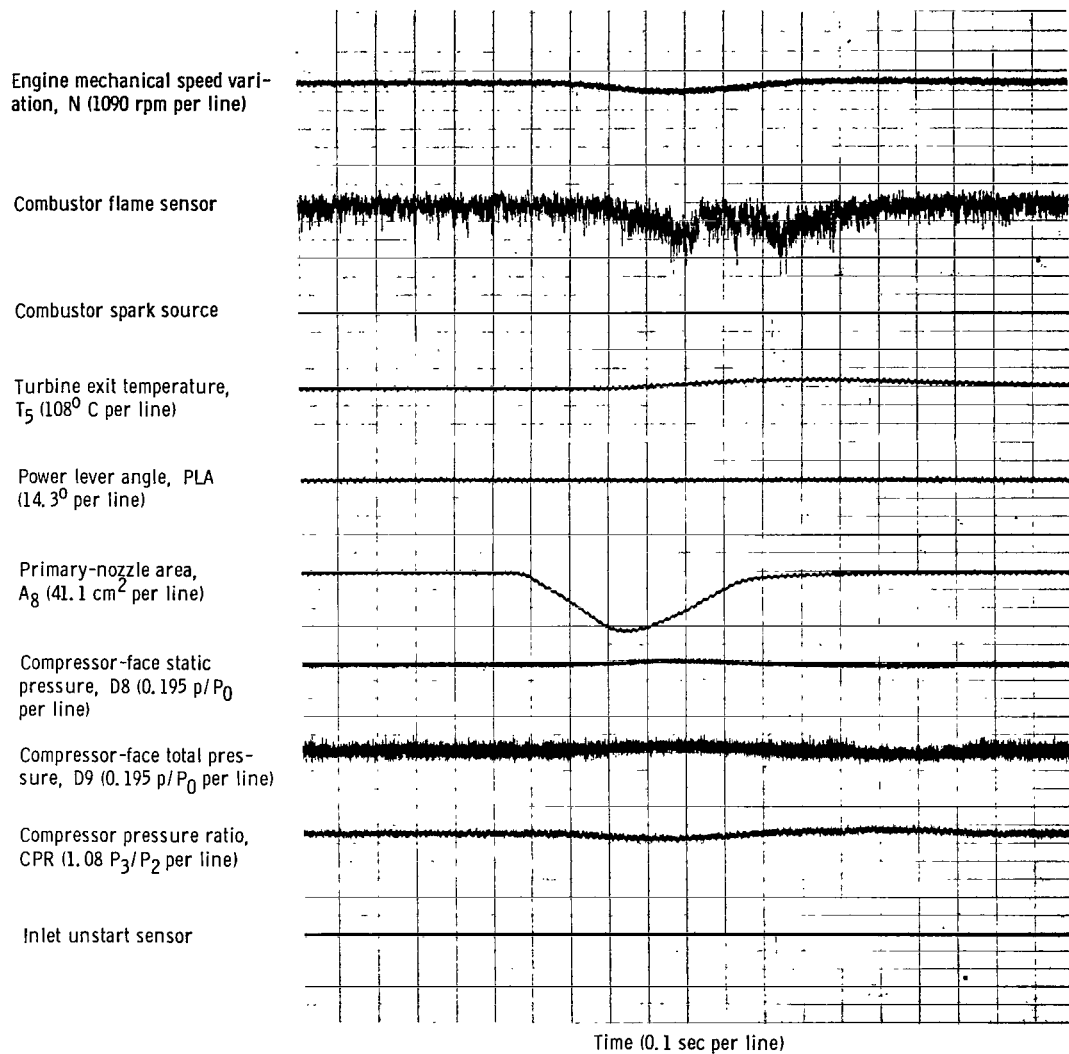
Centerbody translation, x<sub>cb</sub>  
(1.82 cm per line)



Time (0.1 sec per line)

(a) Inlet response.

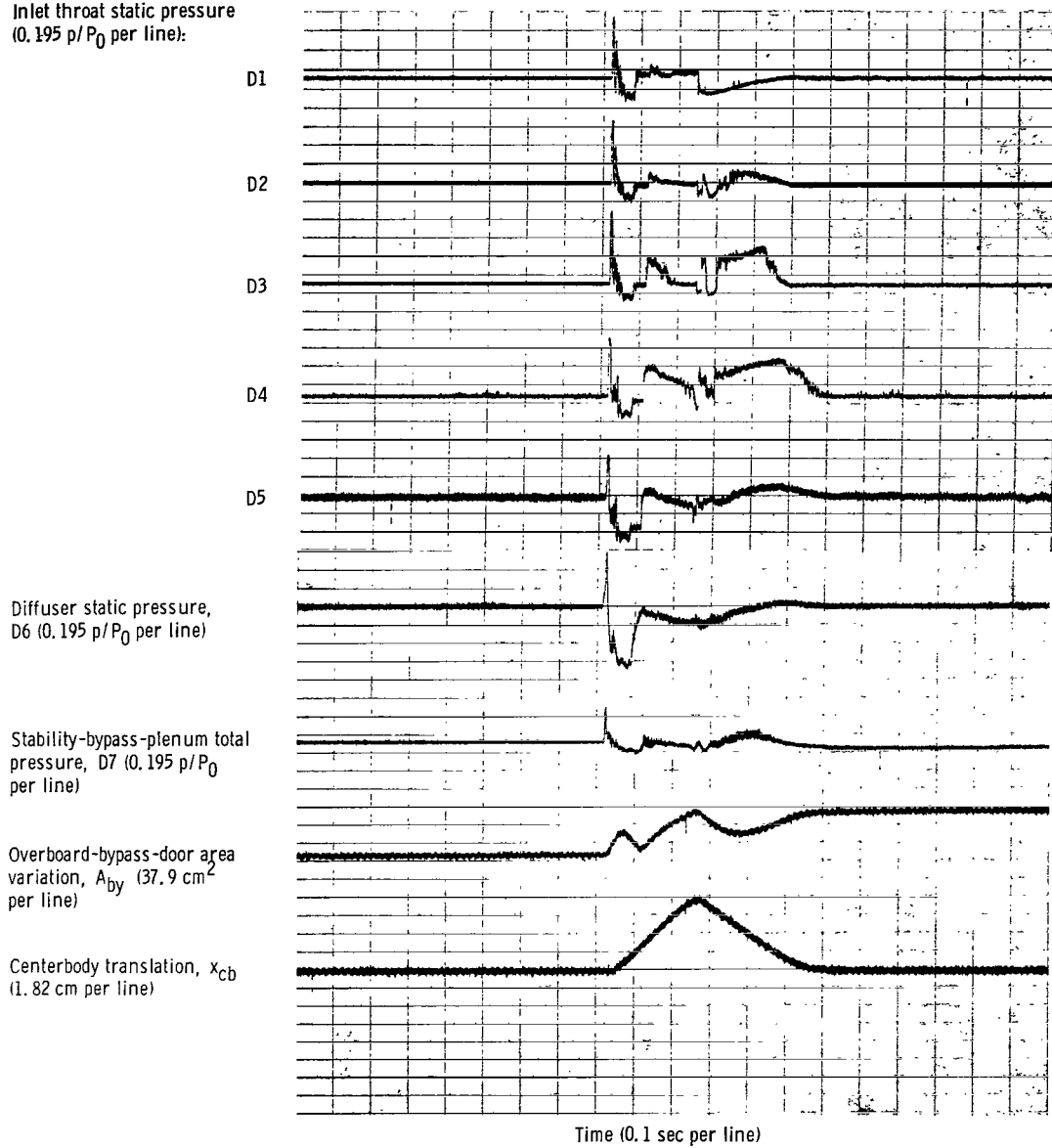
Figure 29. - Transient reduction in primary-nozzle area. Free-stream Mach number, M<sub>0</sub>, 2.5; transient primary-nozzle area, A<sub>g1</sub>, 155 square centimeters; transient pulse frequency, 1/τ, 2 seconds<sup>-1</sup>; corrected engine speed, N/N\* √θ, 0.874; total-pressure recovery, P<sub>2</sub>/P<sub>0</sub>, 0.898; mass-flow ratio, m<sub>2</sub>/m<sub>0</sub>, 0.874; stability bypass total-pressure recovery, P<sub>sb</sub>/P<sub>0</sub>, 0.279; primary-nozzle area, A<sub>g</sub>, 0.0647 square meter.



(b) Engine response.

Figure 29. - Concluded.

Inlet throat static pressure  
(0.195 p/P<sub>0</sub> per line):



(a) Inlet response.

Figure 30. - Engine stall induced by slow, manual reduction in primary-nozzle area. Free-stream Mach number,  $M_0$ , 2.5; corrected engine speed,  $N/N^* \sqrt{\theta}$ , 0.901; total-pressure recovery,  $P_2/P_0$ , 0.906; mass-flow ratio,  $m_2/m_0$ , 0.878; compressor total-pressure recovery,  $P_3/P_2$ , 5.525; stability bypass total-pressure recovery,  $P_{sb}/P_0$ , 0.31; primary-nozzle area,  $A_8$ , 0.0543 square meter.

Engine mechanical speed variation, N (1090 rpm per line)

Combustor flame sensor

Combustor spark source

Turbine exit temperature,  $T_5$  ( $108^\circ$  C per line)

Power lever angle, PLA ( $14.3^\circ$  per line)

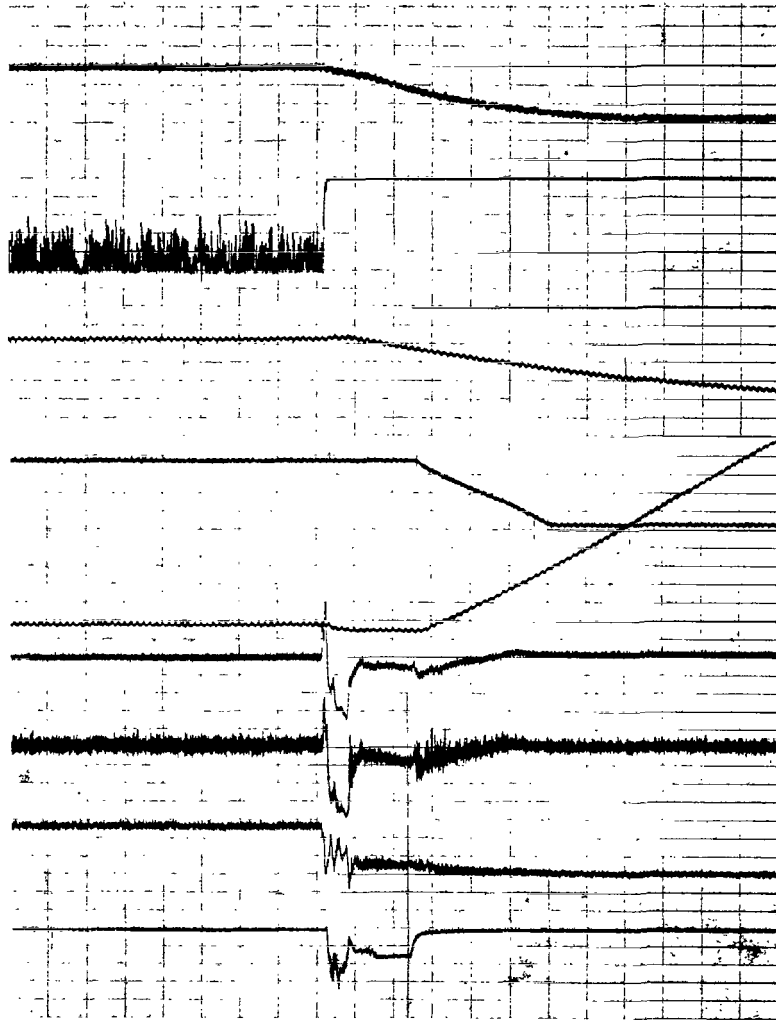
Primary-nozzle area,  $A_8$  ( $41.1 \text{ cm}^2$  per line)

Compressor-face static pressure, D8 ( $0.195 p/P_0$  per line)

Compressor-face total pressure, D9 ( $0.195 p/P_0$  per line)

Compressor pressure ratio, CPR ( $1.08 P_3/P_2$  per line)

Inlet unstart sensor



Time (0.1 sec per line)

(b) Engine response.

Figure 30. - Concluded.



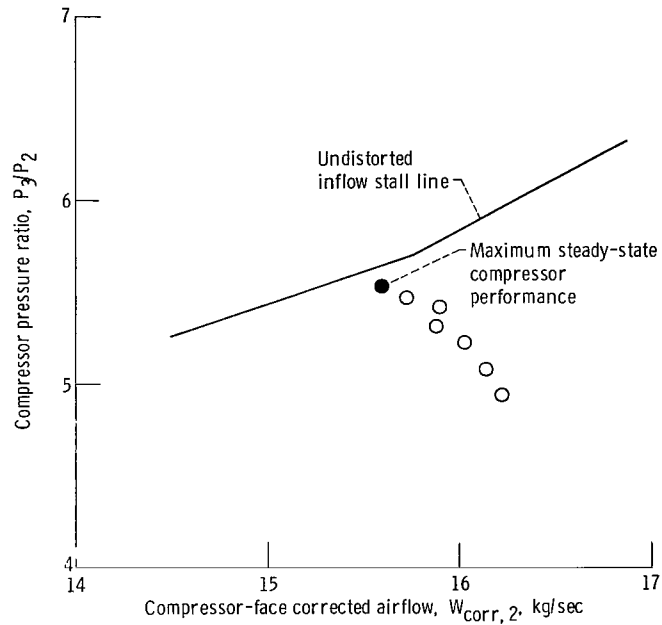
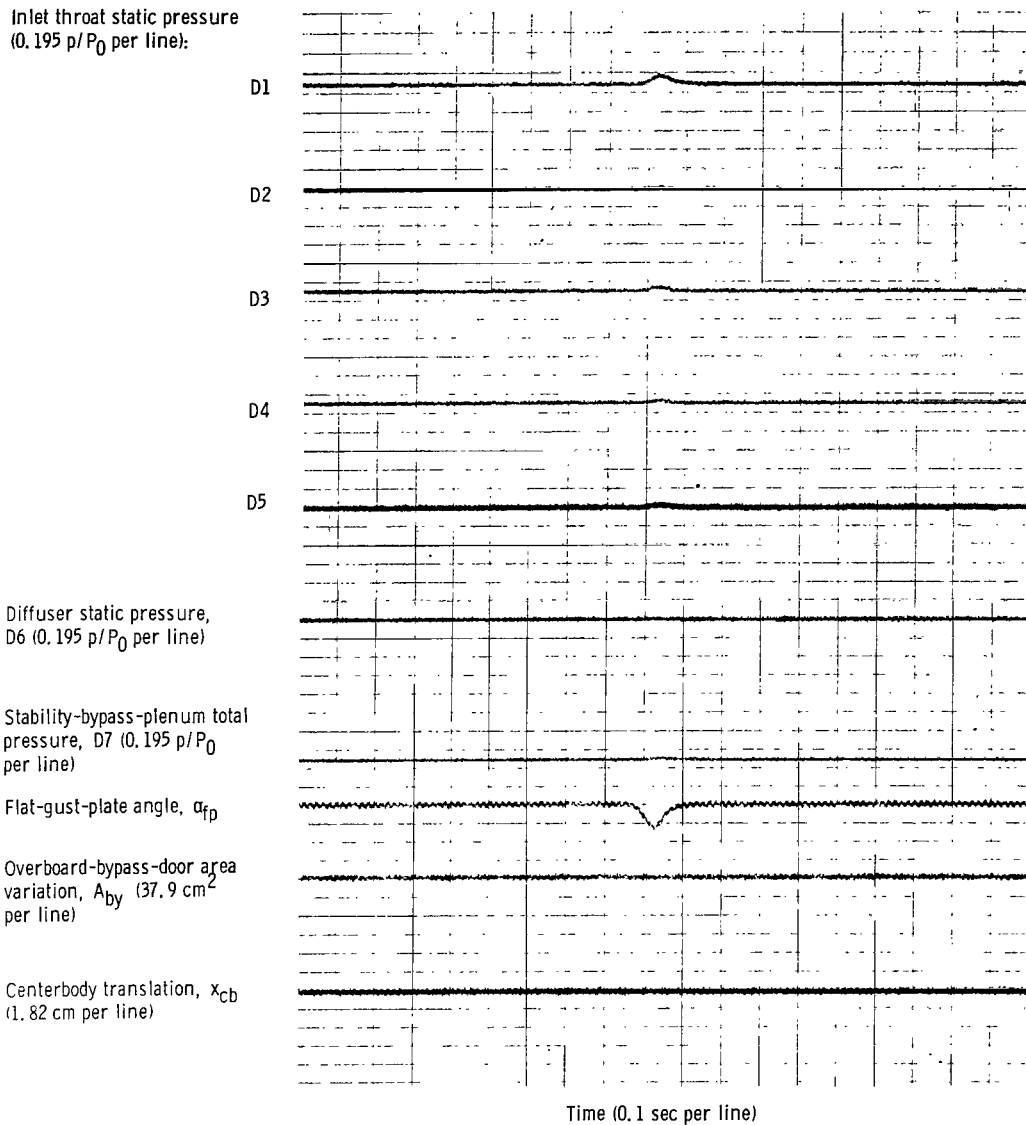
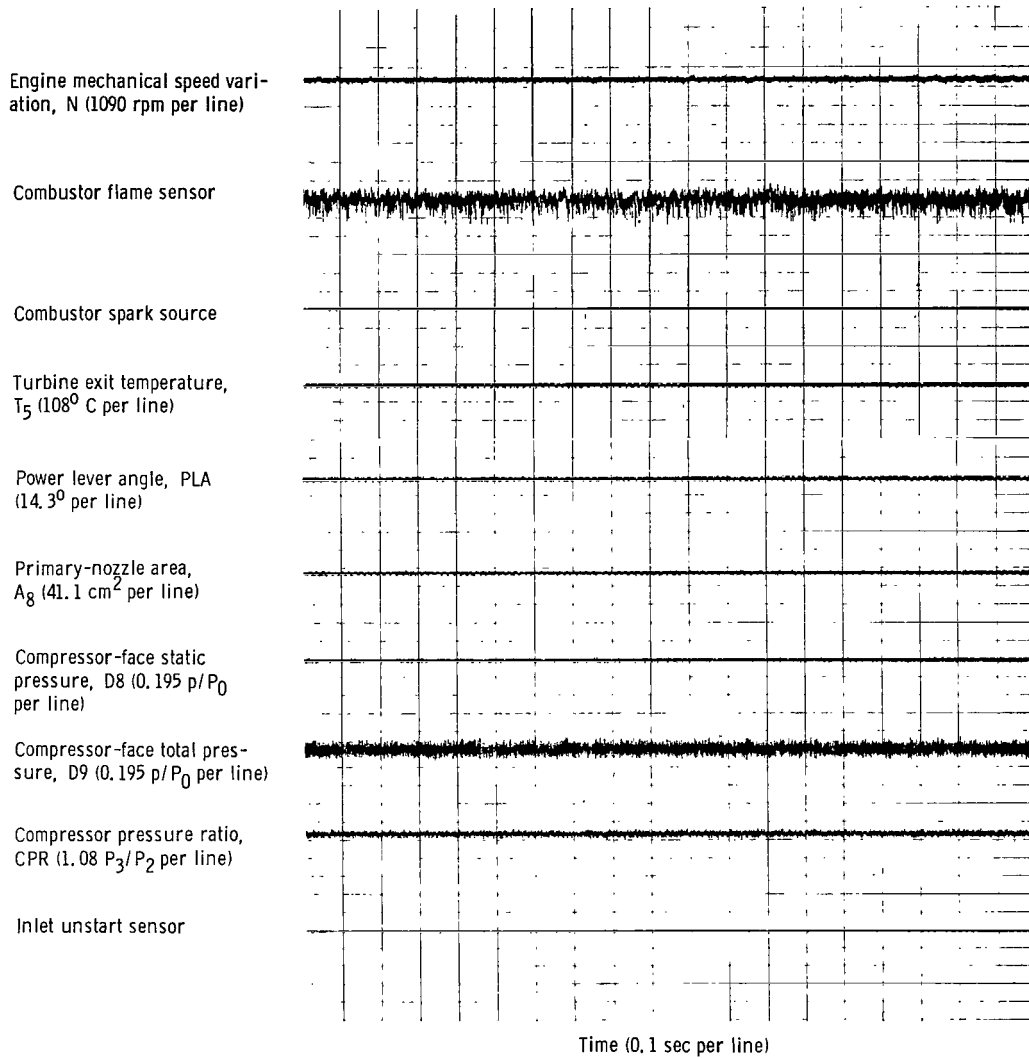


Figure 31. - Compressor performance obtained by reducing primary-nozzle area while maintaining constant corrected engine speed. Free-stream Mach number,  $M_0$ , 2.5; corrected engine speed,  $N/N^* \sqrt{\theta}$ , 0.901.



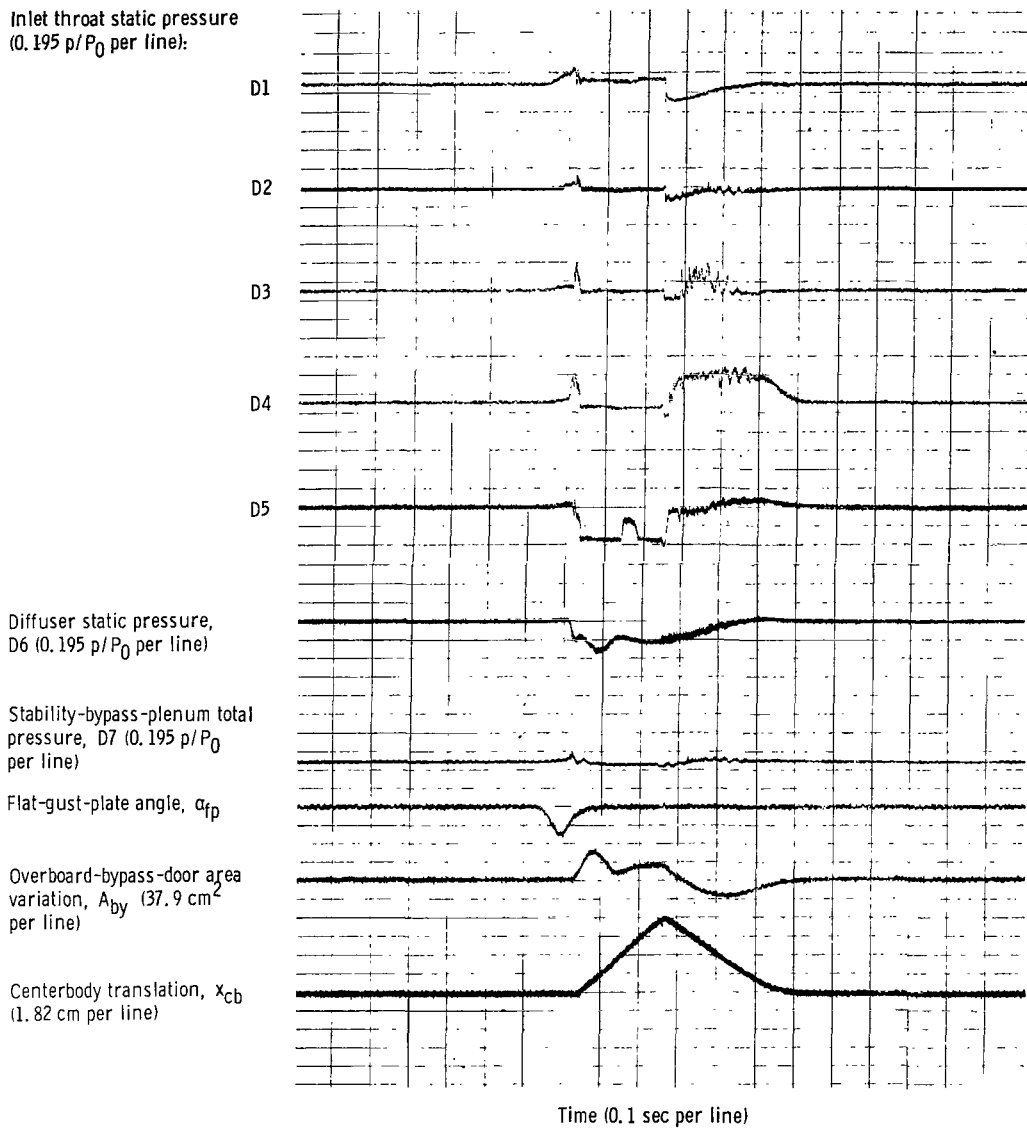
(a) Inlet response.

Figure 32. - External airflow transient induced by flat gust plate - transient flat-gust-plate angle,  $\alpha_{fp,t}$ ,  $1.0^\circ$ . Free-stream Mach number,  $M_0$ , 2.5; transient pulse frequency,  $10 \text{ seconds}^{-1}$ ; corrected engine speed,  $N/N^* \sqrt{\theta}$ , 0.872; total-pressure recovery,  $P_2/P_0$ , 0.901; mass-flow ratio,  $m_2/m_0$ , 0.876; stability bypass total-pressure recovery,  $P_{sb}/P_0$ , 0.278; primary-nozzle area,  $A_8$ , 0.0647 square meter.



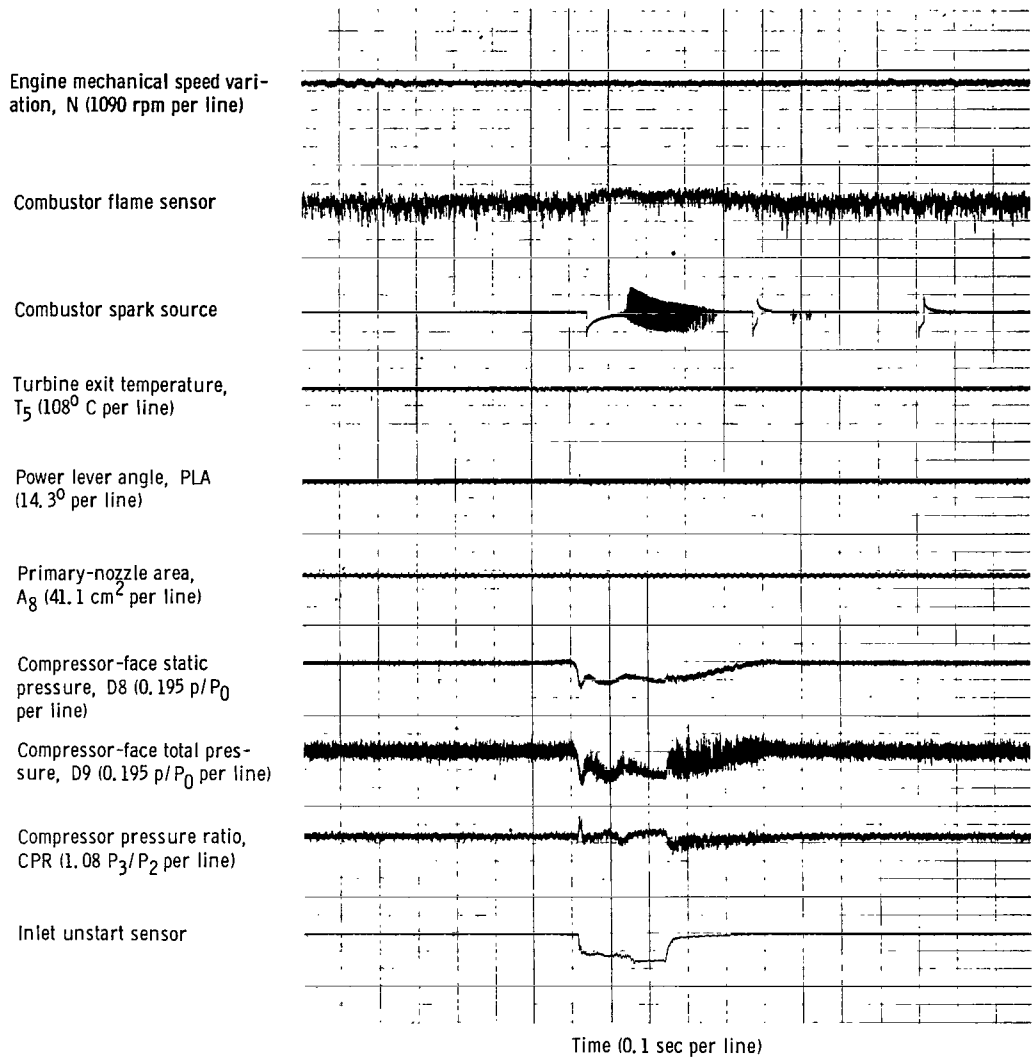
(b) Engine response.

Figure 32. - Concluded.



(a) Inlet response.

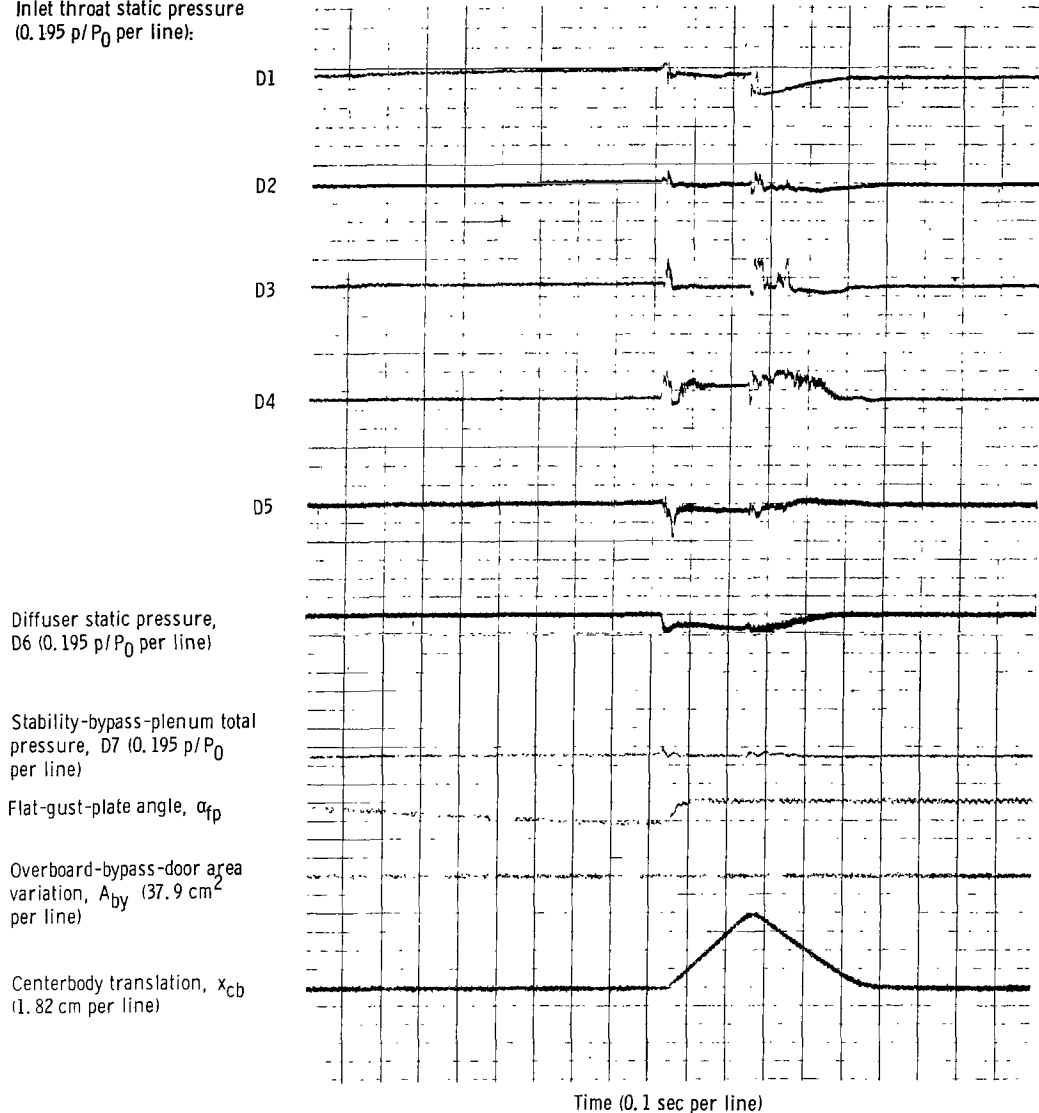
Figure 33. - External airflow transient induced by flat gust plate - transient flat-gust-plate angle,  $\alpha_{fp}$ ,  $t$ , 1.2°. Free-stream Mach number,  $M_0$ , 2.5; transient pulse frequency,  $1/\tau$ , 10 seconds<sup>-1</sup>; engine corrected speed,  $N/N^* \sqrt{\theta}$ , 0.874; total-pressure recovery,  $P_2/P_0$ , 0.898; mass-flow ratio,  $m_2/m_0$ , 0.881; stability bypass total-pressure recovery,  $P_{sb}/P_0$ , 0.279; primary-nozzle area,  $A_8$ , 0.0647 square meter.



(b) Engine response.

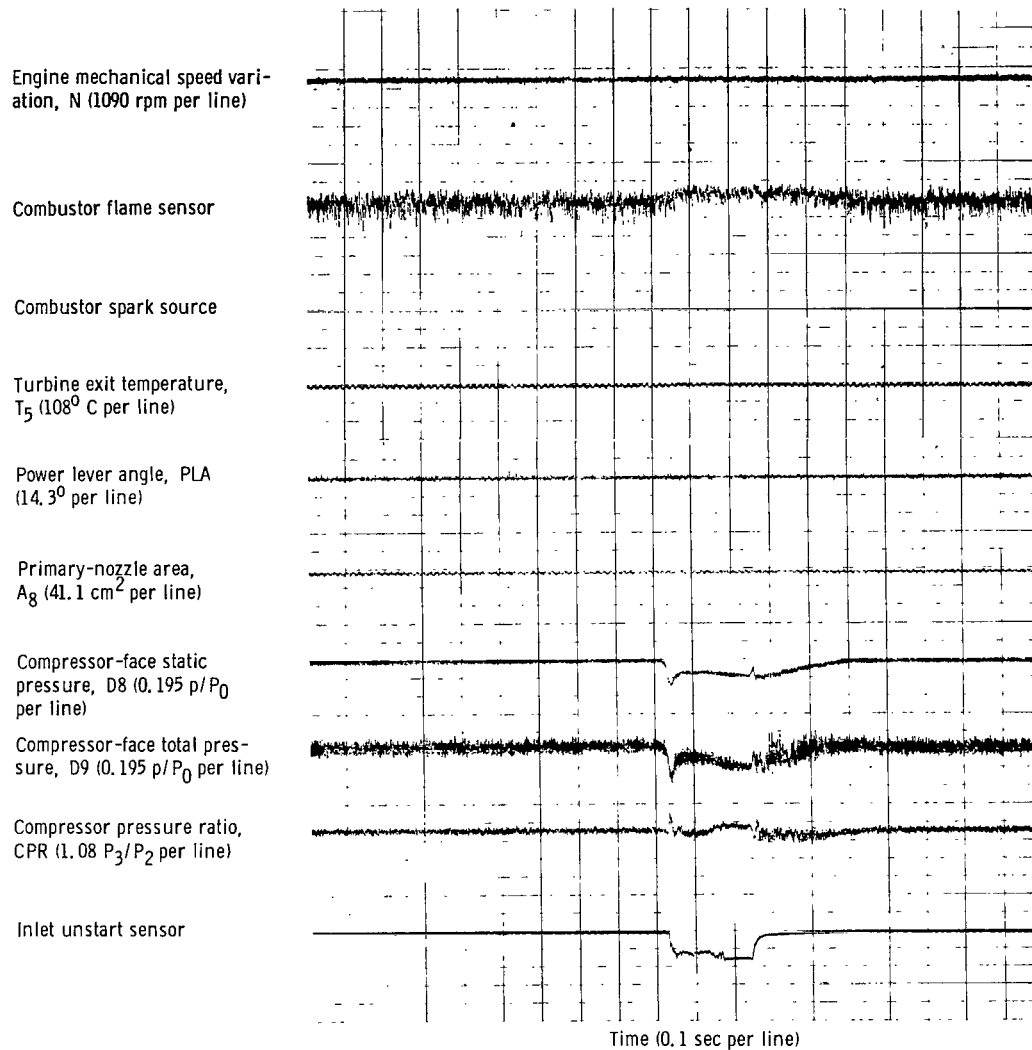
Figure 33. - Concluded.

Inlet throat static pressure  
(0.195  $p/P_0$  per line):



(a) Inlet response.

Figure 34. - Slow, manual variation in flat-gust-plate angle of attack to inlet unstart with no overboard bypass control after inlet unstart. Free-stream Mach number,  $M_0$ , 2.5; corrected engine speed,  $N/N^c \sqrt{\theta}$ , 0.874; total-pressure recovery,  $P_2/P_0$ , 0.897; mass-flow ratio,  $m_2/m_0$ , 0.877; stability bypass mass-flow ratio,  $P_{sb}/P_0$ , 0.279; primary-nozzle area,  $A_8$ , 0.0648 square meter.



(b) Engine response.

Figure 34. - Concluded.

Inlet throat static pressure  
(0.195 p/P<sub>0</sub> per line):

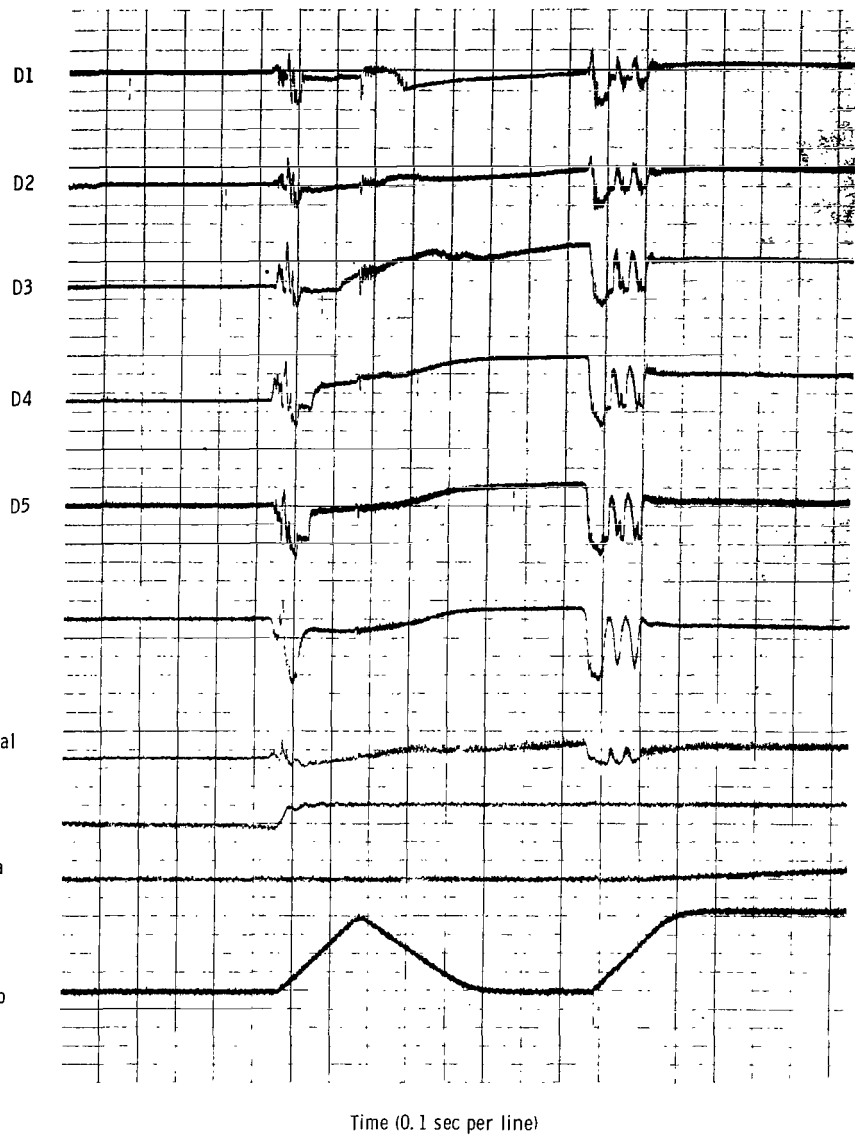
Diffuser static pressure,  
D6 (0.195 p/P<sub>0</sub> per line)

Stability-bypass-plenum total  
pressure, D7 (0.195 p/P<sub>0</sub>  
per line)

Flat-gust-plate angle,  $\alpha_{fp}$

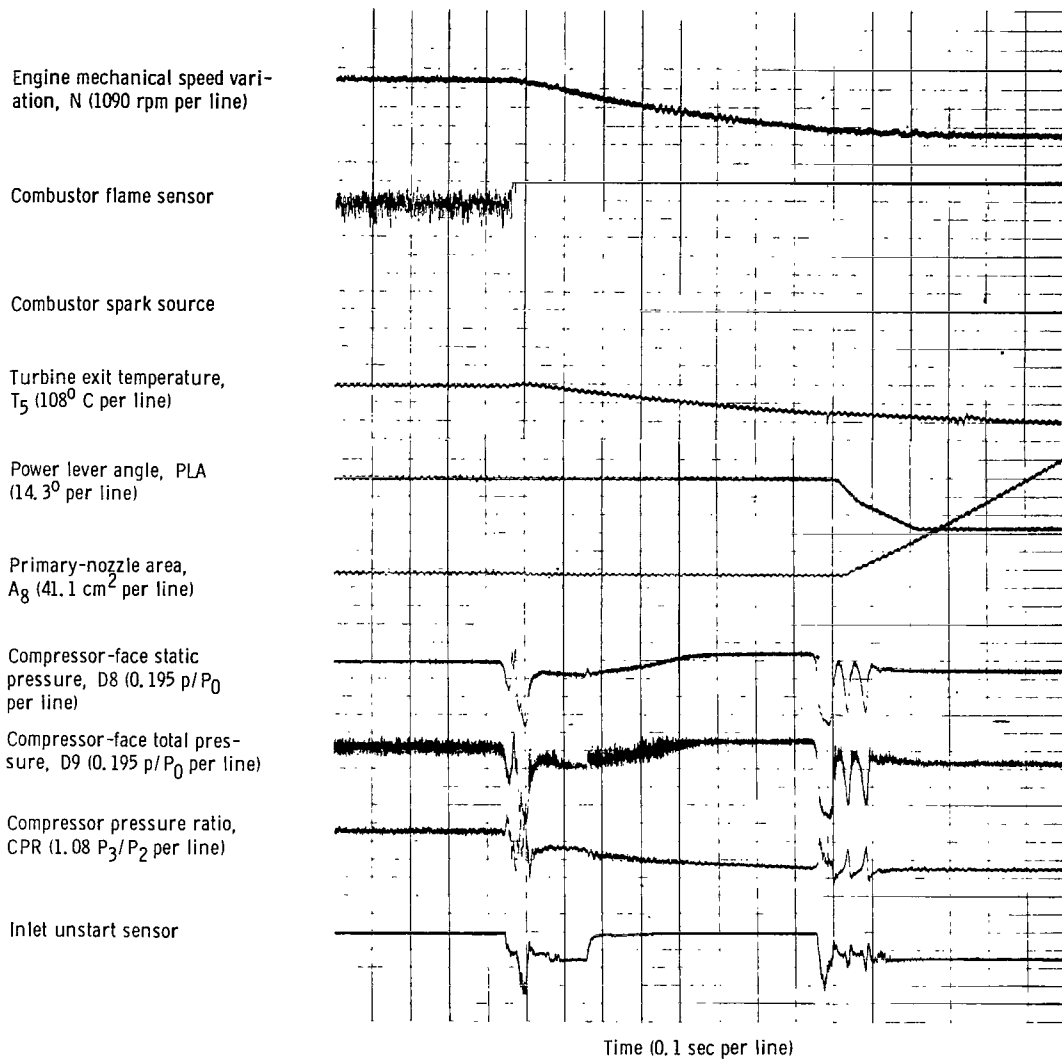
Overboard-bypass-door area  
variation,  $A_{by}$  (37.9 cm<sup>2</sup>  
per line)

Centerbody translation,  $x_{cb}$   
(1.82 cm per line)



(a) Inlet response.

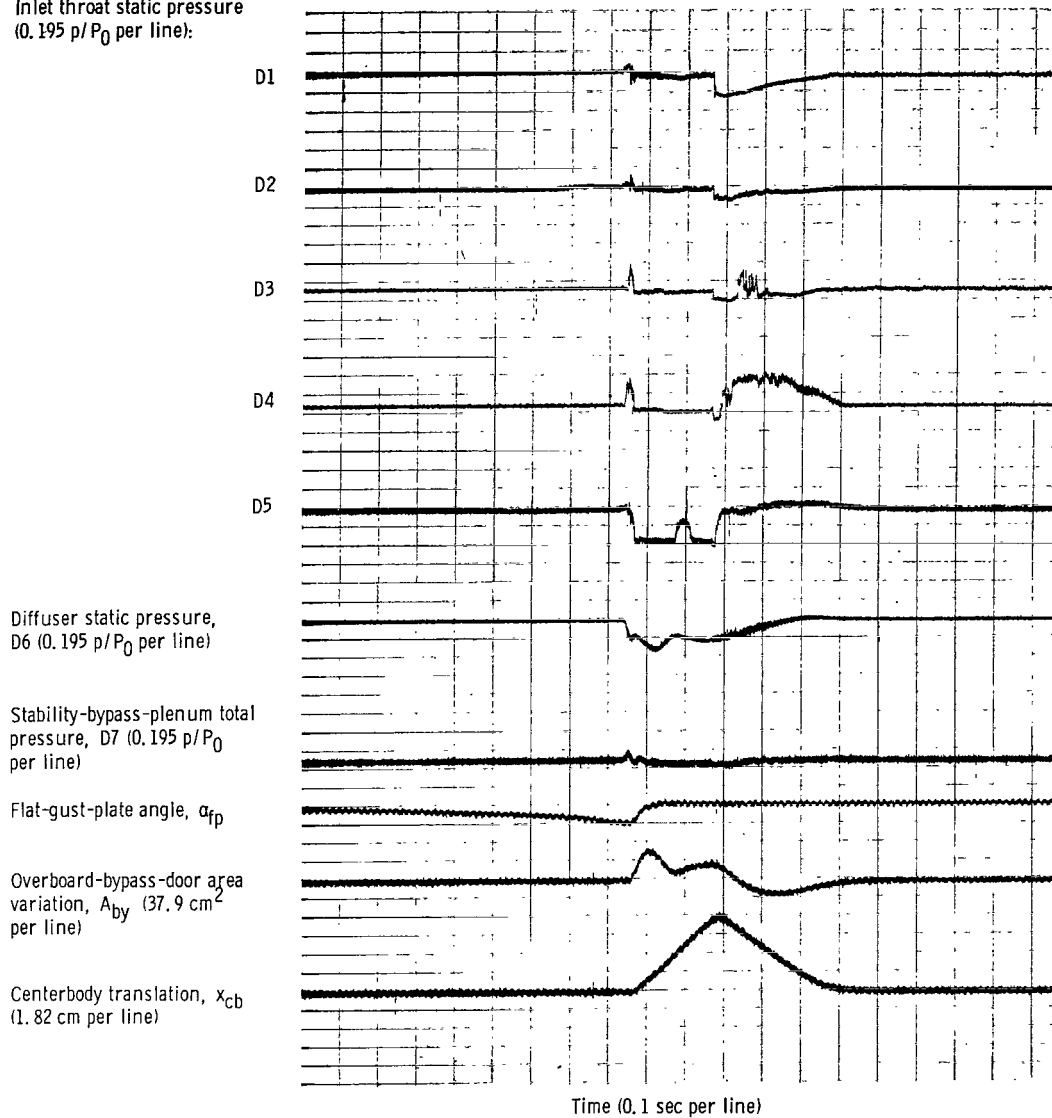
Figure 35. - Conditions of figure 34 repeated 45 seconds later.



(b) Engine response.

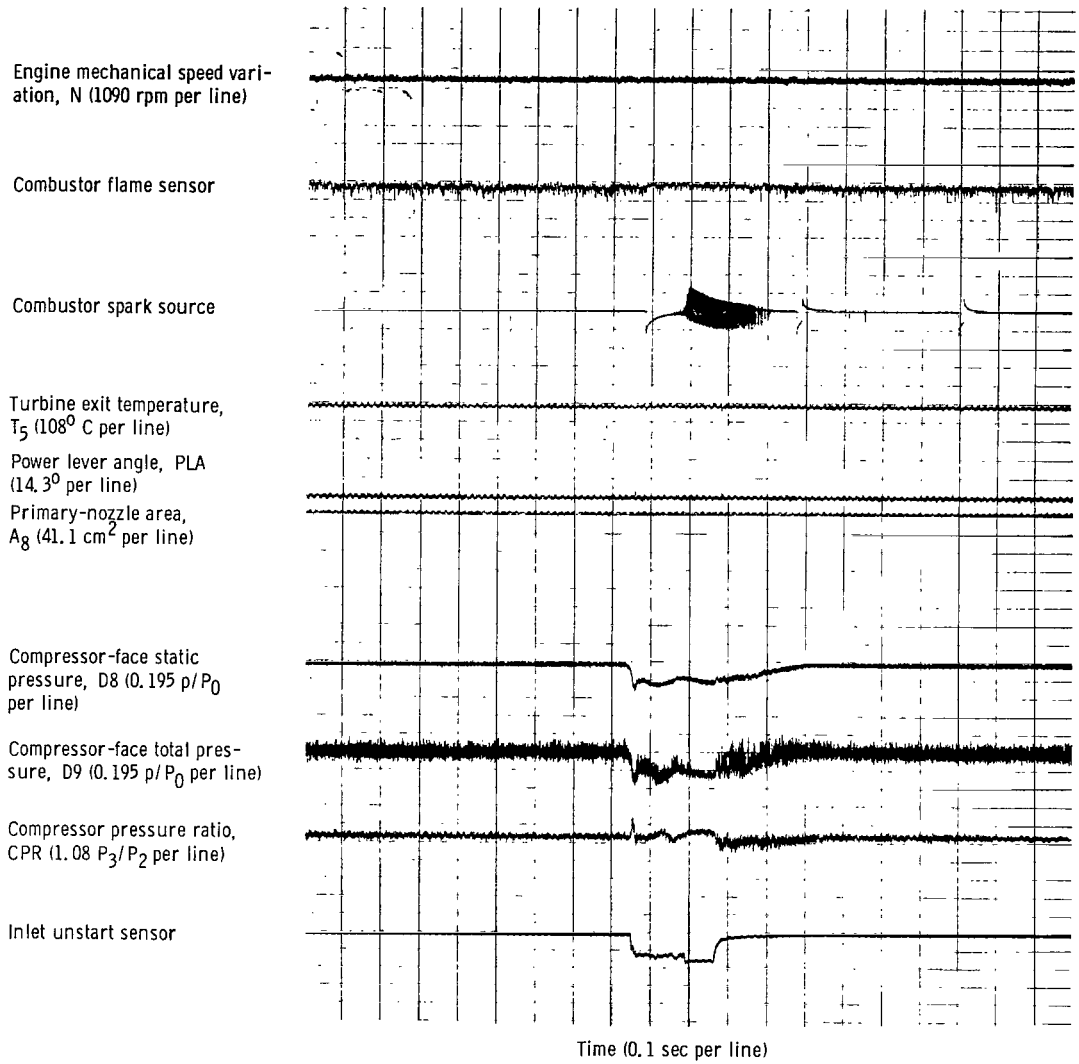
Figure 35. - Concluded.

Inlet throat static pressure  
(0.195 p/P<sub>0</sub> per line):



(a) Inlet response.

Figure 36. - Slow, manual variation in flat-gust-plate angle of attack to inlet unstart with overboard bypass control after unstart. Free-stream Mach number,  $M_0$ , 2.5; corrected engine speed,  $N/N^* \sqrt{\theta}$ , 0.873; total-pressure recover,  $P_2/P_0$ , 0.891; mass-flow ratio,  $m_2/m_0$ , 0.871; stability bypass total-pressure recovery,  $P_{sb}/P_0$ , 0.273; primary-nozzle area,  $A_8$ , 0.0794 square meter.

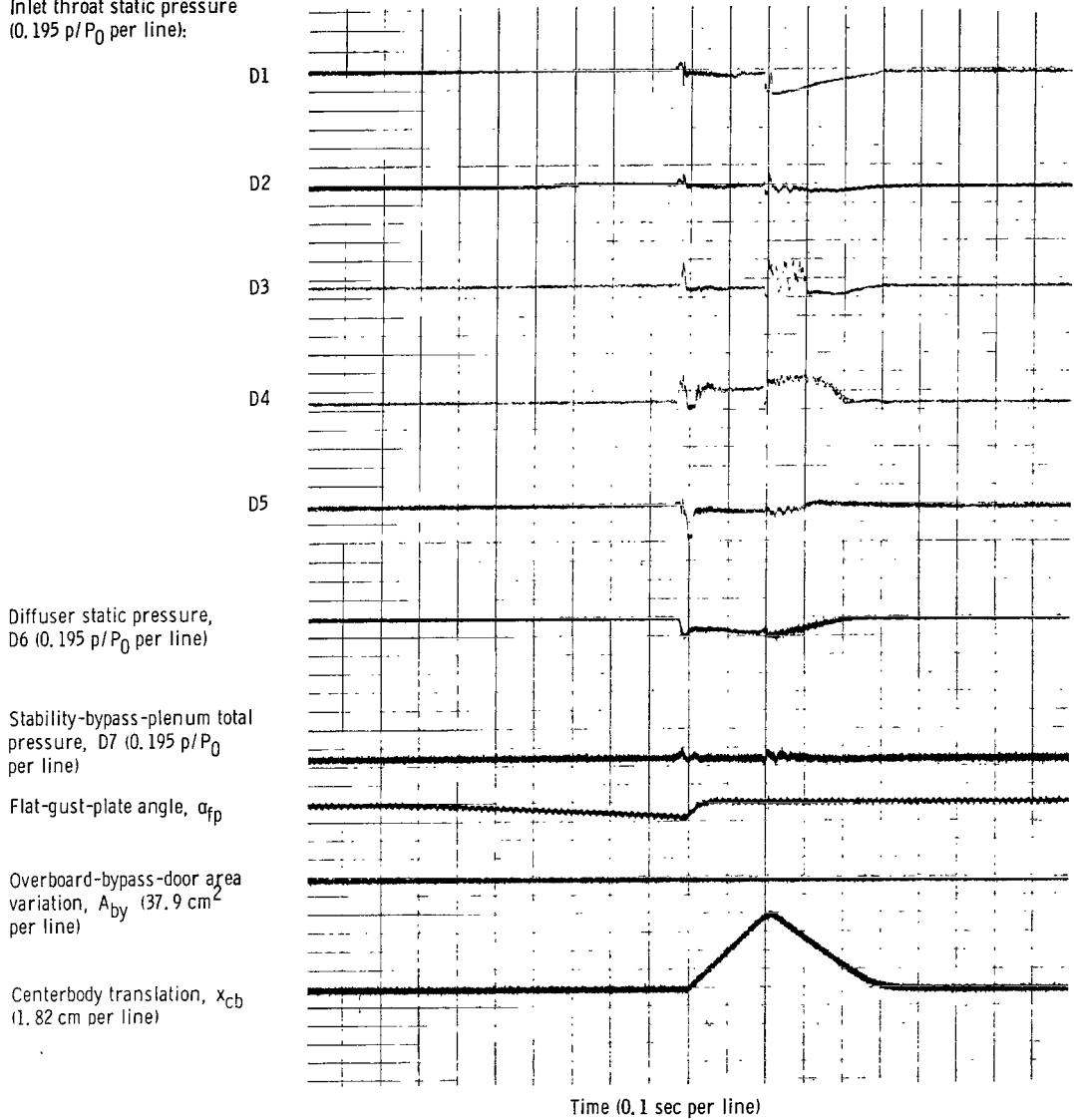


Time (0.1 sec per line)

(b) Engine response.

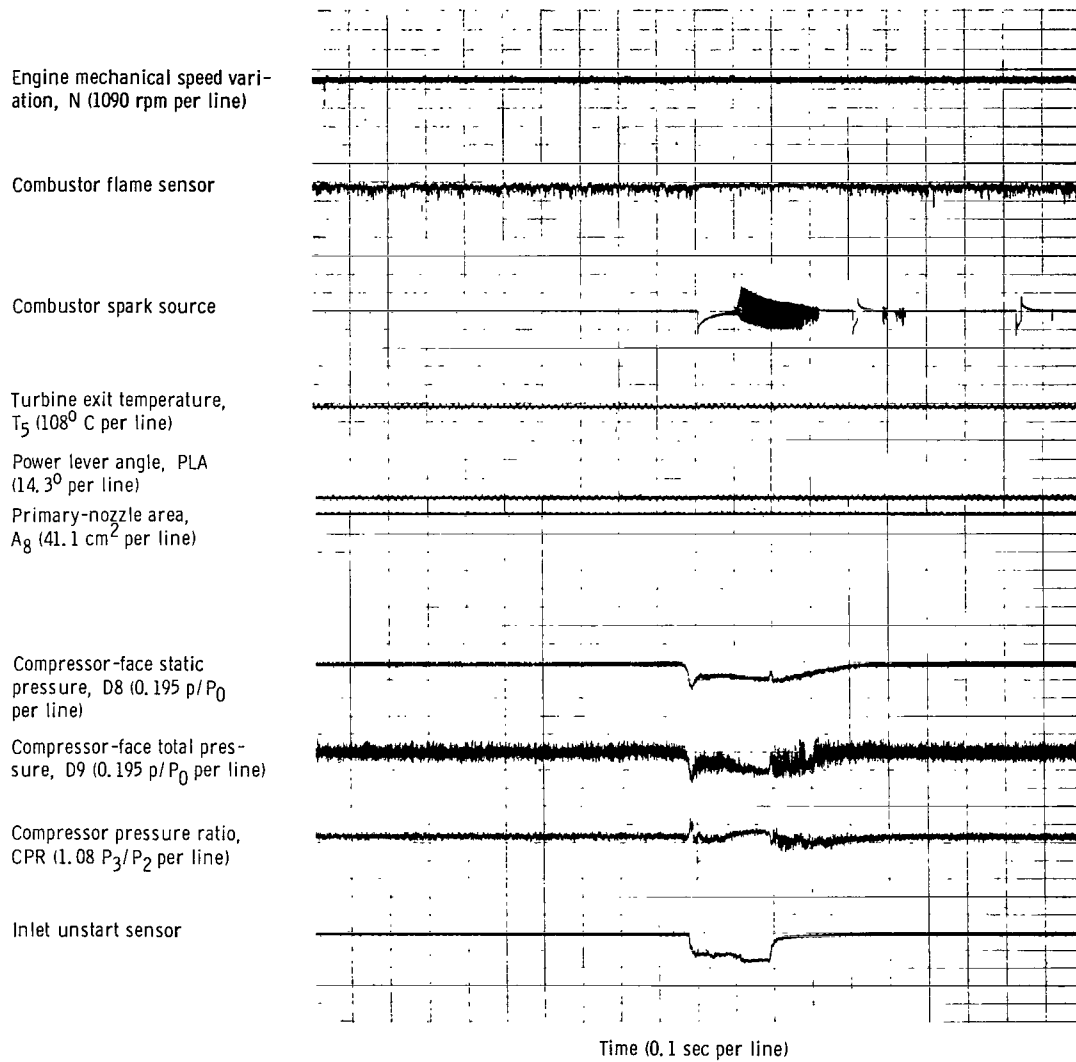
Figure 36. - Concluded.

Inlet throat static pressure  
(0.195 p/P<sub>0</sub> per line):



(a) Inlet response.

Figure 37. - Slow, manual variation in flat-gust-plate angle of attack to inlet unstart with no overboard bypass control after inlet unstart - for larger primary-nozzle area than figure 34. Free-stream Mach number,  $M_0$ , 2.5; corrected engine speed,  $N/N^* \sqrt{\theta}$ , 0.873; total-pressure recovery,  $P_2/P_0$ , 0.891; mass-flow ratio,  $m_2/m_0$ , 0.871; stability bypass mass-flow ratio,  $P_{sb}/P_0$ , 0.273; primary-nozzle area,  $A_8$ , 0.0794 square meter.



(b) Engine response.

Figure 37. - Concluded.

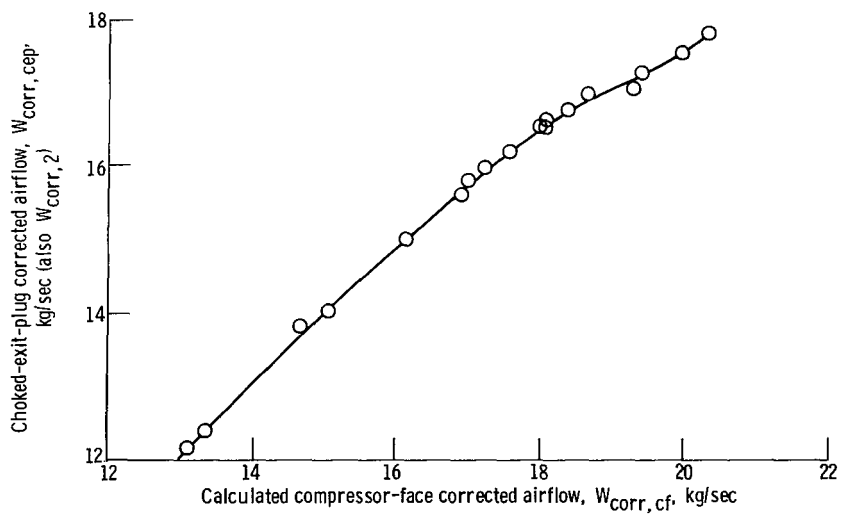


Figure 38. - Compressor-face corrected airflow calibration.

1. Report No. <b>NASA TP-1532</b>	2. Government Accession No.	3. Recipient's Catalog No.
4. Title and Subtitle <b>TURBOJET-EXHAUST-NOZZLE SECONDARY-AIRFLOW PUMPING AS AN EXIT CONTROL OF AN INLET-STABILITY BYPASS SYSTEM FOR A MACH 2.5 AXISYMMETRIC MIXED-COMPRESSION INLET</b>	5. Report Date January 1980	6. Performing Organization Code
7. Author(s) <b>Bobby W. Sanders</b>	8. Performing Organization Report No. <b>E-9468</b>	10. Work Unit No. <b>505-04</b>
9. Performing Organization Name and Address <b>National Aeronautics and Space Administration Lewis Research Center Cleveland, Ohio 44135</b>	11. Contract or Grant No.	13. Type of Report and Period Covered <b>Technical Paper</b>
12. Sponsoring Agency Name and Address <b>National Aeronautics and Space Administration Washington, D. C. 20546</b>	14. Sponsoring Agency Code	
15. Supplementary Notes		
16. Abstract  The throat of a Mach 2.5 inlet that was attached to a turbojet engine was fitted with large, porous bleed areas to provide a stability bypass system that would allow a large, stable airflow range. Exhaust-nozzle, secondary-airflow pumping was used as the exit control for the stability bypass airflow. Propulsion system response and stability bypass performance were obtained for several transient airflow disturbances, both internal and external. Internal airflow disturbances included reductions in overboard bypass airflow, power lever angle, and primary-nozzle area, as well as compressor stall. Nozzle secondary pumping as a stability bypass exit control can provide the inlet with a large stability margin with no adverse effects on propulsion system performance.		
17. Key Words (Suggested by Author(s)) <b>Air intakes; Supersonic cruise inlets; Shock stability; Inlet bleed; Turbojet engine; Nozzle pumping</b>	18. Distribution Statement <b>Unclassified - unlimited STAR Category 07</b>	
19. Security Classif. (of this report) <b>Unclassified</b>	20. Security Classif. (of this page) <b>Unclassified</b>	21. No. of Pages <b>81</b>
		22. Price* <b>A05</b>

\* For sale by the National Technical Information Service, Springfield, Virginia 22161

National Aeronautics and  
Space Administration

Washington, D.C.  
20546

Official Business

Penalty for Private Use, \$300

THIRD-CLASS BULK RATE

Postage and Fees Paid  
National Aeronautics and  
Space Administration  
NASA-451



4 1 10, A, 120379 S00903DS  
DEPT OF THE AIR FORCE  
AF WEAPONS LABORATORY  
ATTN: TECHNICAL LIBRARY (SUL)  
KIRTLAND AFB NM 87117

**NASA**

ion 158  
Postal Manual, DO NOT Return

S